PEGASE

PAN EUROPEAN GRID ADVANCED SIMULATION AND STATE ESTIMATION

Deliverable D5.1

Modeling requirements for the ETN

Part 3: Toolbox for modeling ETN components

Proprietary Rights Statement

This document contains information, which is proprietary to the "PEGASE" Consortium. Neither this document nor the information contained herein shall be used, duplicated or communicated by any means to any third party, in whole or in parts, except with prior written consent of the "PEGASE" Consortium.

Grant Agreement Number: 211407 implemented as Large-scale Integrating Project
Coordinator: Tractebel Engineering S.A.
Project Website: http://www.fp7-pegase.eu

Document Information

Document Name:	D5.1 Part 3: Toolbox for the modeling the ETN components
ID:	**DEL_WP5.1_Part_3_Toolbox_for_modeling_ETN_components_V3.doc**
WP:	5
Task:	5.3 (subtasks 5.3.1, 5.3.2, 5.3.3, 5.3.4)
Revision:	1
Revision Date:	30.06.2011
Author:	UDE, RTU & ESP

Diffusion list

STB, SSB, and Coordinator

Approvals

Final version to be submitted to the European Commission.

	Name	Company	Date	Visa
Author	Antans Sauhats	RTU		
Author	Vladimir Chuvychin	RTU		
Author	Vadims Strelkovs	RTU		
Author	Fekadu Shewarega	UDE		
Author	István Erlich	UDE		
Author	Alexander Rubtsov	ESP		
Task Leader		RTU		
WP Leader		UDE		

Documents history

Revision	Date	Modification	Author
1	01.05.2011	First draft version	RTU, UDE,TE & ESP
		Contribution to the report	
		Contribution to the report	
		Final version	

Table of content

Deliverable D5.1 1

Modeling requirements for the ETN 1

Part 3: Toolbox for modeling ETN components 1

1. Executive Summary 6

2. Introduction 8

3. Simplified wind farm / wind turbine model 9

3.1. Introduction 9

3.2. DFIG based WT system configuration 9

3.3. Detailed (full order) model of the DFIG 10

3.4. The quasi stationary (QS) model of the DFIG 11

3.5. Rotor side converter (RSC) model 11

3.6. Simplified model of DFIG and its control system- the generic model 12

3.7. Model of the full size converter machine and its control system 13

3.8. Current limitation equations 14

3.9. Further extensions and the generic model in its final form 15

3.10. Accuracy of the generic model in comparison with the QSS model 16

3.11. Sign convention and initialization procedure 17

3.11.1. Sign convention 17

3.11.2. Initialization 17

4. Implementation of the wind farm model 18

4.1. Modifications made in EUROSTAG model compared to base model description 18

4.2. Implementation of specific parts of the model 18

4.2.1. Simple lag with variable time constant 18

4.2.2. Current conversion 18

4.2.3. PI block with limitation 18

4.3. Model parameters description 19

4.4. Model testing 20

4.4.1. Sample power grid 20

4.5. Test results 21

4.5.1. Direct (metallic) short-circuit 22

4.5.2. Voltage set-point modification 24

4.6. EUROSTAG limitations 25
4.6.1. Reset feature 26
4.6.2. Limited integrator block with variable limits 27
5. High Voltage Direct Current (HVDC) Transmission System 28
5.1. Introduction 28
5.2. HVDC VSC basics 29
5.3. Control of HVDC VSC 29
5.3.1. Overview 29
5.3.2. Simplified HVDC VSC Dynamic Model 30
5.3.3. DC Link Model 33
5.3.4. Sending-end converter (SEC) model 33
5.4. Demonstration Examples 34
5.4.1. Test network and controller parameters 34
5.4.2. Simulation results 35
6. Implementation of the HVDC VSC model 39
6.1. Versions of implementation 39
6.2. Implementation of specific parts of the model 39
6.2.1. PQ priority block 39
6.2.2. Current conversion 40
6.2.3. Hysteresis block 40
6.2.4. Losses modeling 41
6.2.5. Implementation of converter reactance 41
6.3. Model parameters description 42
6.4. Model testing 42
6.4.1. Sample power grid 42
6.4.2. Test results 44
6.4.3. Conclusion on test results 47
6.5. EUROSTAG limitations 47
7. Digital loss of synchronism protection 49
7.1. Model description 49
7.2. Notes on implementation 50
7.3. Model parameters description 50
7.4. Model testing 50
7.4.1. Sample power grid 50
7.4.2. Test results 51
7.4.3. Conclusion on test results 53

8. Thermal overload protection 53
9. Non-directional instantaneous/definite time over-current protection 62
10. Non-directional inverse time over-current protection 68
11. Directional over-current protection 74
12. Zero (residual) and negative sequence over-current protection 81
13. Differential protection 82
14. Distance protection 92
15. Power swing detection 96
16. Under-voltage and over-voltage protection 103
17. Under-frequency and over-frequency protection 108
18. Under-frequency load shedding 110
19. General protection model 111
20. Special Protection Schemes (SPS) 114
21. References 116

1. Executive Summary

Modelling usually involves a trade-off between the level of detail in the modelling process on the one hand and the capability of the model in reproducing the physical reality and thus the accuracy of the simulation results on the other. To strike an optimal balance between complexity of the model and the efficiency of the simulation tools, therefore, the mathematical model of the system and its components must remain as simple as possible, yet detailed enough to capture the underlying physical phenomena.

As the number of power electronic converters connected to the power system has increased rapidly over the recent past, it was deemed necessary within the context of PEGASE project to assess the accuracy and robustness of the models commonly used to represent these devices. This was prompted by serious concerns expressed in the professional literature to this effect, especially when one considers their overload capability is typically much more limited than the traditional power system components. Included in this consideration are also complex digital and distributed control systems and system protection schemes that have the capability to affect the operation of a wide area of the interconnected system. Because these devices enable a faster control of the system, an accurate representation of their behaviour on different time scales is necessary for reliable system operation.

Previous reports in this work package dealt with modelling and validation of power system components and systems in general, with particular emphasis on power electronic based electronic interfaces, FACTS devices, and digital controllers. Many of the models that are currently in use have been evaluated and the existing modelling gaps elaborated. Furthermore, the problems associated with lack of access to manufacturer specific models and their control algorithms for many modern equipment (such as wind turbines, HVDC VSC, etc.) due to product protection reasons have been highlighted.

This report, building on the results of the previous reports and outputs of other work packages, introduces the general framework for deriving simplified models (which do not necessarily rely on manufacturer or technology specific data) for wind turbines, voltage source converter based HVDC transmission systems and several protection and automation systems. Additionally, the models have been implemented on different computation platforms and results of sample computations provided.

In the process, particular emphasis was placed on wind turbine modelling, as the level of installed wind power generation continues to increase steadily and its impact on power system dynamic behaviour is becoming increasingly significant. The report describes the necessary steps for deriving a simplified model for Type 3 (doubly-fed induction generator) and Type 4 (full converter interface) wind turbines. The models have been implemented and the error in comparison with a more detailed model quantified.

The report subsequently focuses on simplified modelling of HVDC VSC. As is well known, voltage source based HVDC is able to create any voltage phase angle or amplitude almost instantly. Unlike conventional HVDC converters (that normally have a 5% minimum current) the HVDC SVC converter can operate at very low power or even at zero power. As the active and reactive power are controlled independently, in situations of zero active power the full rating can be utilized to transmit reactive power and to support system voltage, especially during disturbances. The clear superiority of HVDC VSC over the classical HVDC also stems from the fact that the outputs of the VSC are determined solely by the control system and not by the AC network's ability to keep the voltage and frequency constant. As this technology gives total flexibility regarding the location of the converters in the AC system, it is quite probable that the number of HVDC VSC installations will increase significantly.

As with the wind turbine, a simplified HVDC VSC model has been derived and implemented. It is shown that without the need for exact representation and the use of complex mathematical relationships (which in any case would not be of much help without reliable parameters) a fairly acceptable error margin in the simulations can be achieved.

Protection and automation devices are handled in the subsequent section of the report. Due to great variety of protection systems in general and special protection schemes and wide area

protection and automation systems in particular it is impossible to create ready to use system models. As a result a library of standard elements as well as standard protection and automation models have been developed, which can be put together or adjusted by the end user to create any complex system needed.

2. Introduction

The number of power electronic converter based equipment and system connected to the European Transmission Network (ETN) has increased rapidly over the recent past. This work package, as part of the overall activities in the PEGASE projected, is devoted to the analysis of the accuracy and robustness of the commonly used models to represent these systems and devices. Another set of activities involves the development of models for complex digital and distributed control systems and special protection schemes that have the capability to affect the operation of a wide area of the interconnected system. Because these devices enable a faster control of the system, an accurate representation of their behaviour on different time scales is necessary.

The intermediate reports submitted so far deal with aspects of the modelling of components of the ETN for different purposes such as state estimation, security assessment, dispatcher training, etc. In addition to power electronic based modern equipment and systems, the reports included discussions of protection and automation systems. The reports also dealt with the definition of accuracy requirements for mathematical models of power system equipment on the one hand and methodologies for the validation of those models to ascertain whether these requirements are met on the other. In addition, to facilitate the sharing of models of the various plant and apparatus used in different countries and control areas of the ETN a common platform for the exchange and the development and improvement of those models is one of the tasks included in this work package.

This report, building on the results of the previous reports and outputs of other work packages, introduces the general framework for deriving simplified models for wind turbines, voltage source converter based HVDC transmission systems and several protection and automation systems. Additionally, the models have been implemented on different computation platforms and results of sample computations provided.

The first two chapters following this introduction deal with the modelling of wind turbines and the implementation of this model on EUROSTAG. The report summarises the necessary mathematical steps leading to a generic wind turbine model applicable for Type 3 (doubly-fed induction generator) and Type 4 (full converter interface) wind turbines. The models have been implemented and the error in comparison with a more detailed model quantified.

The subsequent two chapters focus on simplified modelling of HVDC VSC. As is well known, the active and reactive power in the HVDC VSC transmission system can be controlled independently from one another, and even in situations of zero active power the system can continue to operate to transmit reactive power in support of system voltage during disturbances. As this technology gives total flexibility regarding its location in the AC system, it is quite probable that the number of HVDC VSC installations will increase significantly in the future. As with the wind turbine, a simplified HVDC VSC has been derived and implemented. It is shown that without the need for exact representation and the use of complex mathematical relationships, a fairly acceptable error margin in the simulations can be achieved.

The last two sections of the report are devoted to the modelling of protection and automation devices. Due to great variety of protection systems in general and special protection schemes and wide area protection and automation systems in particular it was found to be impossible to create ready to use models. As a result a library of standard elements as well as standard protection and automation models have been developed, which can be put together or adjusted by the end user to suit any practical application.

3. Simplified wind farm / wind turbine model

3.1. Introduction

As the level of installed wind power generation grows, its impact on power system dynamic behaviour is likely to become increasingly significant. For performing transient stability studies and quantifying the effect of wind farms on the overall performance indices of the system, suitable models of wind turbines and their aggregate models are required. So far about 25 vendor-specific models have been developed [1]. However, the use of vendor specific models that contain proprietary information usually requires prior manufacturer authorization, and therefore such models are not openly available. One possible solution is the development of publicly-available generic wind turbine models that can be parametrically adjusted to any practical implementation. This would also improve over time the quality of the models and their portability across simulation platforms.

For purposes of developing generic models wind turbines are classified as follows:

Type 1 – conventional directly connected induction generator

Type 2 – wound rotor induction generator with variable rotor resistance

Type 3 – doubly-fed induction generator

Type 4 – full converter interface

In this report the necessary steps for deriving a simplified model for Type 3 and Type 4 wind turbines is described.

3.2. DFIG based WT system configuration

The following figure summarizes the major components of a DFIG based wind turbine system and the necessary control tasks. The block denoted as "operating control" is responsible for coordinating the pitch-angle and converter controls, in addition to performing the necessary supervisory control measures for safe and automatic operation, which will not be considered further.

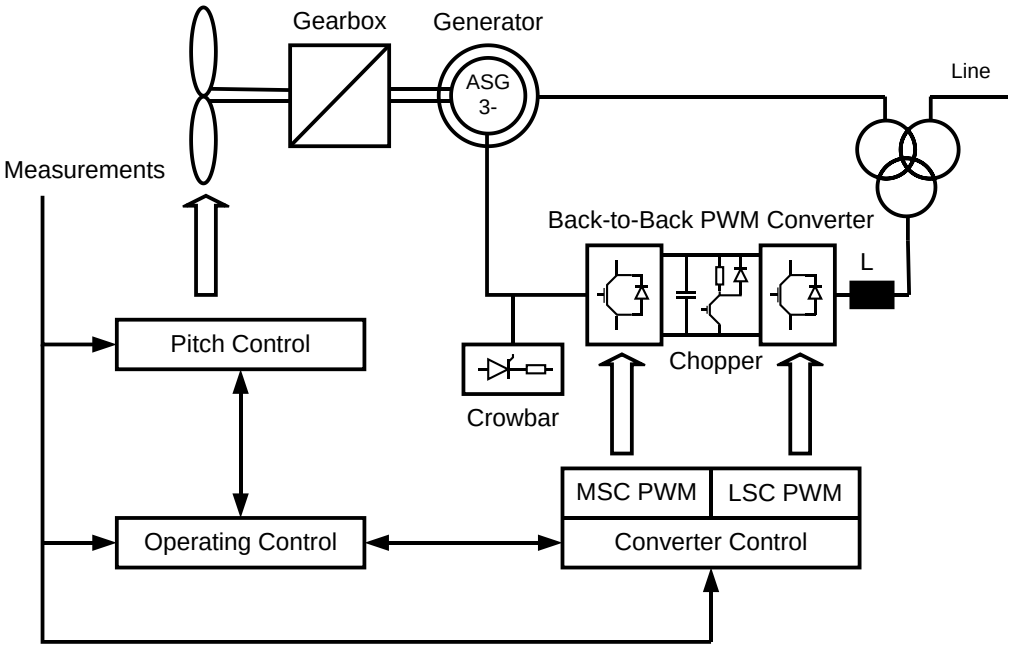

Figure 3-1: DFIG based WT system configuration including the control system

3.3. Detailed (full order) model of the DFIG

The complete set of mathematical relationships that describe the dynamic behaviour of the machine is given below. The superscript $\angle K$ denotes an arbitrary reference frame rotating at the speed ω_K. (If ω_K, for example, is chosen to be ω_0, the voltage, current and flux linkage space-phasors correspond to the ordinary complex phasors).

Voltage equations:

$$\underline{u}_S^{\angle K} = r_S \underline{i}_S^{\angle K} + \frac{d\underline{\Psi}_S^{\angle K}}{dt} + j\omega_K \underline{\Psi}_S^{\angle K} \tag{1}$$

$$\underline{u}_R^{\angle K} = r_R \underline{i}_R^{\angle K} + \frac{d\underline{\Psi}_R^{\angle K}}{dt} + j\left(\omega_K - \omega_R\right)\underline{\Psi}_R^{\angle K} \tag{2}$$

Flux equations:

$$\underline{\psi}_S^{\angle K} = l_S \underline{i}_S^{\angle K} + l_h \underline{i}_R^{\angle K} \tag{3}$$

$$\underline{\psi}_R^{\angle K} = l_h \underline{i}_S^{\angle K} + l_R \underline{i}_R^{\angle K} \tag{4}$$

With

$$l_S = l_h + l_{\sigma S} \tag{5}$$

and

$$l_R = l_h + l_{\sigma R} \tag{6}$$

Equation of motion:

$$\frac{d\omega_R}{dt} = \frac{1}{T_m}\left(m_W + \left(\Psi_{Sd} i_{Sq} - \Psi_{Sq} i_{Sd}\right)\right) \tag{7}$$

Where:

l_h:	Main-field inductance	l:	Inductance
m_W:	Torque at the turbine-shaft	r:	Resistance
T_m:	Inertia constant	u:	Voltage phasor
$\underline{\psi}$:	Complex flux-linkages	ω_K:	Angular velocity of the reference frame
ω_0:	Synchronous angular velocity		

Superscripts/subscripts

S, R	Stator, rotor	d, q	Direct, quadrature axis component
σ	leakage inductance	$\angle K$	In arbitrary reference frame (speed ω_K)

The voltage equations (resolved into real and imaginary parts together with the equation of motion (7) constitute the detailed (full order model) of the doubly-fed induction machine. The terminal voltage $\underline{u}_S^{\angle K}$ forms the link to the rest of the network.

In the following sections, this detailed (EMTP-type) model will be simplified for use in simulations based on phasor approximation in the following steps.

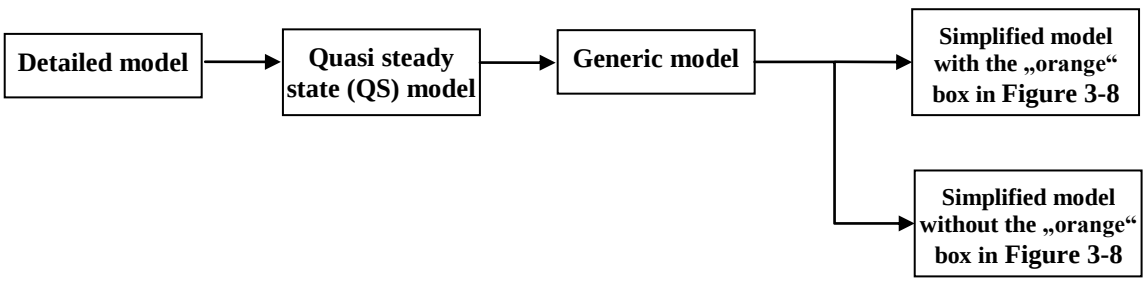
Detailed model
Quasi steady state (QS) model
Generic model
Simplified model with the „orange“ box in Figure 3-8
Simplified model without the „orange“ box in Figure 3-8

3.4. The quasi stationary (QS) model of the DFIG

The quasi-stationary mode underlies the assumption that in the synchronously rotating reference frame the transformer voltage in the stator winding can be neglected against the much greater speed voltage, i.e.

$$\left| j\omega_K \cdot \underline{\Psi}_S^{\angle K} \right| \gg \left| \frac{d\underline{\Psi}_S^{\angle K}}{dt} \right| \tag{8}$$

Using a reference frame rotating at angular speed corresponding to the grid frequency ω_0 the quasi stationary machine model can then be given in Figure 3-2 and also in block diagram form in

(lower part):

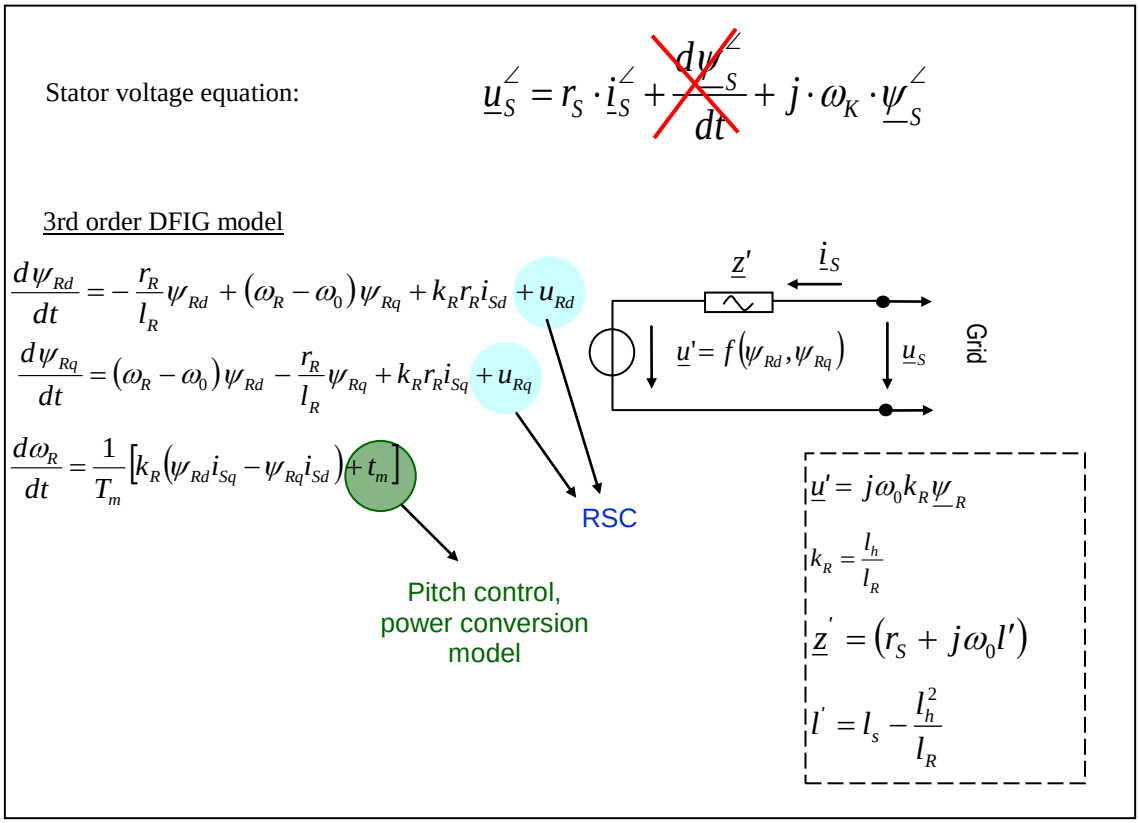
Stator voltage equation:
$\underline{u}_S^{\angle} = r_S \cdot \underline{i}_S^{\angle} + \frac{d\underline{\psi}_S^{\angle}}{dt} + j \cdot \omega_K \cdot \underline{\psi}_S^{\angle}$
3rd order DFIG model
$\frac{d\psi_{Rd}}{dt} = -\frac{r_R}{l_R}\psi_{Rd} + (\omega_R - \omega_0)\psi_{Rq} + k_R r_R i_{Sd} + u_{Rd}$
$\frac{d\psi_{Rq}}{dt} = (\omega_R - \omega_0)\psi_{Rd} - \frac{r_R}{l_R}\psi_{Rq} + k_R r_R i_{Sq} + u_{Rq}$
$\frac{d\omega_R}{dt} = \frac{1}{T_m}\left[k_R(\psi_{Rd} i_{Sq} - \psi_{Rq} i_{Sd}) + t_m\right]$
RSC
Pitch control, power conversion model
$\underline{z}'$
$\underline{i}_S$
$\underline{u}' = f(\psi_{Rd}, \psi_{Rq})$
$\underline{u}_S$
Grid
$\underline{u}' = j\omega_0 k_R \underline{\psi}_R$
$k_R = \frac{l_h}{l_R}$
$\underline{z}' = (r_S + j\omega_0 l')$
$l' = l_s - \frac{l_h^2}{l_R}$

Figure 3-2: The quasi stationary mathematical model of the DFIM.

3.5. Rotor side converter (RSC) model

The RSC control in a DFIG is responsible for the control of active and reactive power. The active power reference is derived from the tracking characteristic of the turbine with the objective of adjusting the generator speed for maximum power generation corresponding to a given wind speed. The outer power control loop of the RSC provides the set values for the inner rotor current loop.

After setting the derivative term in the voltage equation to zero and some re-arrangement, we have:

$$\underline{u}_R = r_R \cdot \underline{i}_R + js \cdot \left(x_h \cdot \frac{\underline{u}_S - jx_h \cdot \underline{i}_R}{jx_S} + x_R \cdot \underline{i}_R \right) \tag{9}$$

The voltage drop over the rotor resistance is used as an auxiliary signal to be controlled by a PI controller. With the feed forward terms accounted for, the PI rotor current controller only needs to put into effect the transition of the rotor current to the set value and compensate for the stator and rotor resistances. The corresponding current control loop is shown in

Figure 3-3 (upper part).

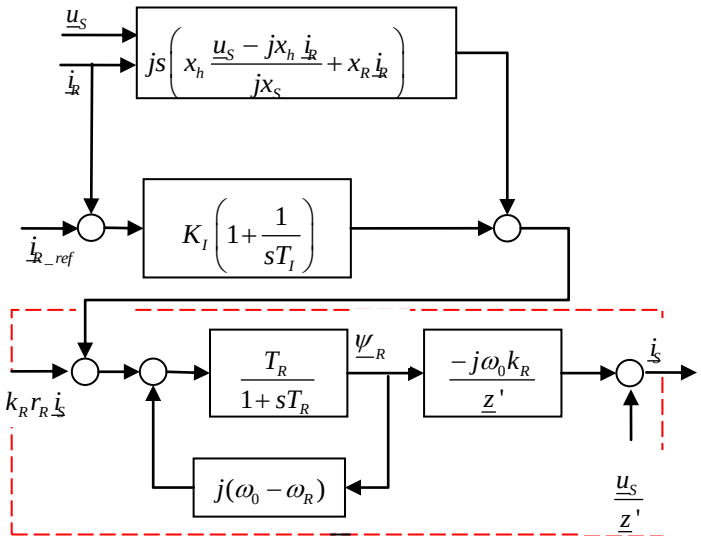

Figure 3-3: Block diagram of quasi stationary model of DFIG including rotor current control.

The line side converter (LSC) primarily controls the DC link voltage, which in simplified simulations can be assumed to remain constant around the rated value and thus not considered. However, the magnitude of the current set value for the LSC is limited in accordance with the converter rating with a priority for the active current. Although the model of the LSC is not incorporated explicitly, the current limitation will be considered in the generic model, as will be shown later.

3.6. Simplified model of DFIG and its control system- the generic model

A comprehensive system study for a large system such as the UCTE involves the simulation of a large interconnected system, spanning national boundaries, operated by different transmission system operators (TSO), and incorporating wind turbines of multiple manufacturers and technologies. While the manufacturer-specific models (together with reliable parameters) enable the simulation of individual units as well as wind farms, the effort required to put together such a large data set makes this approach impractical. For preliminary system studies or estimating grid code compliance, therefore, the current trend is directed at the use of open source generic models with parameters that can be calibrated to conform to any given technology or topology.

The generic model is derived with the quasi stationary model as the basis by making the following simplifications:

- The term rotor flux feedback through (jΔω) is neglected
- The block containing the slip (s) a factor is not considered
- The rotor current in per unit is assumed to be the stator current (magnetization current is neglected)
- The line side converter is not considered explicitly.

Simplification of the quasi stationary model in accordance with the above list results in a generic model shown in. As stated above, the LSC model is not included. Also, the air gap torque of the machine is assumed to remain constant, and thus the equation of motion is not considered.

As a result of the assumptions and simplifications, direct calculation of the model parameters is not possible. One possible way to determine the parameters is comparing the simulation results based on the simplified model with measurement results and employing a heuristic optimization to determine parameters that minimize the error.

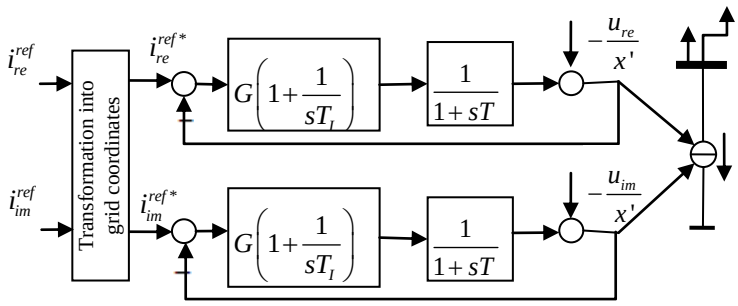

Figure 3-4: Generic model of variable speed machine.

3.7. Model of the full size converter machine and its control system

The machines used in conjunction with the full size converter are separately or permanent magnet excited generator (SG) and asynchronous generator (ASG). But due to the presence the dc link capacitor, the machine including the machine side converter (MSC) do not directly influence the grid behaviour. The generator and the MSC can therefore be modelled as just a controllable current source.

A typical configuration for the full size converter machine is shown in Figure 3-5.

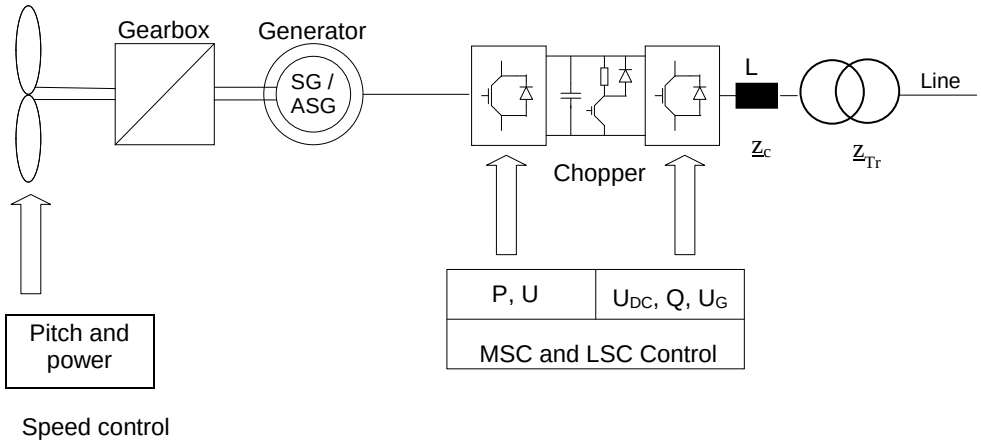

Figure 3-5: Full size converter based WT system configuration including the control system.

Assuming that $\underline{z}_c$: the impedance of the converter choke, $\underline{z}_{Tr}$: the transformer impedance, the current source can be determined as:

$$\underline{i}_{SC} = -\frac{\underline{v}_c}{\underline{z}}, with\ \underline{v}_c = voltage\ injected\ by\ the\ converter\ and\ \underline{z} = \underline{z}_c + \underline{z}_{Tr}$$

The corresponding Norton equivalent circuit is given in Figure 3-6.

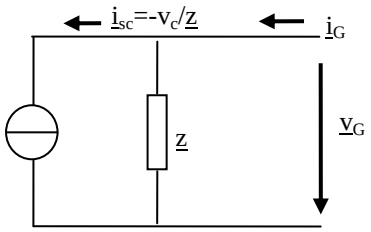

Figure 3-6: The current source (Norton) equivalent of the generator and the MSC.

As stated above, the machine itself can be considered a controlled current source and the converter as a first order delay. The resulting block diagram of the full converter machine including the control system is given in Figure 3-7.

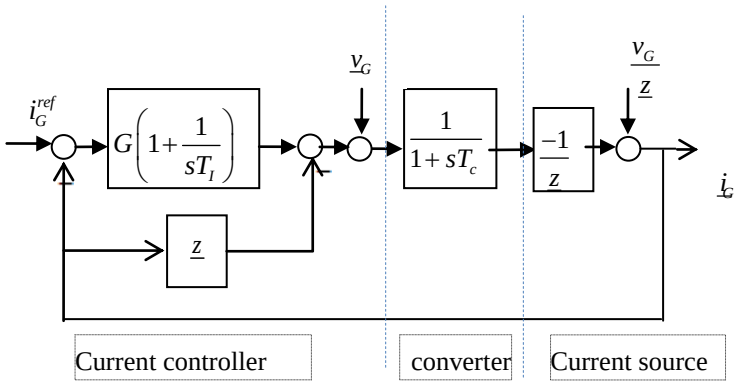

Figure 3-7: Block diagram of current controller, converter and current source.

This representation, after some simplification and re-arrangement, leads to the same generic model developed for the DFIG (Figure 3-4).

3.8. Current limitation equations

The output current limitation may be necessitated by physical, control or dynamic limits. Short term thermal current limitations define physical limits for the maximum current the system can feed into the grid. For the DFIG and full converter machine, these current limits are determined by the converter, which has a much shorter time constant than the generator. Normally active current priority is applicable during steady state operation, while reactive current priority may be used during very low or high voltage conditions. Depending on the type of priority setting applicable, the maximum allowable active or reactive current can be defined as follows:

$$i_{p\_\max} = \sqrt{i_{\max}^2 - i_q^2} \text{ or } i_{q\_\max} = \sqrt{i_{\max}^2 - i_p^2}$$

Where i_{max} = maximum allowable current, i_{p_max} = maximum allowable active current, i_{q_max} = maximum allowable reactive current, i_p = actual active current, i_q = actual reactive current,

Active and reactive current output may further be limited as a function of the voltage. Some of the reasons that may necessitate the reduction of the active current may be reactive current priority during grid faults, active current restriction to fulfil specific grid code requirements, active current restriction as the result of the voltage going outside the standard operating range and grid stability limits, especially at weak connection points. Similarly, reactive current limitation may be needed as a result of active current priority during steady state operation.

Dynamic control limits are needed to allow for an improved representation of active power restoration process following a grid fault. Common reasons that give rise to ramp rate limitation after a grid fault are the need to limit shaft and gear box loads and due to limits on rate of change of the dc link voltage. Control delays in the converter, the settling time needed by the PLL to re-synchronize after deep voltage dips and phase angle jumps following fault clearance may act to slow the active power increase. Manufacturers implement the delay as first order lag or as a linear ramp rate limitation. The model preferably should allow for both implementations.

3.9. Further extensions and the generic model in its final form

Fault Ride-Through (FRT) is now a general requirement on wind turbines. Accordingly, wind turbines must remain connected to the grid during faults by introducing new technologies, if need be. FRT of wind turbines is necessary at least for two reasons:

- To be able to continue with active power in-feed immediately after the fault clearance.
- To provide voltage support during and after the fault period to reduce the size of the voltage dip area within the grid.

The model is extended to account for this operational requirement by incorporating a block which increases or reduces the reactive power in-feed whenever the voltage exits a dead-band of 10 % above or below the rated value.

Figure 3-8 represents the model in its final form. The model as a whole (both with and without the "orange box") constitutes the simplified model. The only difference between the two options (including or excluding the "orange box") is the level of simplification, which one chooses to adopt for a particular simulation.

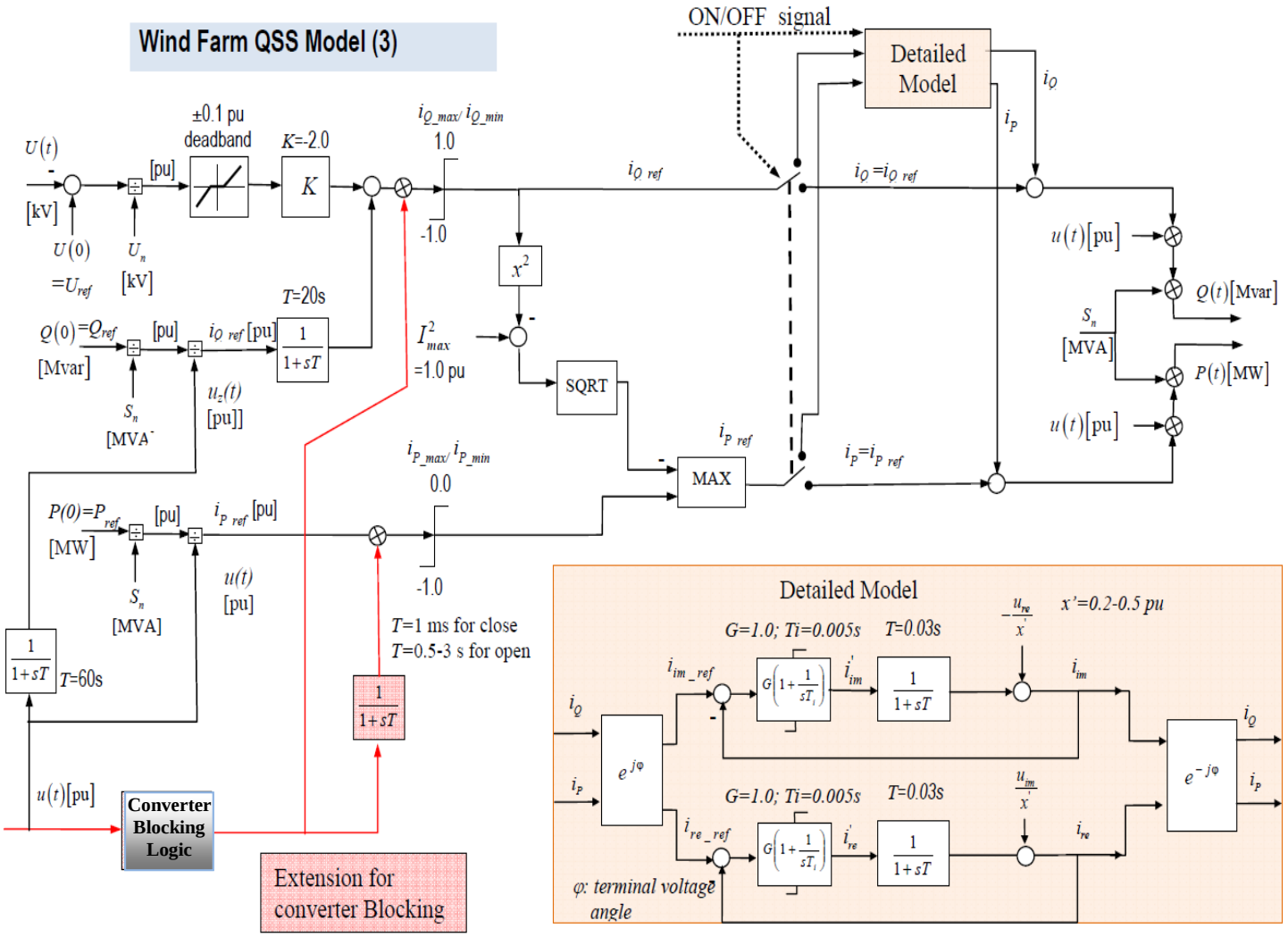

Figure 3-8: Simplified model including converter blocking option.

3.10. Accuracy of the generic model in comparison with the QSS model

The purpose of a generic model is to keep the model of the wind turbine as simple as possible by keeping the accompanying loss in accuracy for preliminary system studies or estimating grid code compliance within acceptable limits. The generic model will inevitably involve simplification compared to the detailed model. The only thing that needs to be ascertained is that these simplifications should not stunt the model to the extent that the underlying physical phenomena are no longer visible.

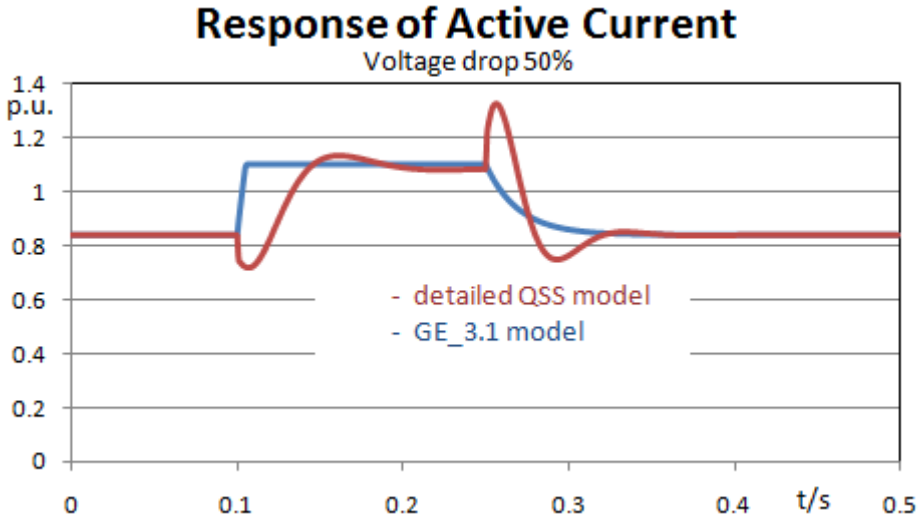

Figure 3-9: Effect of different levels of simplification on the simulation result.

Although a general statement with regard to loss of accuracy as a result of the use of the generic model is not possible, Figure 3-9 exemplifies the nature of the error one commits in using the generic model. The blue curve describes the behavior of active current following a grid fault leading to a voltage dip to 50 % (of the pre-fault value), when the switch (in Figure 3-8) is "ON". The red curve represents the same situation, when the generic model is incorporated, i.e. the switch in "OFF" position.

3.11. Sign convention and initialization procedure

3.11.1. Sign convention

- Generated active power is negative (or alternatively consumed active power is positive)
- Inductive reactive power (under-excited generation mode) is positive (or capacitive reactive power (overexcited generation mode) is negative
- U(t) [kV] and u(t) [pu] represents the magnitude of the terminal voltage

3.11.2. Initialization

<u>After incorporating the "Detailed Model":</u>

Assume "Detailed Model" is switched on at t_{ON}, then initialize as follows:

- set first order delay block and integral outputs = $i_m(t_{on}) + \frac{u_{re}(t_{on})}{x_r}$ (upper branch)
- set first order delay block and integral outputs = $i_{re}(t_{on}) - \frac{u_{im}(t_{on})}{x_r}$ (lower branch)

After initialization, simulation is continued by incorporating the "Detailed Model".

<u>After switching-off the "Detailed Model":</u>

Assume "Detailed Model" is switched off at t_{OFF}, then proceed with the initialization as follows:

- Set all block outputs and state variables zero

4. Implementation of the wind farm model

4.1. Modifications made in EUROSTAG model compared to base model description

Base model was slightly modified to make it more coherent to EUROSTAG computational environment. The changes include the following:

1. Model inputs are supplied directly with voltage, active and reactive power in p.u.
2. Model outputs provide active and reactive current instead of power. This modification was made to improve model performance in EUROSTAG.
3. Simple lag with time constant T=0.001 s is applied to model outputs to avoid algebraic loops in EUROSTAG.

4.2. Implementation of specific parts of the model

4.2.1. Simple lag with variable time constant

This block used in converter blocking model was represented as simple lag with feedback loop with variable gain K (Figure 4-1).

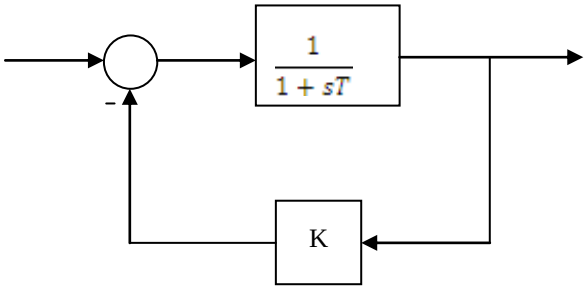

Figure 4-1: Simple lag with variable time constant

4.2.2. Current conversion

Current conversion from terminal voltage reference frame (I_P, I_Q) to synchronous reference frame (I_{re}, I_{im}) is performed according to the formulas below

$$I_{re} = I_P \cos\varphi + I_Q \sin\varphi$$

$$I_{im} = I_P \sin\varphi - I_Q \cos\varphi$$

where φ - terminal voltage angle

4.2.3. PI block with limitation

The PI block (shown in the detailed model as the figure below) is modeled using the scheme given in Figure 4-2).

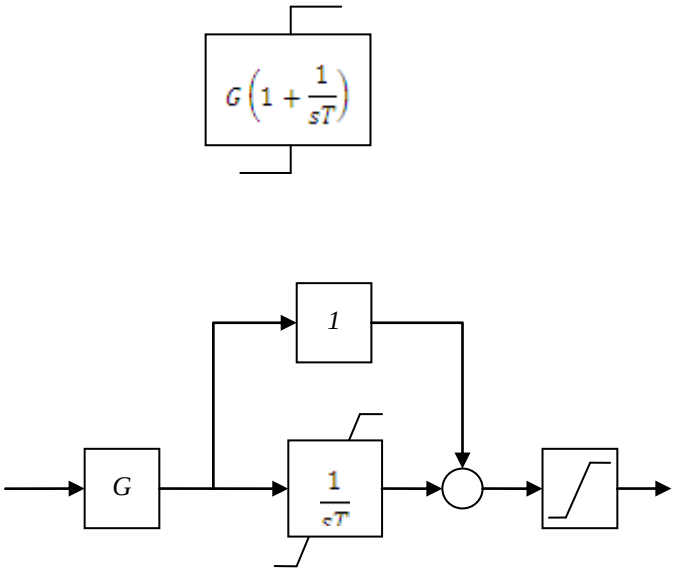

Figure 4-2: PI block with limits

4.3. Model parameters description

Description of model parameters adjustable by user and their default values are given in the table below.

Table 1: Acronyms and default values of model parameters

Name	Default value	Unit	Description
Active and reactive power control			
DBMAX	0.1	p.u.	Deadband limits in voltage channel
DBMIN	-0.1	p.u.	
KU	-2.	p.u.	Gain in voltage channel
IMAX	1.	p.u.	Converter current limit
IPMAX	0.	p.u.	Limits applied to active current value
IPMIN	-1.	p.u.	
IQMAX	1.	p.u.	Limits applied to reactive current value
IQMIN	-1.	p.u.	
TQ1	60.	s	Time constants in reactive power channel
TQ2	20.	s	
Model of converter blocking			
UBLCK	.15	p.u.	Voltage level at which converter is blocked
TC	0.001	s	Time constant for close (shut down) of converter
TO	3.	s	Time constant for open (recover) of converter
Detailed model			
IIMMAX	5.	p.u.	Limits applied to PI block
IIMMIN	-5.	p.u.	
IREMAX	5.	p.u.	
IREMIN	-5.	p.u.	
KG	1.	p.u.	Gain
TI	0.005	s	Lag parameters
TI2	0.03	s	
X	0.5	p.u.	Equivalent reactance

4.4. Model testing

4.4.1. Sample power grid

The simple scheme shown Figure 4-3 has been used for testing purposes.

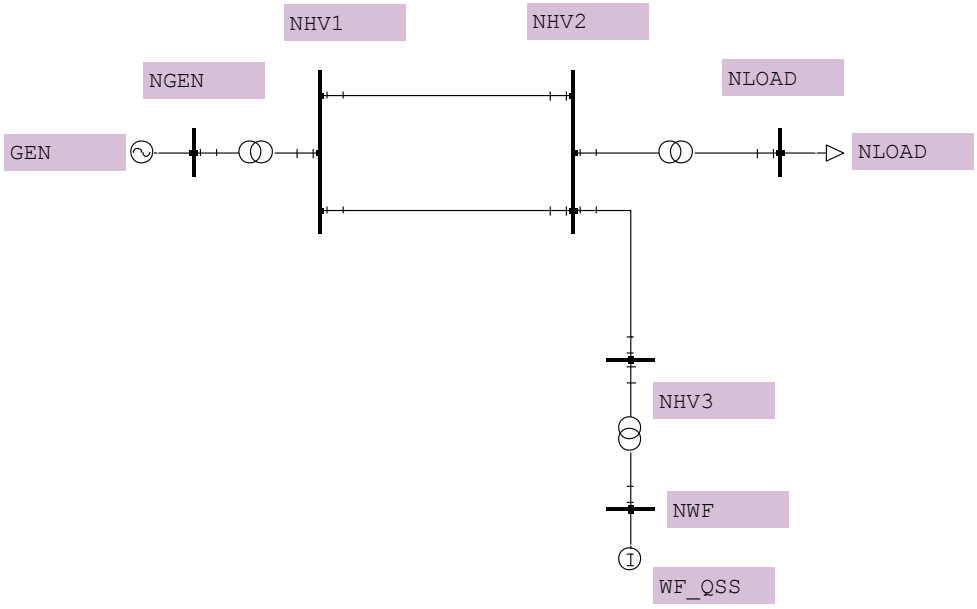

Figure 4-3: Test network

Synchronous generator is connected to NGEN node. It is equipped with turbine governor and AVR. NGEN is considered as a slack bus in steady state computation.

Load is connected to NLOAD node. It is modeled with constant active and reactive power.

QSS Wind Farm model is used to control the injector, which is connected to NWF node. NHW node is modeled as PV-node in steady state computation.

Network data are shown in the tables below.

Table 2: Network power flow data

Node name	Base voltage	Generated power		Load power	
		Active	Reactive	Active	Reactive
	kV	p.u.	p.u.	p.u.	p.u.
NGEN	24.000	1.969	0.374	0.000	0.000
NHV1	380.000	0.000	0.000	0.000	0.000
NHV2	380.000	0.000	0.000	0.000	0.000
NLOAD	150.000	0.000	0.000	3.459	1.715
NHV3	380.000	0.000	0.000	0.000	0.000
NWF	24.000	1.500	-0.852	0.000	0.000

Table 3: Test network branch data

Sending and receiving node names	Base power	Resistance	Reactance	Semi shunt conductance	Semi shunt susceptance	Ratio
	MVA	p.u.	p.u.	p.u.	p.u.	p.u.
NHV1-NHV2-1	1000	0.002	0.023	0.000	0.279	
NHV1-NHV2-2	1000	0.002	0.023	0.000	0.279	
NHV2-NHV3-0	1000	0.001	0.011	0.000	0.134	
NGEN-NHV1	1300	0.00018	0.007690	0	0	1.05
NHV2-NLOAD	1000	0.00021	0.017990	0	0	1.0
NHV3-NWF	300	0.00018	0.007690	0	0	1.05

Results of steady state computation are shown in the tables below.

Table 4: Power flow result - bus data

Node name	Base voltage	Voltage magnitude	Voltage angle
	kV	p.u.	rad
NGEN	24.000	1.021	0.067
NHV1	380.000	1.077	0.080
NHV2	380.000	1.073	0.099
NLOAD	150.000	1.043	0.154
NHV3	380.000	1.084	0.085
NWF	24.000	1.036	0.076

Table 5: Line power flow

Sending and receiving node names	Power flow	
	Active	Reactive
	MW	MVAR
NHV1-NHV2-1	75.4	-35.5
NHV1-NHV2-2	75.4	-35.5
NHV2-NHV1-1	-75.3	-28.3
NHV2-NHV1-2	-75.3	-28.3
NHV2-NHV3-0	-149.9	-111.7
NHV3-NHV2-0	150.0	83.2
NGEN-NHV1	150.8	-69.1
NHV2-NLOAD	300.2	168.2
NHV3-NWF	-150.0	-83.2
NHV1-NGEN	-150.7	71.0
NLOAD-NHV2	-300.0	-150.0
NWF-NHV3	150.0	85.1

4.5. Test results

Model was tested in several test cases to verify it operates correctly.

4.5.1. Direct (metallic) short-circuit

This test case is intended to show the model behavior during fast transient (both in detailed and simplified versions) as well as to verify that converter blocking is implemented correctly.

Metallic short circuit on NHV3 bus is modeled at time t=60 s.

Wind farm power output, its terminal voltage magnitude and angle for simplified model simulation are shown at the figure below.

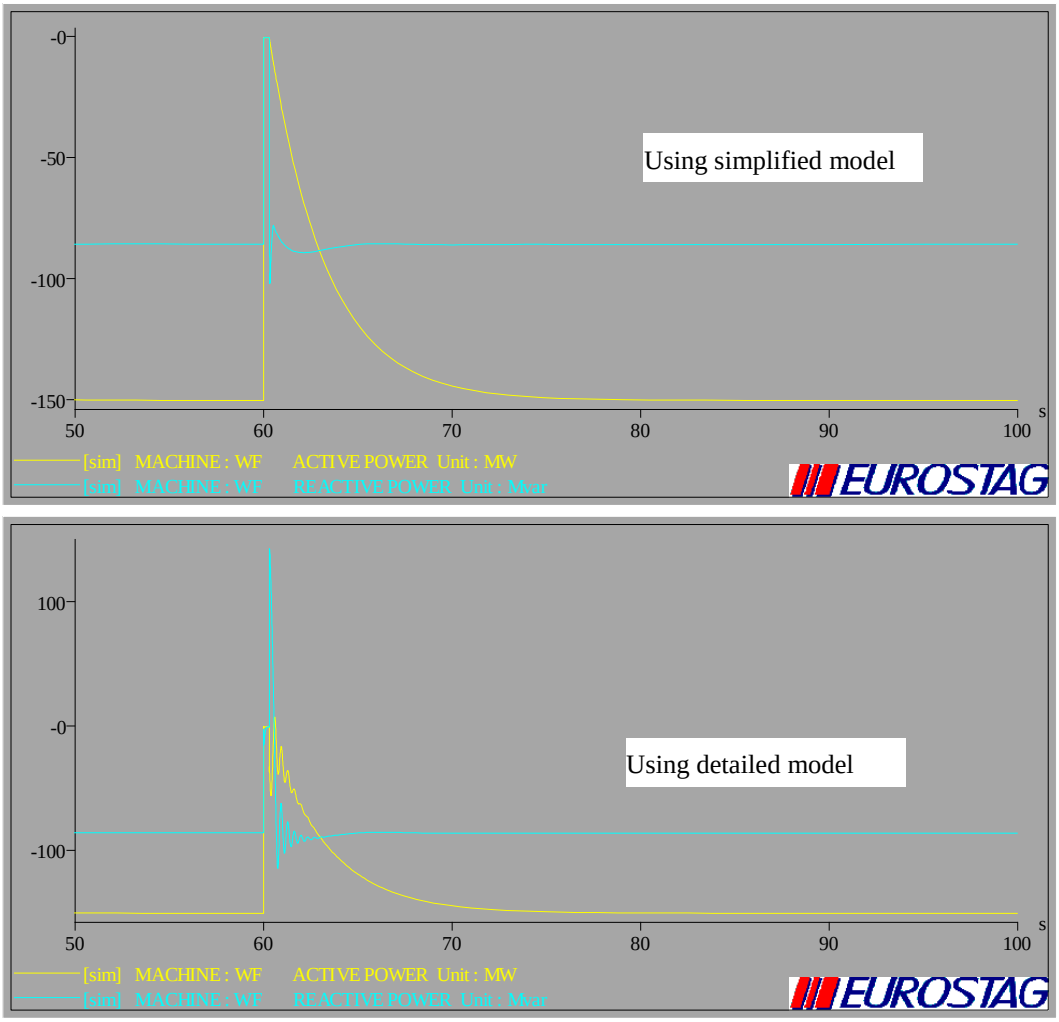

Figure 4-4: Active/reactive power following a fault

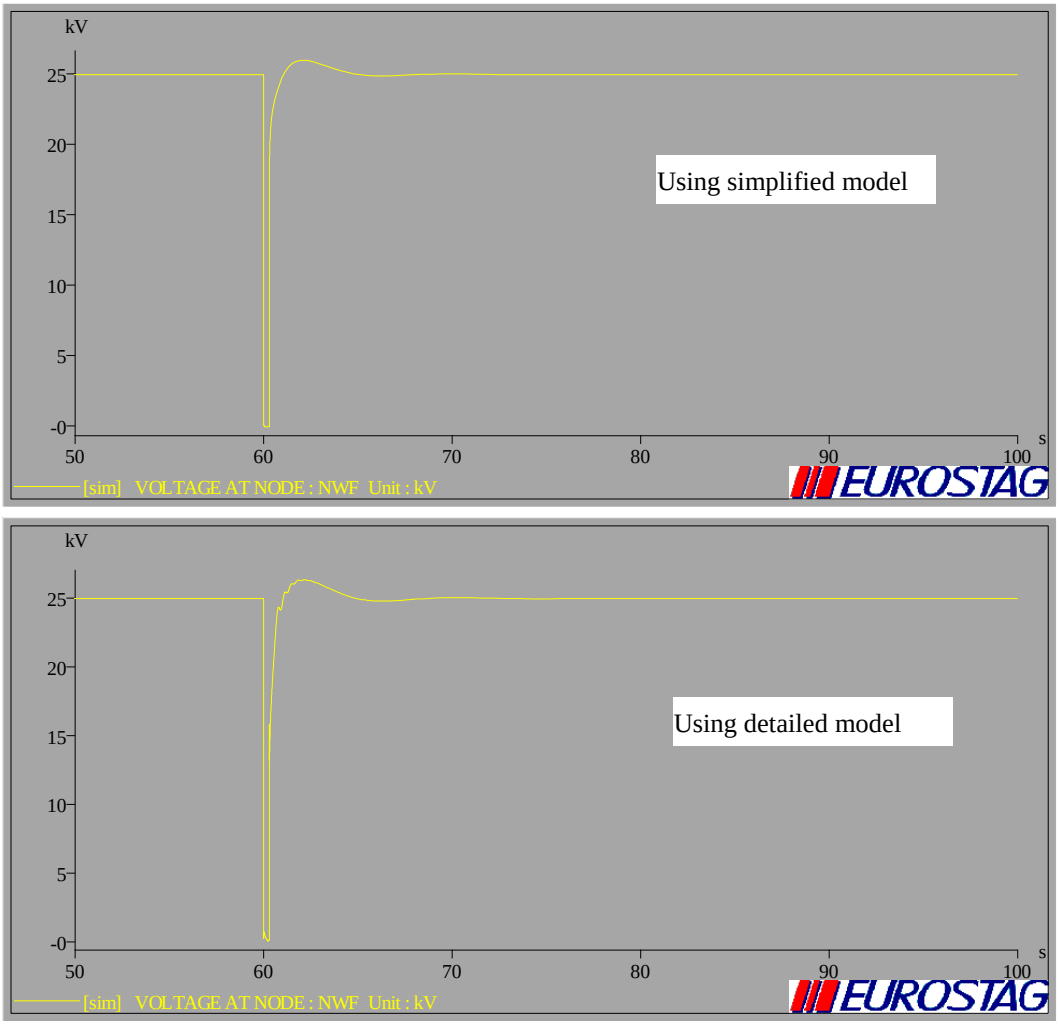

Figure 4-5: Bus voltage after a fault

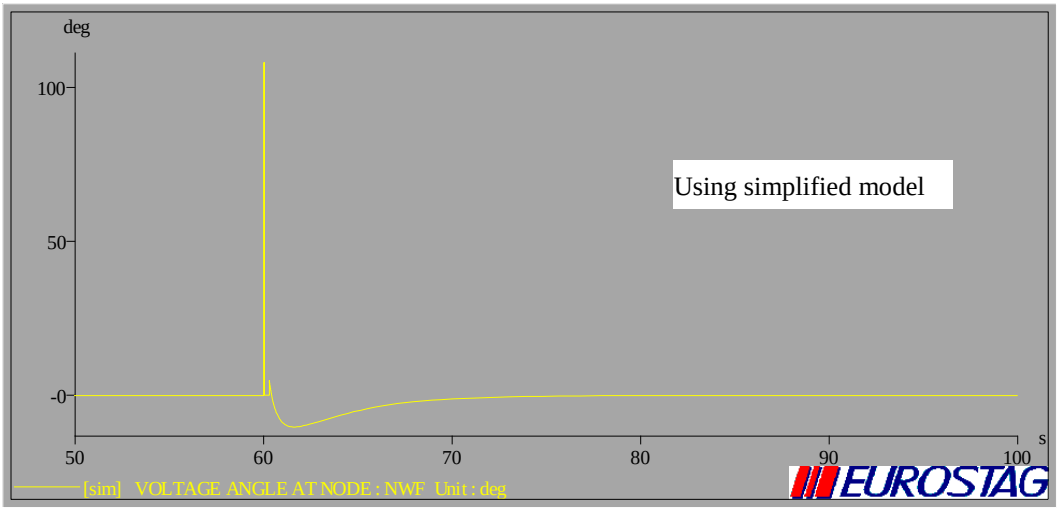

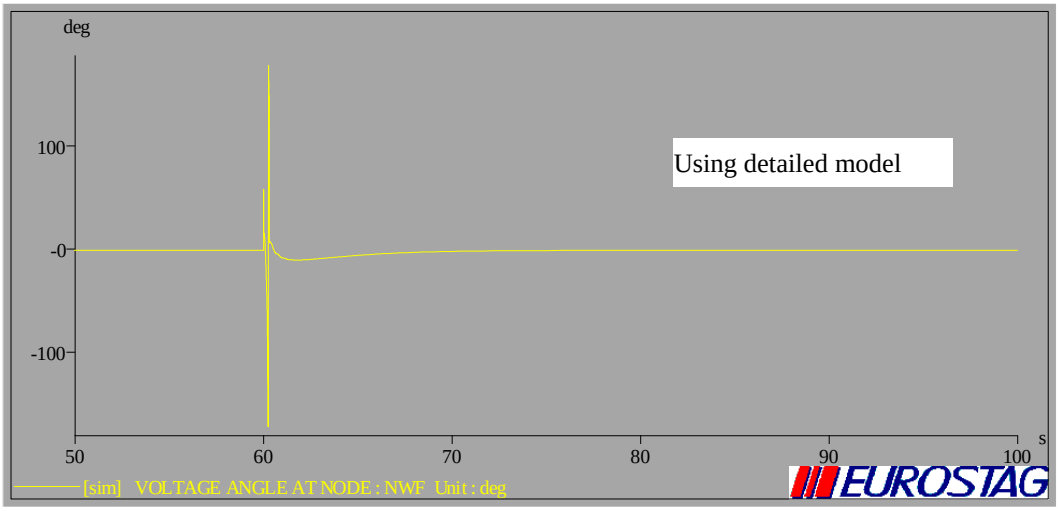

Figure 4-6: Voltage angle after a fault

This test case shows proper model operation in case of voltage drop. Both active and reactive power dropped when fault begins due to converter blocking. After short circuit is eliminated, fast recovery of reactive power output and slow recovery of active power can be seen.

The same curves for detailed model simulation are shown below.

4.5.2. Voltage set-point modification

The purpose of this test case is to verify correct modeling of current limiter.

Set point modification was modeled at time t=10 s. As a result of this action reactive power output of the WF shall increase.

As current limitation is modeled the same way in detailed and simplified model, only simplified model was tested with this test case.

Active and reactive power current output of the WF is shown at the figure below.

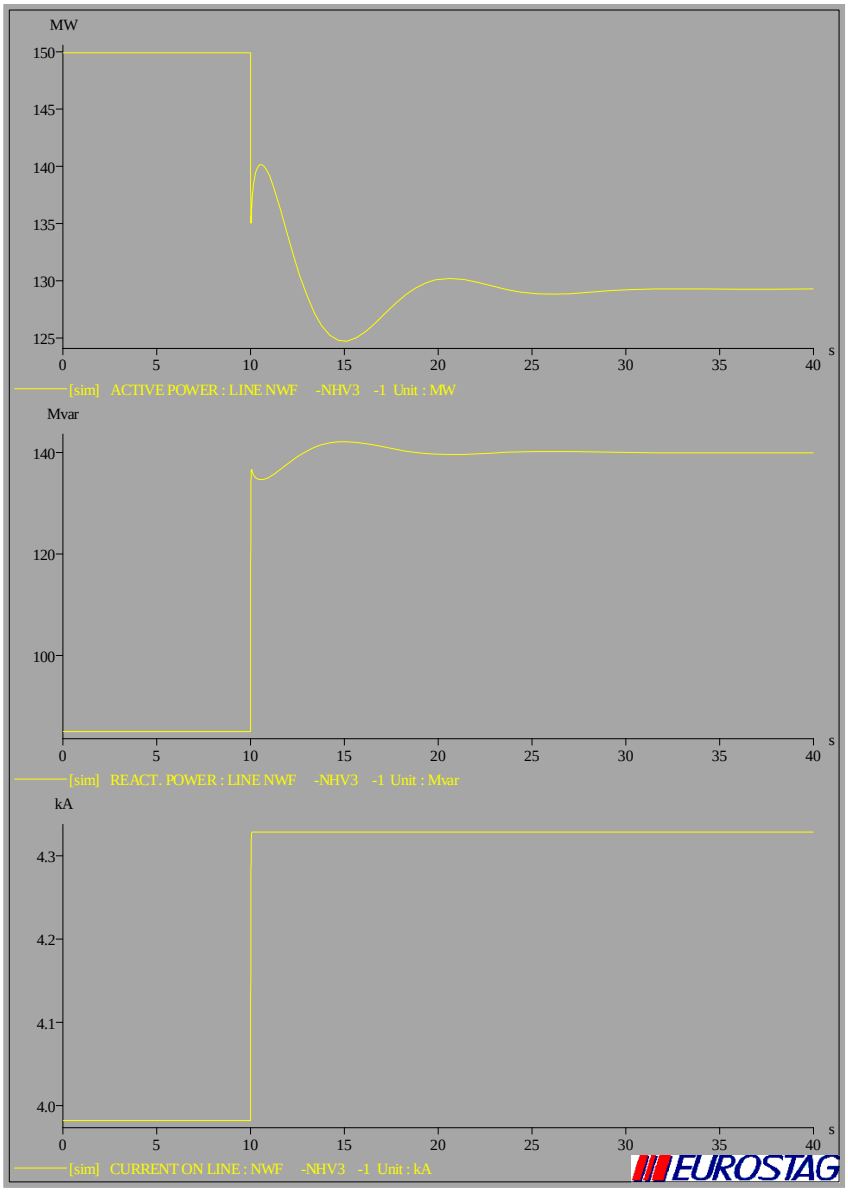

Figure 4-7: Change in voltage set-point

As seen from the figure reactive power output rises after set-point modification. Consequently total current output rises and hits the current limit. Then active power output is decreased to keep the current in the range.

This shows correct operation of current limitation block in the model.

4.6. EUROSTAG limitations

The following EUROSTAG limitations were discovered during WF model implementation (all this limitations prevents simple implementation of switching from detailed to simplified model of WF at runtime):

1. EUROSTAG has no features for disabling or enabling parts of the model at runtime. Therefore proposed switching from detailed to simplified model of WF at runtime may be implemented only using some workaround.
2. EUROSTAG has no ability to change memory block (such as integrator, simple lag etc.) state at runtime.
3. There is no limited integrator block with variable limits.

Some of these limitations may be overridden by use of special techniques. Below we describe some of them.

4.6.1. Reset feature

Integrator and simple lag block with reset feature may be modelled with the following schemes

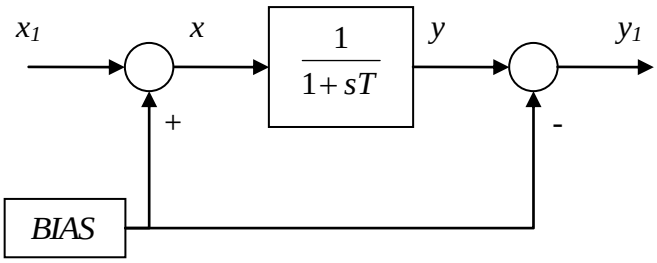

Figure 4-8: Modeling of simple lag block with reset feature

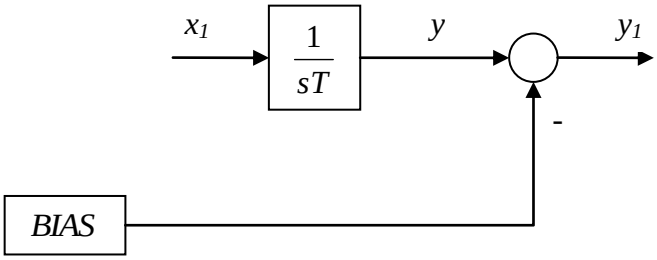

Figure 4-9: Modeling of integrator block with reset feature

To reset block at specific moment t_s one must change at that moment the value BIAS to $y(t_s)$.
The problem with this approach is that SINGLE SETPOINT MODIFICATION EVENT from EUROSTAG .seq file has no access to model outputs, i.e. it can't read the value of $y(t_s)$. The solution is to use USER AUTOMATON because SINGLE SETPOINT MODIFICATION EVENT from USER AUTOMATON EVENTS collection can modify setpoint with value read from model.
The approach is illustrated at the figure below.

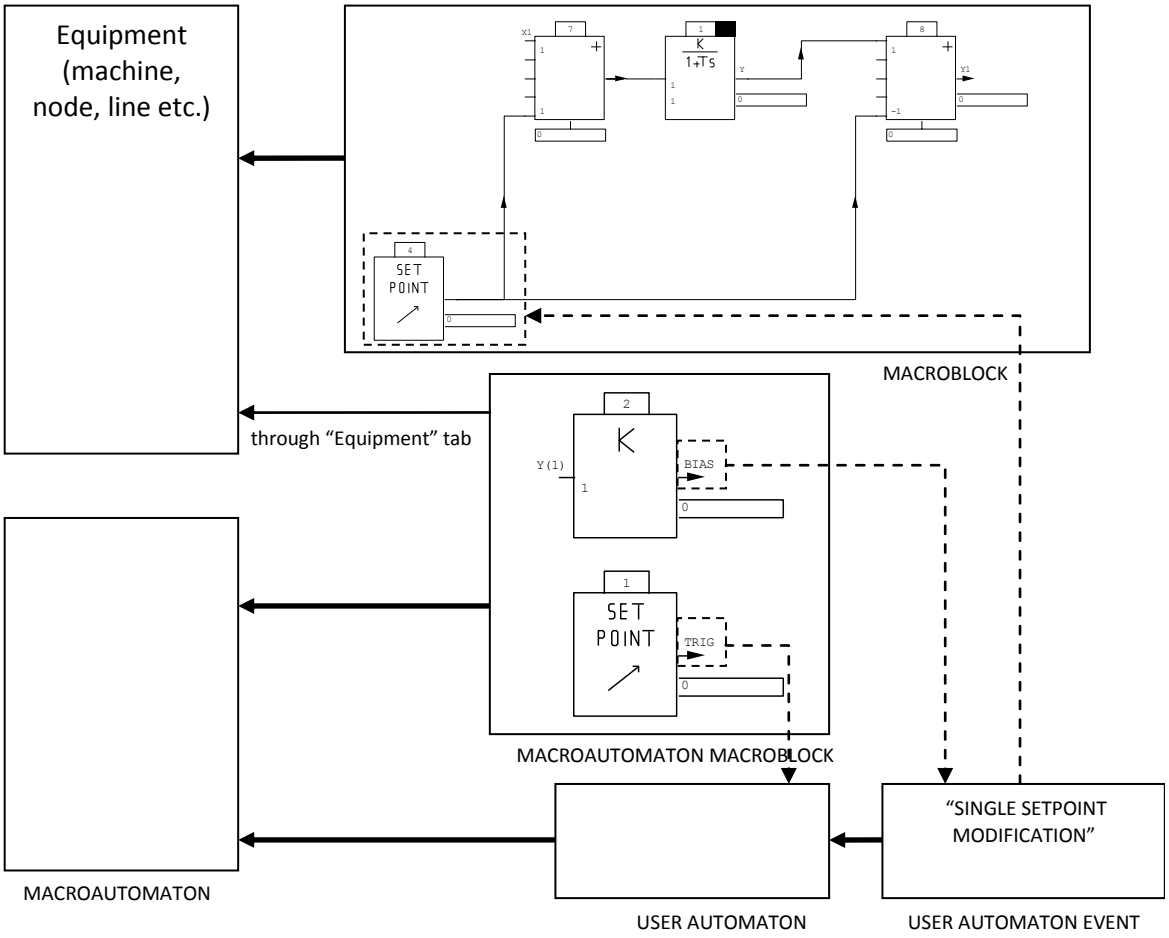

Figure 4-10: Implementation of simple lag block with reset in EUROSTAG

The scheme works as follows: the reset of simple lag block is initiated by modification of setpoint block in MACROAUTOMATON MACROBLOCK that may be done by event in .seq file. This must trigger USER AUTOMATON which in its turn initiates setpoint modification in target MACROBLOCK.

4.6.2. Limited integrator block with variable limits

Limited integrator block may be modeled by manually controlling limit crossing. An example of implementation of this approach is shown at the figure below.

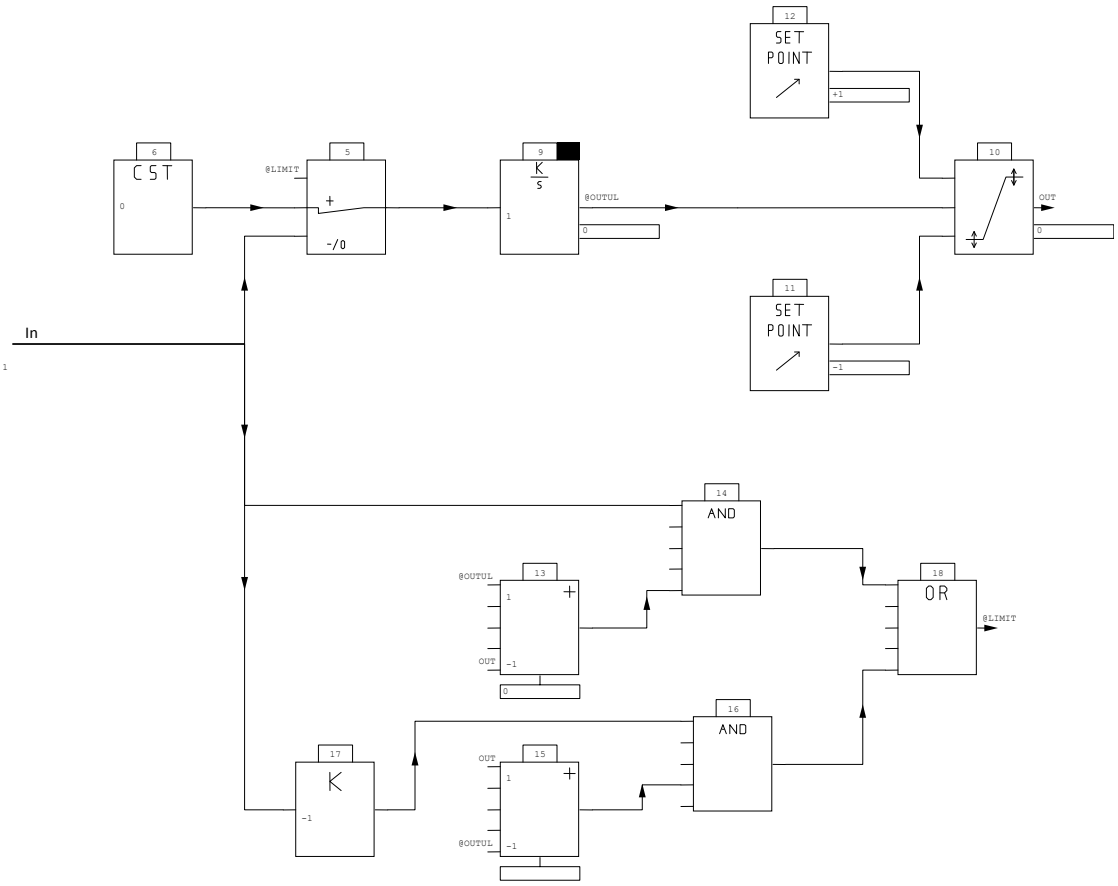

Figure 4-11: Implementation of limited integrator block with variable limits in EUROSTAG

5. High Voltage Direct Current (HVDC) Transmission System

5.1. Introduction

Modern HVDC transmission systems use voltage source converters (VSC) based on self-commutated switching devices. The superiority of HVDC VSC over the classical HVDC stems from the fact that the outputs of the VSC are determined solely by the control system and not by the AC network's ability to keep the voltage and frequency constant. This gives total flexibility regarding the location of the converters in the AC system since the requirement on the AC network in terms of short-circuit capacity (SCR) is no longer a limiting factor. In other words, HVDC SVC can feed power even into a passive network. Classic HVDC terminals can provide limited control of reactive power by means of switching of filters and shunt banks and to some degree through firing angle control.

But the HVDC VSC control makes it possible to create any voltage phase angle or amplitude, which can be accomplished almost instantly. Unlike conventional HVDC converters that normally have a 5% minimum current, the HVDC SVC converter can operate at very low power or even at zero power. As the active and reactive power are controlled independently, at zero active power the full rating can be utilized to transmit reactive power. If and when the need arises the same converter can even be used as an SVC.

5.2. HVDC VSC basics

The converters use a set of six valves, two for each phase, which are equipped with high-power Insulated Gate Bipolar Transistors (IGBT). The valves are controlled by a control system using pulse-width modulation (PWM). Since IGBTs can be switched on or off as desired, output voltages and currents on the AC side can be controlled precisely, and the control system thus enables the control of voltage, frequency, and active and reactive power flow according to the needs of the network. Additionally, HVDC VSC has the capability to rapidly control active and reactive power independent of one another.

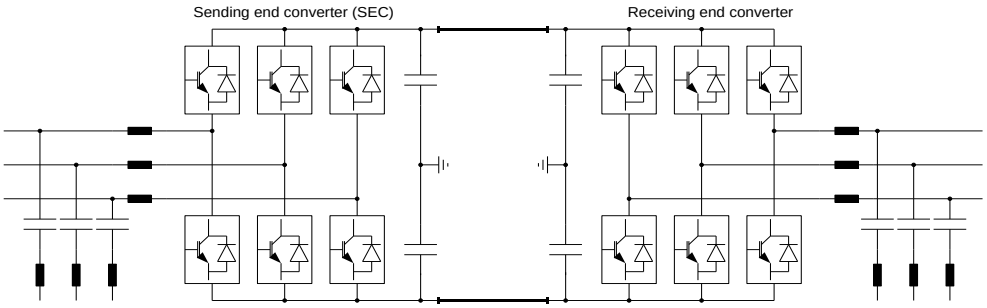

Figure 5-1: Circuit diagram of a VSC based HVDC (HVDC light)

Active power transfer can be quickly reversed without any change of the control mode, and without any filter switching or converter blocking. The power reversal is obtained by changing the direction of the DC current without the need for changing the DC voltage polarity as opposed to conventional HVDC.

HVDC VSC enables a decoupled control of active and reactive power and allows the connection of weak or even passive networks. Additionally, the high switching frequencies of approximately 1–2 kHz reduce the filter size and the IGBT valves themselves have a smaller size compared to thyristor valves in classical HVDC systems. This leads to a smaller footprint of the converter stations and thus makes it more suitable for applications, where space requirement is a critical issue.

5.3. Control of HVDC VSC

5.3.1. Overview

HVDC VSC consists of two voltage source converters, one operating as a rectifier and the other as an inverter. Both ends of the HVDC line are connected to an AC circuit, and the HVDC line linking the two transmits the power from the rectifier to the inverter station.

The control functions of HVDC VSC converter include AC and DC voltage control, active and reactive power control, and the inner current control together with current output limitation and internal converter voltage limitations. For a two-terminal HVDC VSC system, one of the converters controls the DC voltage and the other the active power. Additionally, each of the converters can optionally be set in either AC voltage control or reactive power control mode. The basic control functions are summarized in Figure 5-2.

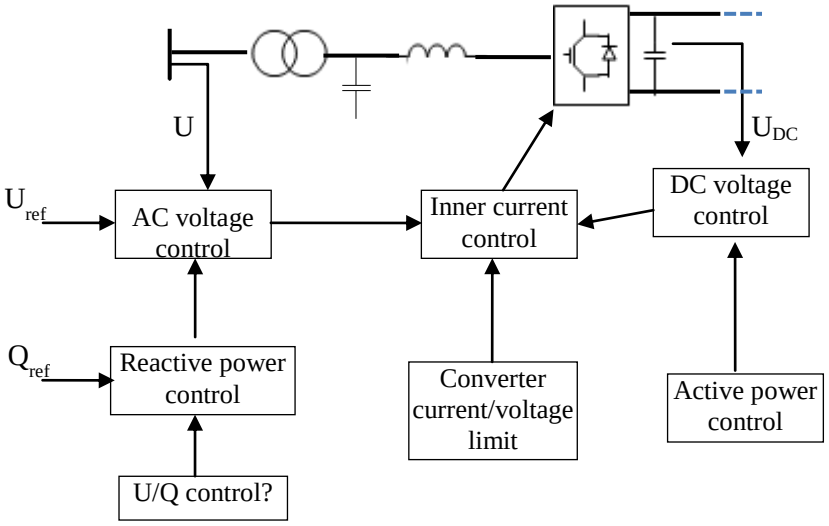

Figure 5-2: Overview of HVDC VSC control functions

The active power control function aims to fulfil system-wide objectives such as power flow control and congestion management. As a result, during normal operation the power and voltage settings are determined by the system operator [6]. The lower level control functions are attuned to these prescriptions and the reference values are determined accordingly. The current control operates in a coordinate system that is phase synchronous with the fundamental frequency in the network, and provides a symmetrical three-phase current to the converter regardless of whether the AC network voltage is symmetrical or not. The use of PWM makes it possible that fast control of the active and reactive power is achieved. This capability is beneficial when support of the AC network, particularly during disturbances, is needed, since the control can be optimized to obtain a fast and stable performance during AC system fault recovery. The DC voltage control provides DC voltage control using the current as a control variable. The AC voltage-dependent current limiter acts to keep the AC bus voltage within its upper and lower limits.

5.3.2. Simplified HVDC VSC Dynamic Model

The two AC networks, linked to one another by the HVDC line, can be represented by their Thévenin or Norton equivalent circuits, with the control actions adjusting the voltage or the current source, as shown in Figure 5-3 and Figure 5-4.

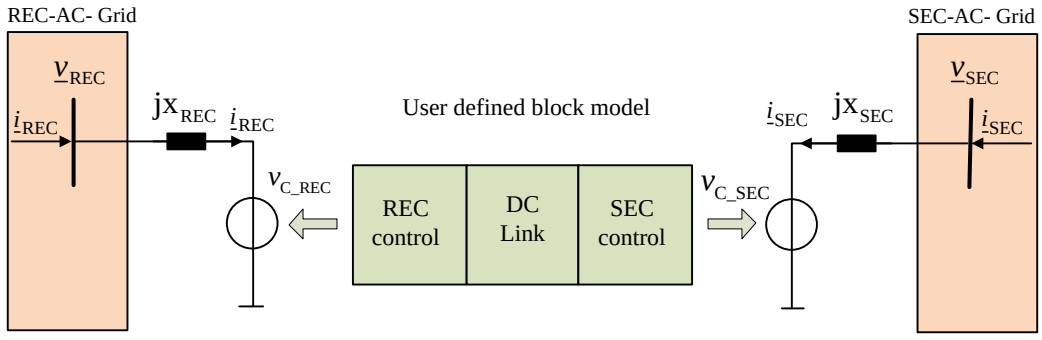

Figure 5-3: The Thevenin equivalent circuit of HVDC VSC

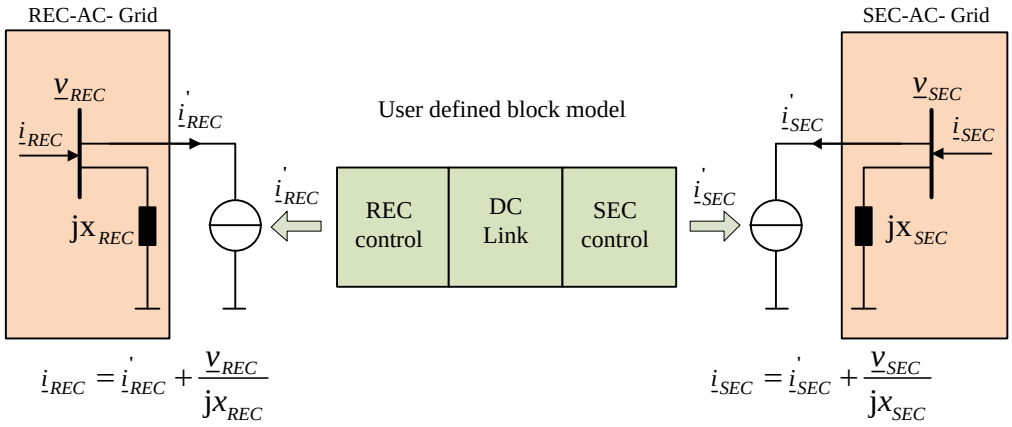

Figure 5-4: The Norton equivalent circuit of HVDC VSC

The acronyms used in Figure 5-4 have the following meaning:

REC: Receiving end converter; SEC: Sending end converter

DC: Direct current; AC: Alternating current

The impedances X_{REC} and X_{SEC} represent the equivalent Thevenin impedances (with resistances neglected) of both external AC circuits.

a. Receiving-end converter (REC) model

The function of REC is to transfer the active power fed by the SEC into the HVDC line to the AC grid by maintaining the DC voltage level. Active current is used to regulate the DC link voltage. The reactive current control loop can be used to control the REC terminal voltage on the AC side or to guarantee a constant power factor at the AC grid terminal, and also to support the grid voltage during faults.

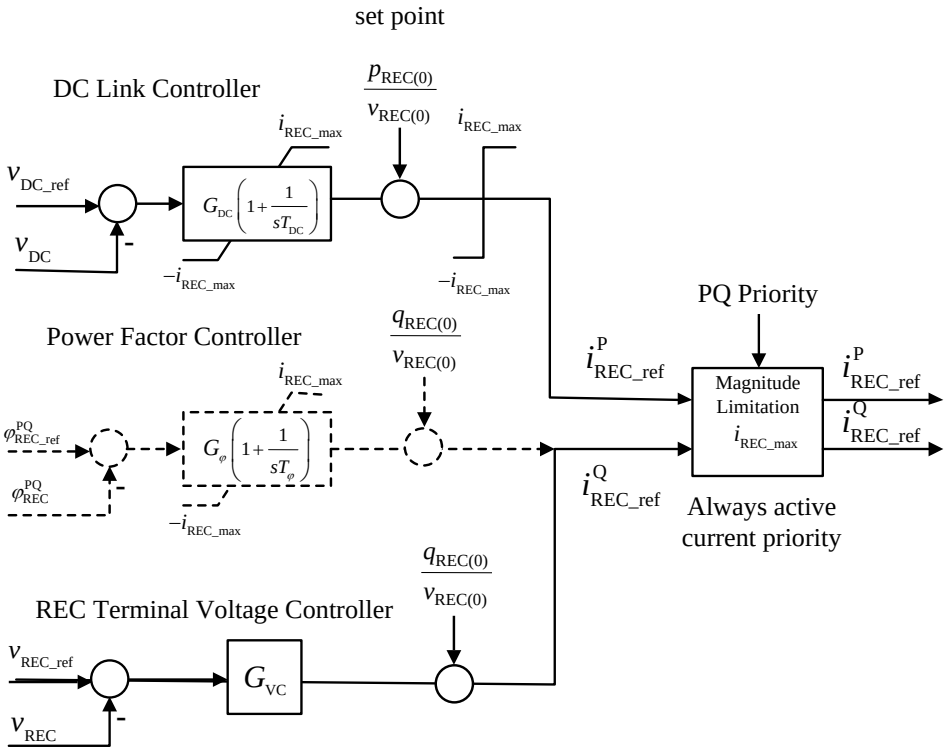

Figure 5-5: REC control

The REC control structure is shown in Figure 5-5, which implements the following three core functions:

– The PI-controller maintaining the DC voltage with the active converter current as a control variable.

– The current magnitude limitation block with active current priority during normal operation

– The AC voltage control block (or alternatively the power factor control (dashed lines)).

The voltage controller is a fast-acting proportional controller, which can include a dead band so that the control action is only then activated when the voltage error is larger than a pre-specified value, for example 0.1 p.u. This block is also responsible for grid voltage support during faults. In steady-state operation the DC voltage control and by implication the d-axis component of the REC current has priority. In case of grid fault, however, the priority is switched to reactive current to provide fast voltage support.

b. Calculation of active/reactive current reference and inner current control loop

The converter control is based on a vector control approach with its rotating reference frame aligned with the grid voltage reference or with the terminal voltage chosen as the reference. As a result, active power can be controlled through d- axis and reactive power through q- axis component of the converter current, both independently of one another.

Alternative 1: Grid synchronous coordinates

If the controller operates in the grid reference frame then the current phase position should be modified as shown in Figure 5-6 so that the real and imaginary parts of the current correspond to the active and reactive parts of the current, respectively. As a result of this modification controller variables change with grid frequency.

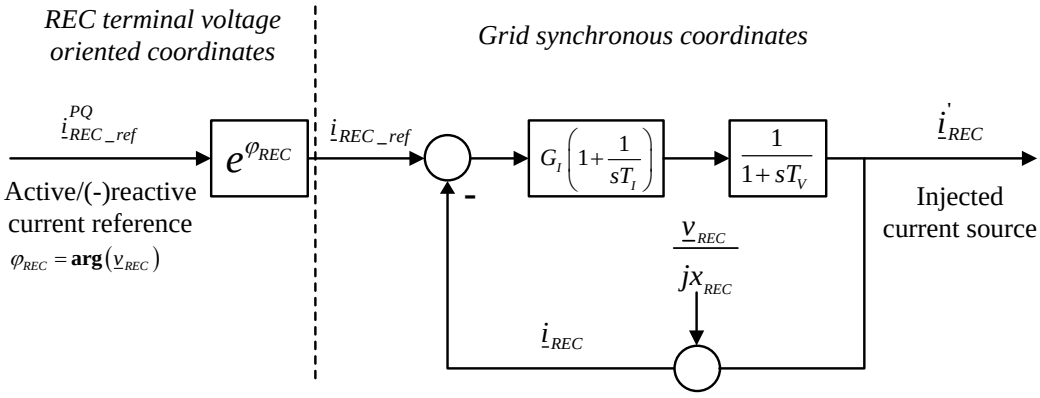

Figure 5-6: Current controller in synchronous reference frame

Alternative 2: Terminal voltage oriented coordinates

If the controller operates in RSC terminal voltage oriented coordinates the controller variables remain constant in steady state conditions in spite of changes in grid frequency. In this case, the RSC terminal voltage is the reference, i.e. it lies along the real axis, and the necessary variations in terms of input and output variables is shown in **Error! Reference source not found.**.

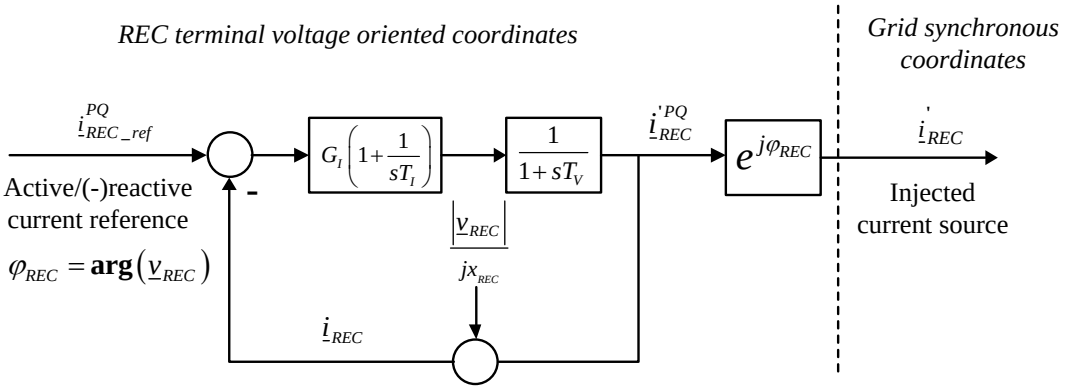

Figure 5-7: Current controller in terminal voltage reference frame

The current control structure makes use of standard PI controllers, as shown in Figure 5-6 and Figure 5-7. The output in both cases is the current source shown in Figure 5-4.

5.3.3. DC Link Model

The model of the DC link capacitance and the DC chopper are shown in Figure 5-8. The model also accounts for the power dissipated by the resistance of the chopper if and when it is activated, and a block indicating that the corresponding block becomes active only when the DC voltage increases beyond a pre-specified threshold.

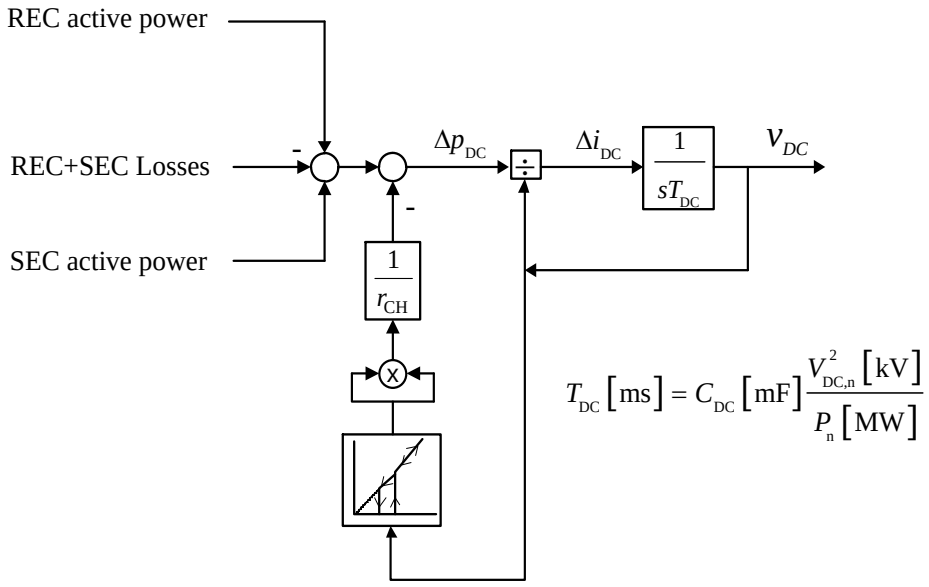

Figure 5-8: DC link model

5.3.4. Sending-end converter (SEC) model

The SEC is responsible for transmitting the active power injected in to the sending end of the transmission system by maintaining the AC voltage set point. The sending-end current controller and connection to the grid is similar to the REC model. Active current reference is calculated from the desired power active power to be transmitted through the HVDC line. The reactive current control loop can be used to control the SEC terminal voltage on the AC side or to guarantee a constant power factor injection to the AC grid. Again, this is similar to the REC side controller.

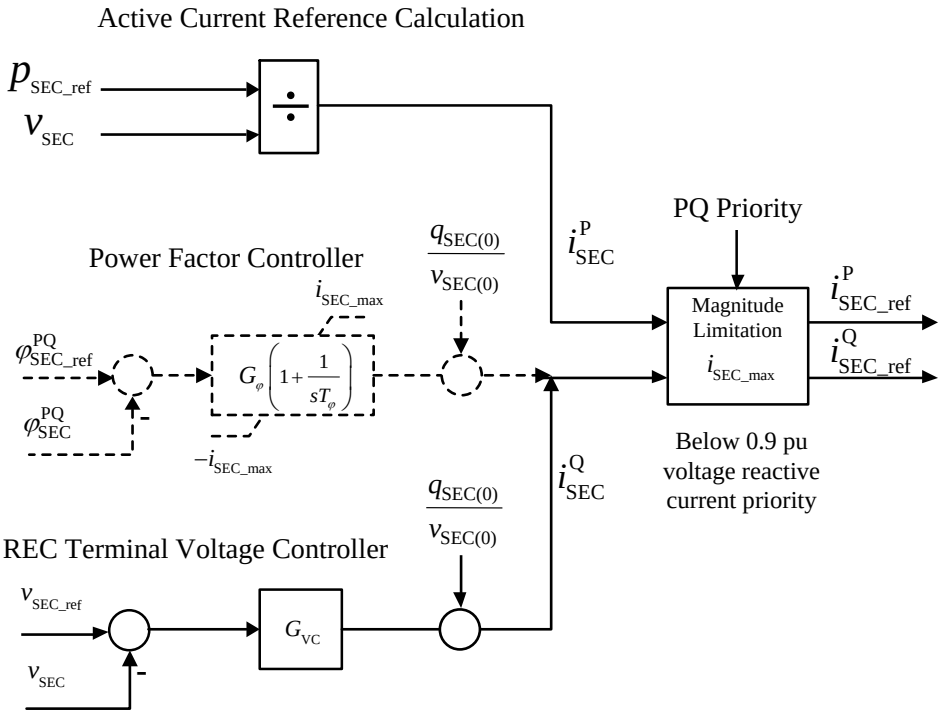

Figure 5-9: Sending-end converter model

5.4. Demonstration Examples

5.4.1. Test network and controller parameters

To illustrate the usage of the models and the plausibility of the results, typical scenarios involving voltage and power step changes have been simulated. The configuratiion and parameters of the test system are summarised below.

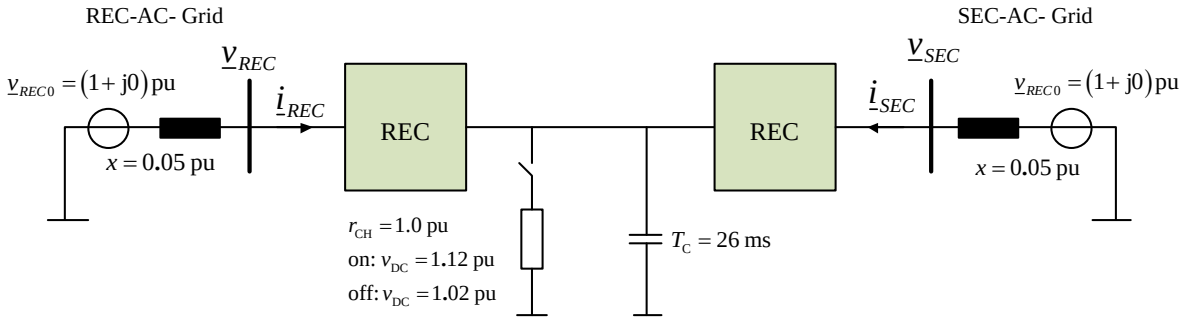

Table 6: Controller parameters

REC and SEC current controller (parameters of REC and SEC are the same):			
$G_I = 0.4$ pu	$T_V = 0.005$ s	$T_I = 0.02$ s	$x_{REC} = x_{SEC} = 0.13$ pu
Additional REC model parameters and settings:			
$G_{DC} = 3.5$ pu	$T_{DC} = 0.1$ s	$G_{VC} = 5.0$ pu	$i_{REC\_max} = 1.25$ pu

Additional SEC model parameters and settings:		
$G_{VC} = 5.0\,pu$	$i_{SEC\_max} = 1.25$ pu	$p_{Losses} = l\left(\left\|p_{REC}\right\| + \left\|p_{SEC}\right\|\right) \quad l = 0.01$ (1% of the power passing through each converter)

5.4.2. Simulation results

a. Example 1 –SEC reference power changed from 1.0 p.u. to 0.9 p.u

For a step changing involving SEC reference power, the behavior of power at both at the sending- and receiving ends as well as the DC voltage are shown in

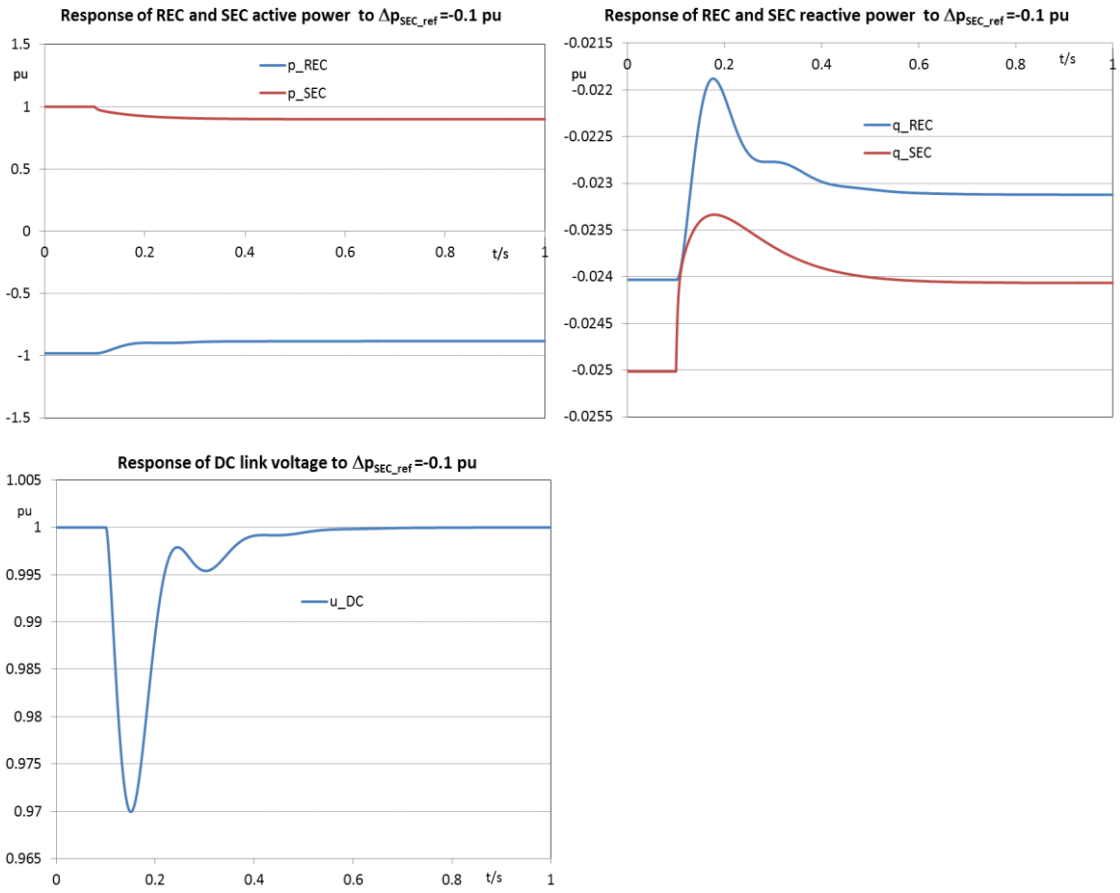

Figure 5-10: Response to a SEC power step change

b. Example 2 – A step change of SEC reference power from 1.0 p.u. to 0.5 p.u

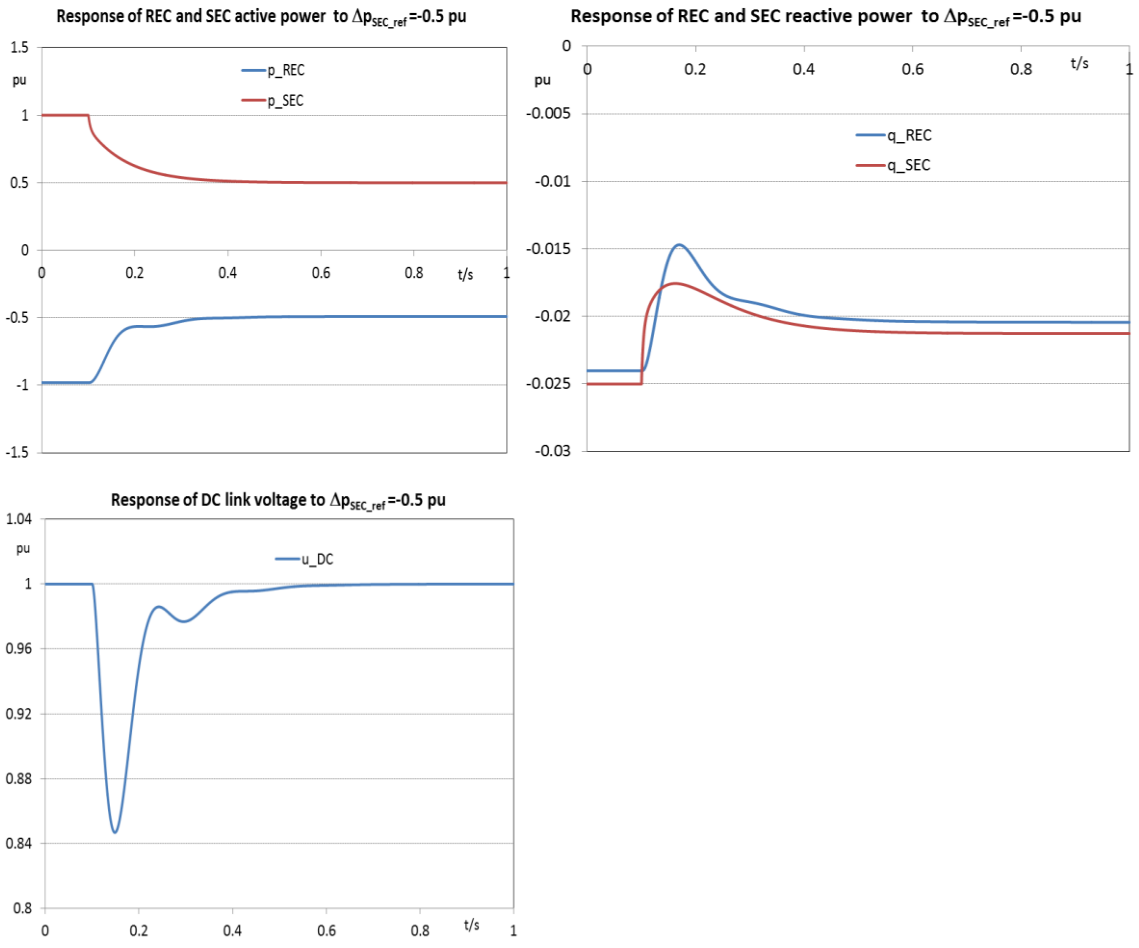

Figure 5-11: A step change involving 50 % SEC power

c. Example 3 – A step change of SEC AC voltage reference from 1.0 p.u. to 0.7 p.u

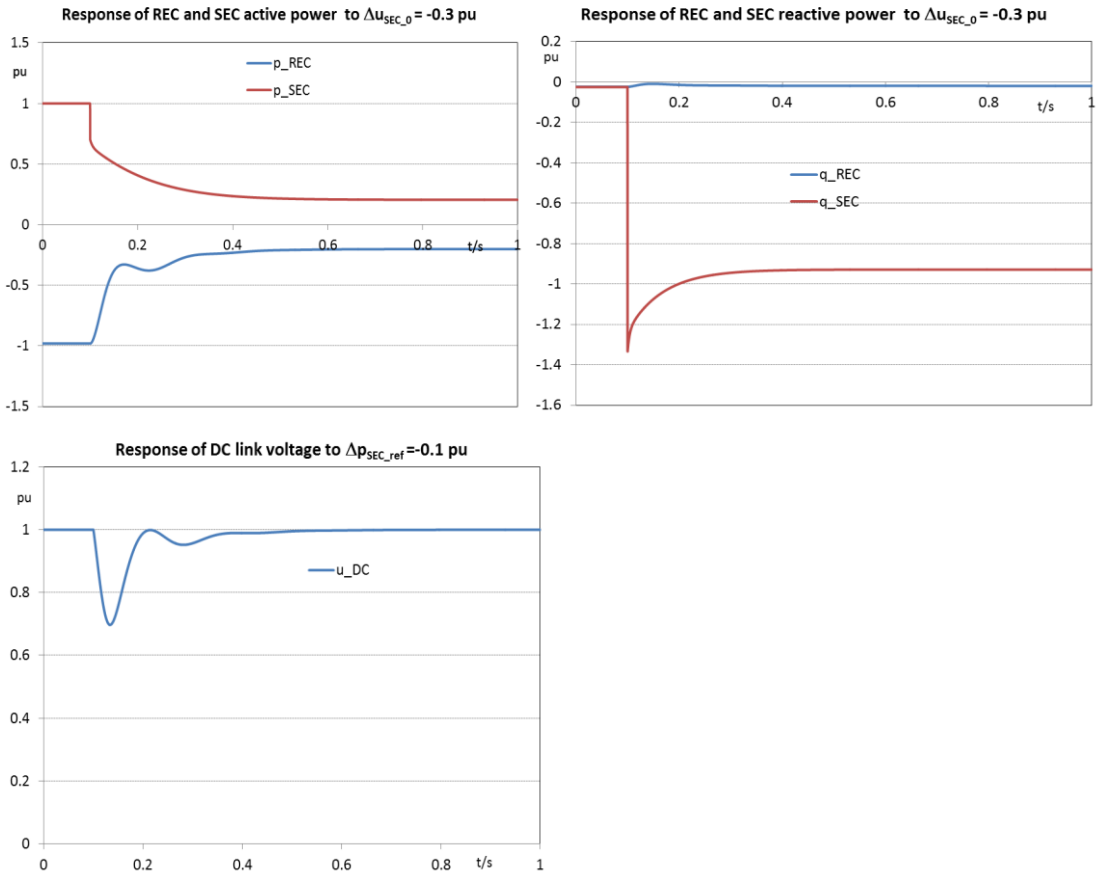

Figure 5-12: Voltage step change at the sending end

d. Example 4 – A step change of REC AC voltage reference from 1.0 p.u. to 0.7 p.u

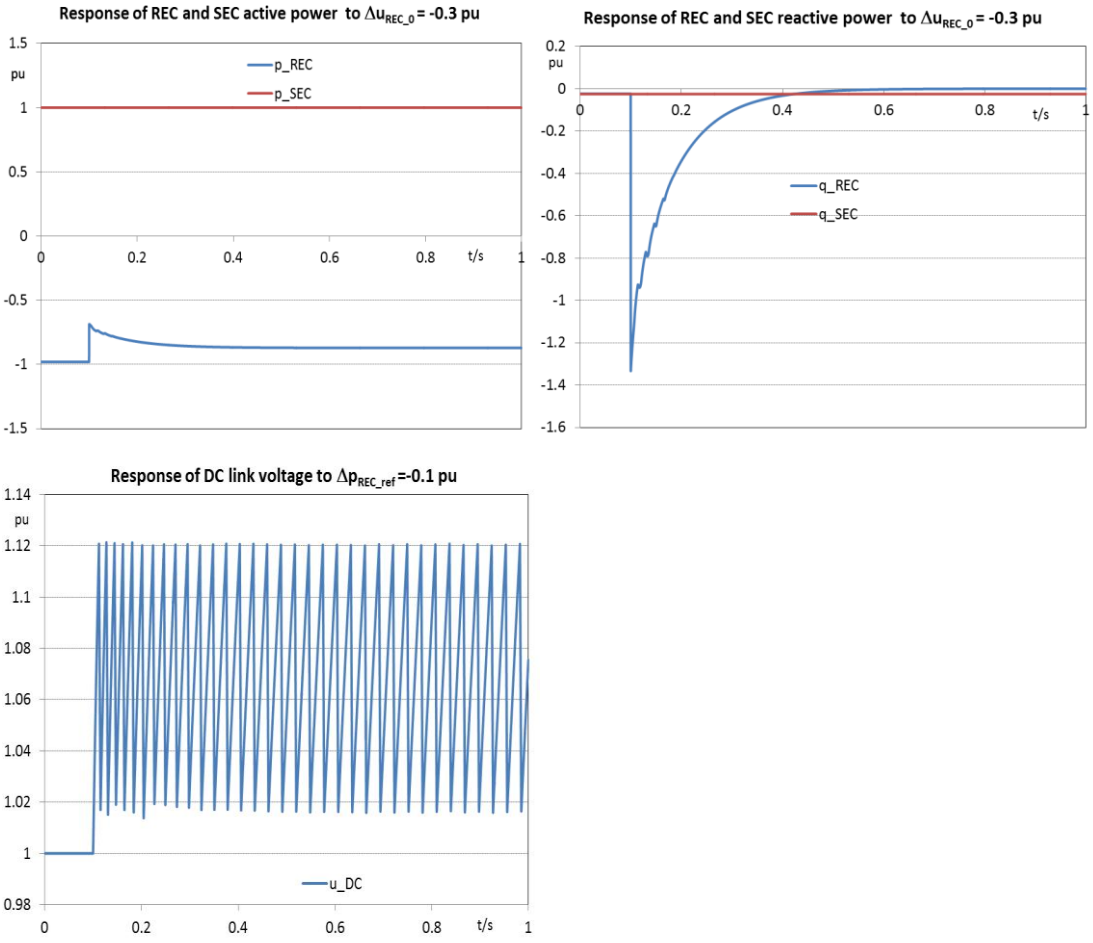

Figure 5-13: Response of a voltage change at the receiving-end

6. Implementation of the HVDC VSC model

The HVDC VSC model was then implemented on EUROSTAG. The results were then compared with those obtained using another power system simulation package known as PSD, an in-house simulation software used by UDE.

6.1. Versions of implementation

Base VSC HVDC model includes complex DC link model with capacitor charging and discharging modelling. It was implemented in two versions (referred as Version 1 and Version 2). In Version 1 converter reactance is modelled inside VSC HVDC model whereas in Version 2 it must be accounted in power flow file.

Since complex DC link model slows down overall computational process two simplified models were proposed (Model A and Model B) that are based on Version 2 model (which is also referred henceforth as Model 0). In Model A simplified model for DC link is used. In Model B in addition to this model of current controller is also simplified.

For Model 0, Model A, Model B two alternatives are available: in "Alternative 1" current controller model is computed in grid synchronous frame and in "Alternative 2" it is computed in terminal voltage frame. In sense of implementation in EUROSTAG these versions may differ in number of additional time constant blocks added to avoid algebraic loops.

The table below shows summary of VSC HVDC implementations that are available for EUROSTAG.

Table 7: Alternative simulations

Version name	Alternative 1	Alternative 2	Reactance in power flow file
Version 1	+	-	no
Version 2/Model 0	+	+	yes
Model A	+	+	yes
Model B	+	+	yes

6.2. Implementation of specific parts of the model

6.2.1. PQ priority block

PQ priority blocks are used in both sending (SEC) and receiving (REC) end converter models. The implementation of this block with selection of either active or reactive current priority depending on voltage level (@VSEC) is shown in Figure 6-1.

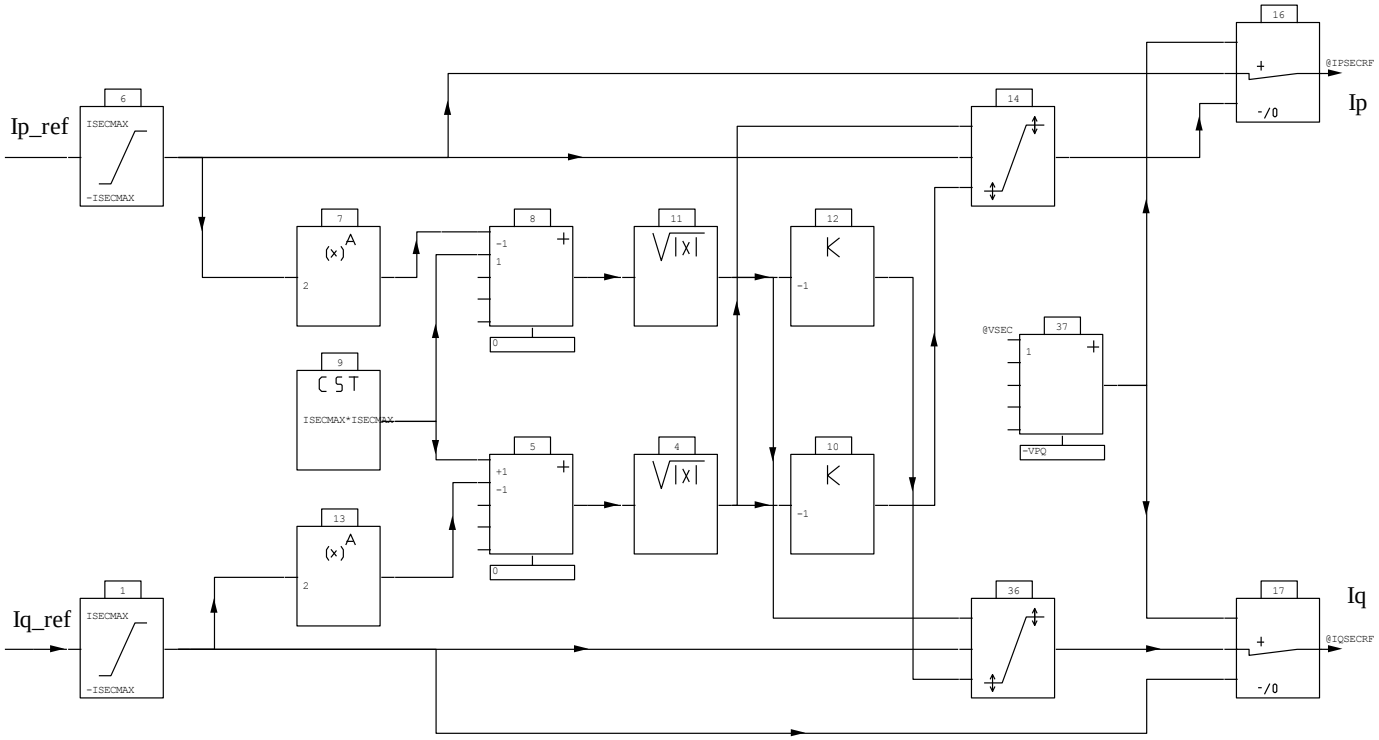

Figure 6-1: Implementation of PQ priority blocks

6.2.2. Current conversion

Current conversion from terminal voltage reference frame (I_P, I_Q) to synchronous reference frame (I_{re}, I_{im}) is performed according to the formulas below

$$I_{re} = I_P \cos\varphi + I_Q \sin\varphi$$

$$I_{im} = I_P \sin\varphi - I_Q \cos\varphi$$

where φ - terminal voltage angle

6.2.3. Hysteresis block

DC link model requires a hysteresis block to model "chopper" resistance switching. Unfortunately built in Schmidt-trigger block (that may be found in EUROSTAG) causes abnormal model behavior during simulation. An attempt was made to implement hysteresis block utilizing SET-RESET block of EUROSTAG, but it produced the same picture.

Eventually hysteresis block was implemented with use of time constant block as shown in Figure 6-2.

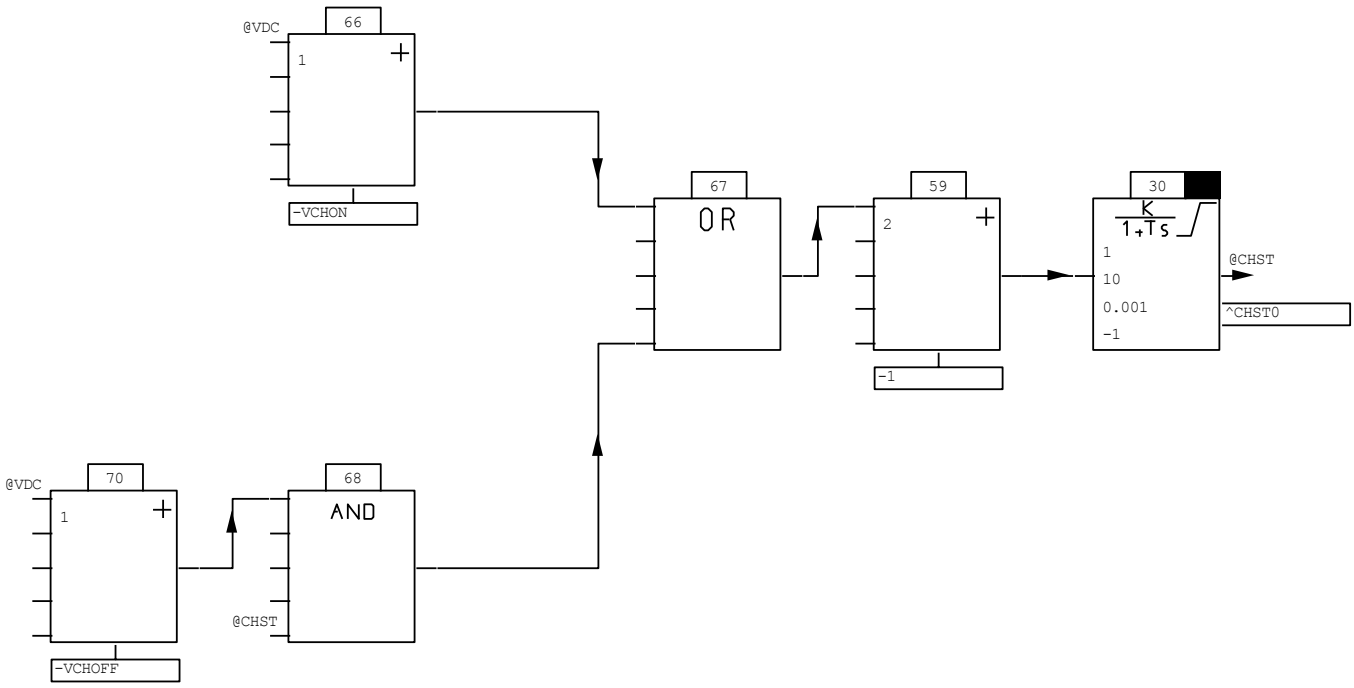

Figure 6-2: Implementation of hysteresis block

Here @VDC is an input and @CHST is an output of hysteresis block.

This implementation gives decent quality of modeling, but invokes a warning message at initialization phase of time domain simulation. This message shall be ignored.

6.2.4. Losses modeling

Losses in the converters are modeled approximately as a proportion of active power transferred through SEC. Parameter KLOS determines the proportion. KLOS is set directly in parameters for Version 1 and Version 2 models. For Model A and Model B it is calculated by equation

$$KLOS = \frac{1-FLOSS}{1+FLOSS},$$

where FLOSS determines losses in each converter.

In the load flow the following equation must be accounted:

$$|P_{SEC}| - |P_{REC}| = KLOS \cdot |P_{SEC}|$$

6.2.5. Implementation of converter reactance

In model Version 1 converter reactance is accounted inside model MACROBLOCK. For other implementations (Model 0, Model A, Model B) the reactance must be included in EUROSTAG network file. To do this it is sufficient to fill in “Shunt capacitor” field for REC and SEC nodes in EUROSTAG Network Editor with the following value

$$Q = -\frac{\mathrm{SBASE}}{\mathrm{X}} \cdot \left(\frac{U0}{VBASE} \right)^2,$$

where X is XREC or XSEC in p.u. as set in model parameters file, U0 is voltage at the node in steady state, SBASE and VBASE are base power and voltage of the node.

Please note the sign of the reactive power.

6.3. Model parameters description

Description of model parameters adjustable by user and their default values are given in the table below.

Table 8: Model parameters

Name	Default value	Unit	Description
INTERRC			
GDC	3.5	p.u.	Gain in DC link controller
GI	0.4	p.u.	Gain in current controller
GVC	5.0	p.u.	Gain in voltage controller
IRECMAX	1.25	p.u.	Converter current limit
KLOS	0.02	p.u.	Losses coefficient (Version 1, Version 2)
FLOSS	0.01	p.u.	Losses coefficient (Model A, Model B)
RCH	1.0	p.u.	Chopper resistance
TDC	0.1	s	Time constant in DC link controller
TDCL	0.026	s	Time constant in DC link model
TI	0.02	s	Time constant in current controller
TV	0.005	s	Time constant in current controller
VCHOFF	1.02	p.u.	Voltage at which the chopper is switched off
VCHON	1.12	p.u.	Voltage at which the chopper is switched on
VDC0	1.0	p.u.	Initial DC voltage
XREC	0.13	p.u.	VSC reactor
INTERSC			
GI	0.4	p.u.	Gain in current controller
GVC	5.0	p.u.	Gain in voltage controller
ISECMAX	1.25	p.u.	Converter current limit
TI	0.02	s	Time constant in current controller
TV	0.005	s	Time constant in current controller
XSEC	0.13	p.u.	VSC reactor

6.4. Model testing

6.4.1. Sample power grid

The model was tested in a simple scheme shownFigure 6-3.

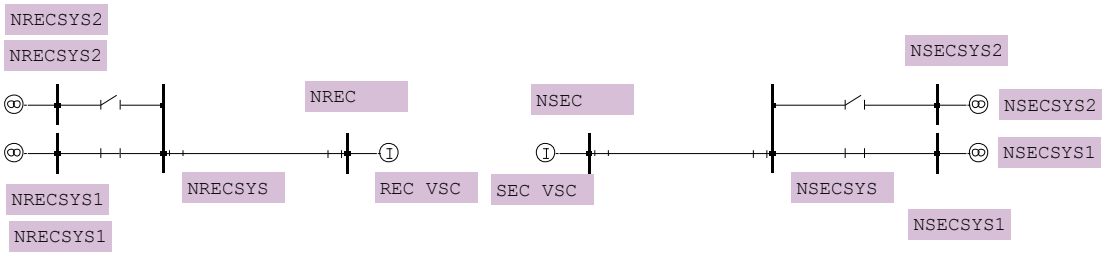

Figure 6-3: Test system

This network represents test case on which VSC HVDC model was tested on UDE software. It is separated into two synchronous zones each containing INJECTOR representing VSC (REC or SEC) and two infinite bus nodes. Number of infinite buses was doubled to enable switching of their voltage that is required by some testing procedures.

Table 9: Bus data

Node name	Base voltage	Generated power		Load power	
		Active	Reactive	Active	Reactive
	kV	p.u.	p.u.	p.u.	p.u.
NREC	220	0.98	0	0	0
NRECSYS	220	0	0	0	0
NRECSYS1	220	0	0	0	0
NRECSYS2	154	0	0	0	0
NSEC	220	-1.00	0	0	0
NSECSYS	220	0	0	0	0
NSECSYS1	220	0	0	0	0
NSECSYS2	154	0	0	0	0

Table 10: Branch data

Sending and receiving node names	Base power	Resistance	Reactance	Semi shunt conductance	Semi shunt susceptance	Ratio
	MVA	p.u.	p.u.	p.u.	p.u.	p.u.
NREC-NRECSYS	100	0	0.05	0	0	0
NRECSYS-NRECSYS1	100	0	0	0	0	0
NRECSYS-NRECSYS2	100	0	0	0	0	0
NSEC-NSECSYS	100	0	0.05	0	0	0
NSECSYS-NSECSYS1	100	0	0	0	0	0
NSECSYS-NSECSYS2	100	0	0	0	0	0

Results of steady state computation are shown in the tables below.

Table 11: Power flow results – bus voltages

Node name	Base voltage	Voltage magnitude	Voltage angle
	kV	p.u.	degree
NREC	220	1	2.81
NRECSYS	220	1	0
NRECSYS1	220	1	0
NRECSYS2	220	0.7	0
NSEC	220	1	-2.86
NSECSYS	220	1	0
NSECSYS1	220	1	0
NSECSYS2	220	0.7	0

Table 12: Power flow result - line flows

Sending and receiving node names	Power flow	
	Active	Reactive
	MW	MVAR
NREC-NRECSYS	98.0	2.4
NRECSYS-NREC	-98.0	2.4
NSEC-NSECSYS	-100.0	2.5
NSECSYS-NSEC	100.0	2.5

6.4.2. Test results

The models was tested according to test program prepared by UDE. The results was compared to those acquired from UDE modeling environment that was considered as reference.

The program includes for test cases:

- change of P_{SEC_ref} from 1.0 to 0.9 p.u.
- change of P_{SEC_ref} from 1.0 to 0.5 p.u.
- change of V_{SEC} from 1.0 to 0.7 p.u.
- change of V_{REC} from 1.0 to 0.7 p.u.

For each test active power of SEC and REC, reactive power of SEC and REC and DC voltage (for Model 0 version) were measured and compared to the reference. Simulation output from EUROSTAG is shown together to that obtained from UDE on the same diagrams.

All diagrams are in per units over time in seconds.

Tests show that the model developed produce results close to the reference in most cases with some exceptions described below.

1. In Test 1 small difference in REC reactive power and DC voltage may be observed.

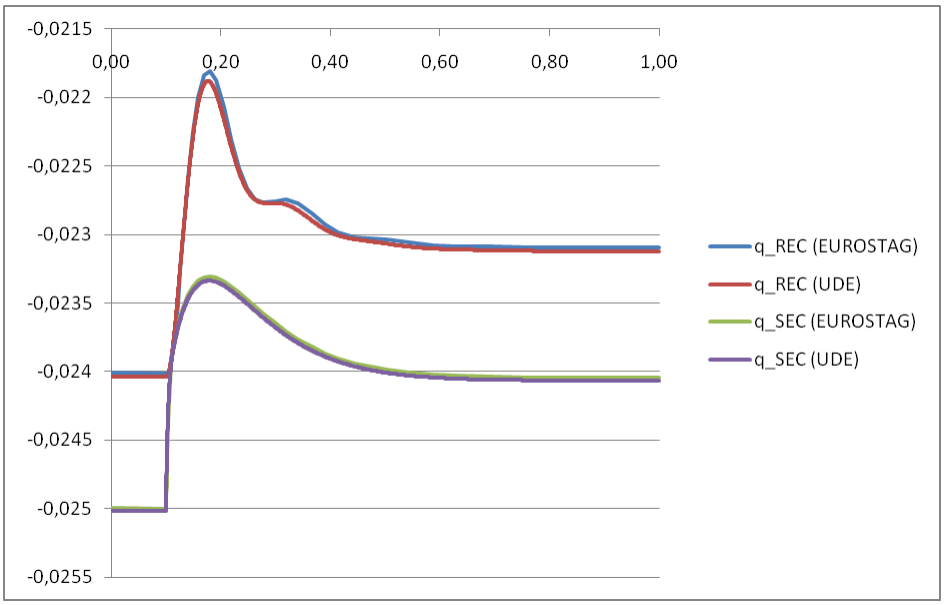

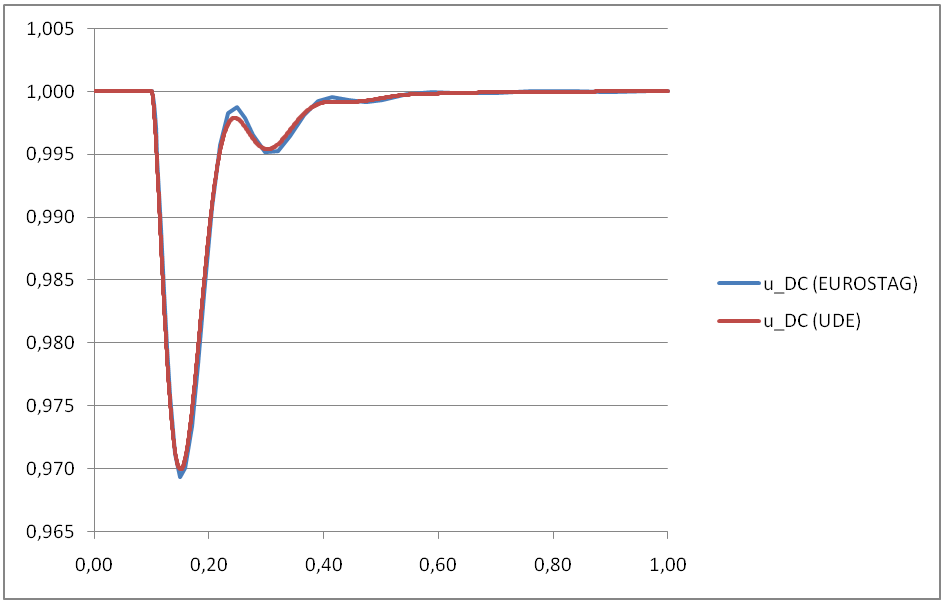

Figure 6-4: Test 1 results for Model 0 (there is small difference in results)

This is probably caused by lag blocks that were added to EUROSTAG model to avoid algebraic loops. The difference is insignificant in absolute value and may be notice only when parameter measured changes very slightly. As seen from the figures below when chnageo of reactive power or DC voltage is higher, the difference is almost unnoticable:

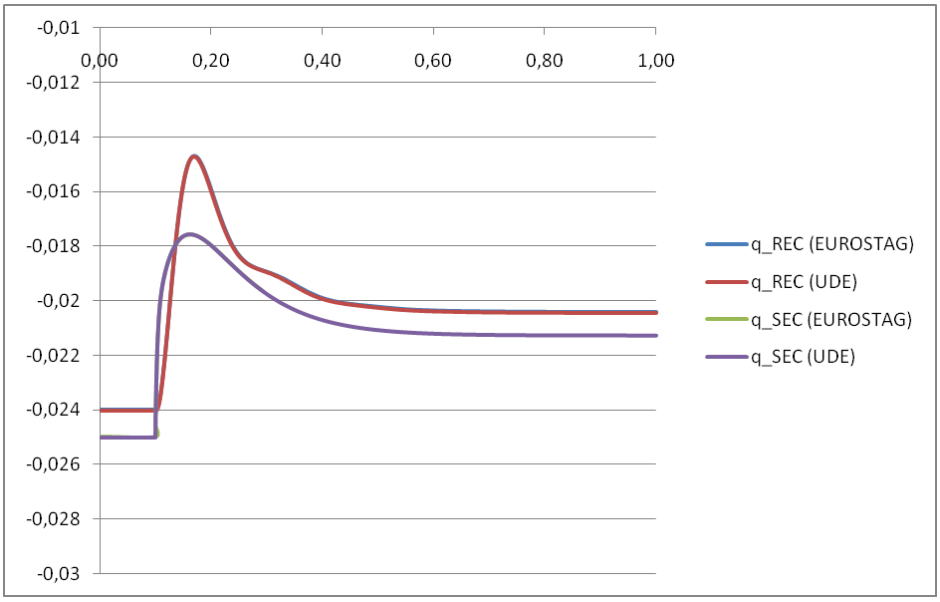

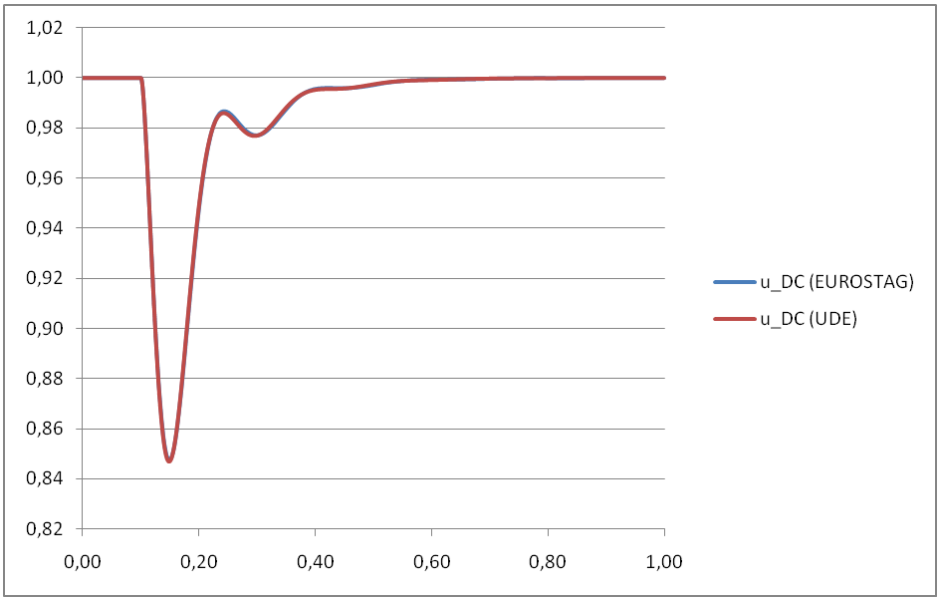

Figure 6-5: Test 2 results for Model 0 (difference cannot be identified)

2. When alternating chopper switching on and off occurs (as in Test 4) the difference in DC voltage may be observed:

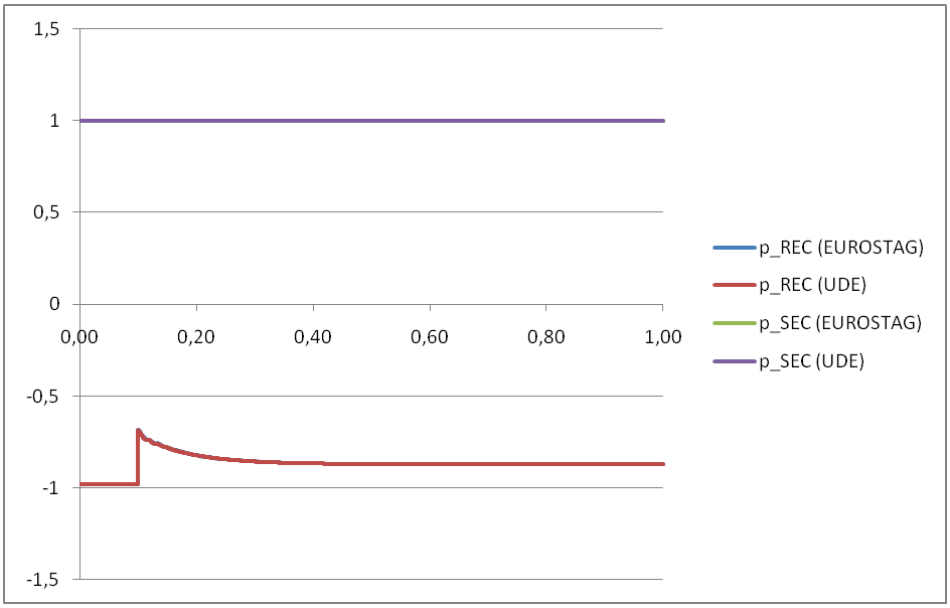

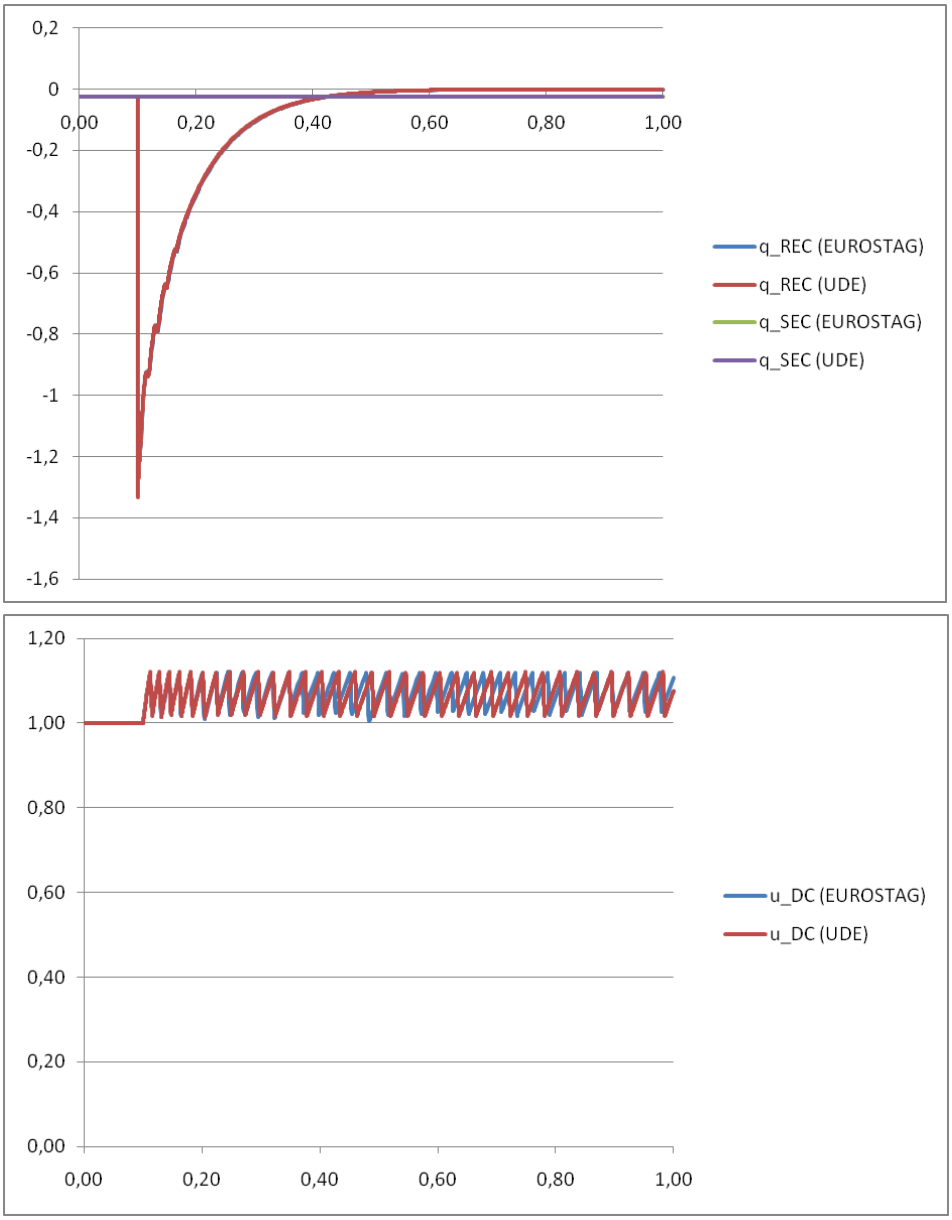

Figure 6-6: Test 4 results for Model 0 (difference in DC voltage doesn't influence on active and reactive power)

This can be explained by the difference in the way EUROSTAG and UDE software handles discontinuities. In any case this difference doesn't influence on active and reactive power calculated.

6.4.3. Conclusion on test results

Tests made prove that EUROSTAG implementation of VDC HVDC model in general follows UDE prototype. Some differences may be observed but they are not significant and do not produce any notable error in sense of modeling the whole power system.

6.5. EUROSTAG limitations

The following limitation on the usage of the Schmidt block to model hysteresis has been found.

The figure below shows block diagram that uses Schmidt-trigger block. This model is derived from VSC HVDC REC model and simplified to leave only the parts that are essential for demonstration.

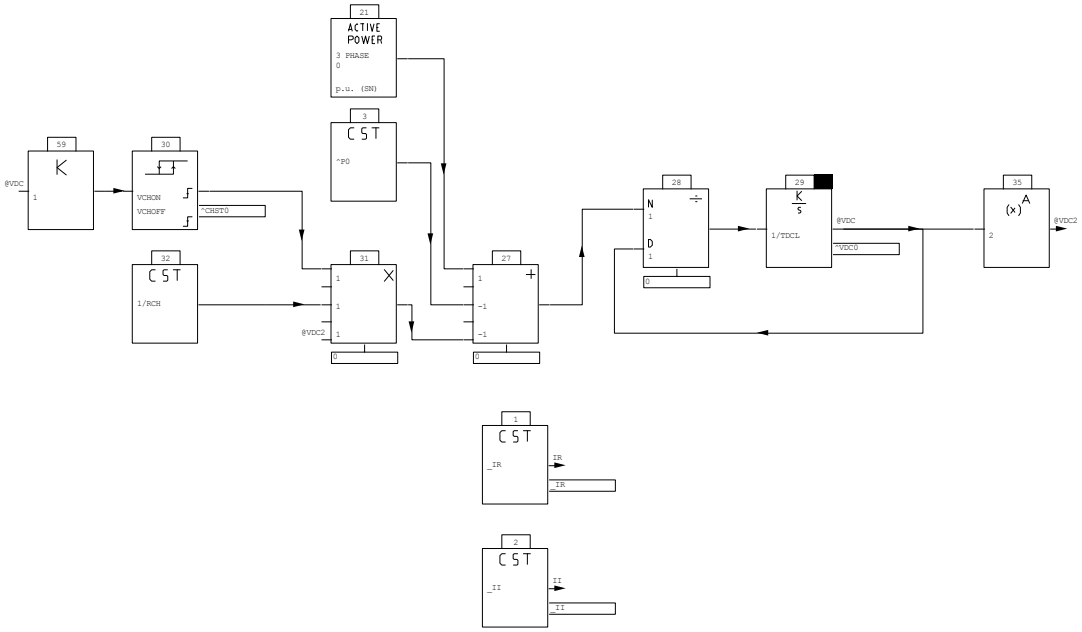

Figure 6-7: Block diagram that demostrates abnormal behaivor of EUROSTAG

The model has been correctly compiled and is used to control current injector in conditions of fourth test case (see 6.4.2). During simulation the output produced by the integrator (block 29) was inconsistent with its input. The figure below shows the input and the output of the block.

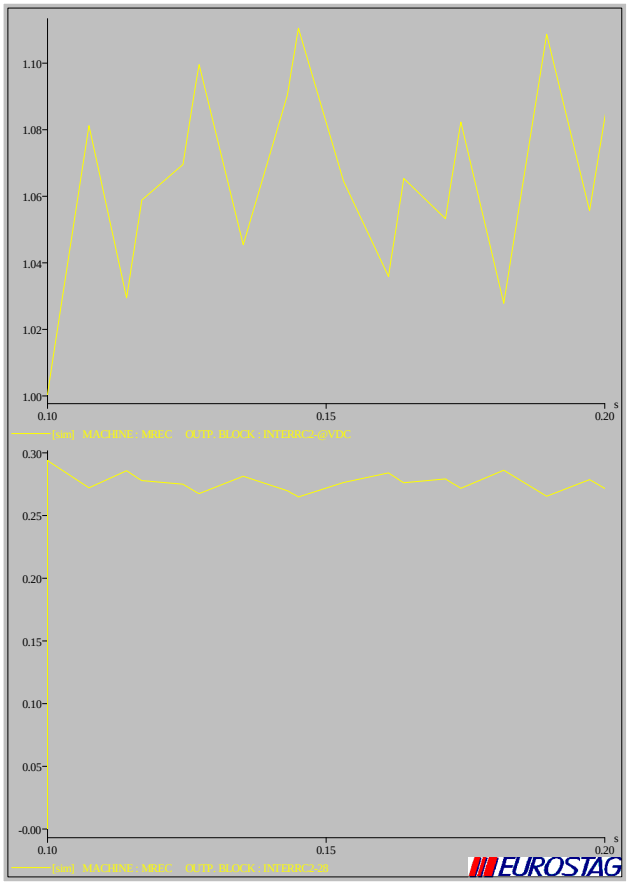

Figure 6-8: The input (bottom) and the output (top) of the integrator (block 29).

The figure shows that while the input is positive at given time period, the output doesn't grow steadily as it should, but experience random variations.

Nevertheless this modeling issue has been solved using the scheme described in 6.2.3with acceptable results.

7. Digital loss of synchronism protection

7.1. Model description

Loss of synchronism automation (ALAR) is a device designed to detect asynchronous mode of operation in power system and to initiate separation of asynchronously operating parts to prevent further fault propagation.

ALAR is a local automation device, i.e. it detects asynchronous mode on specific line and initiates the line tripping.

Principles of asynchronous mode detection may vary. They may base on measurements of active power, current, or impedance. Modern type devices detect loss of synchronism by comparing phase angle between voltage phasors on the ends of power transmission line. Voltage phasor on one end is measured while phasor on the opposite end is calculated.

The model of power transmission line used for calculation is shown at the figure.

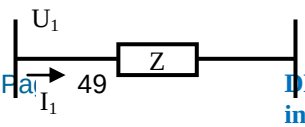

Phasors of U_1 and I_1 are measured and U_2 phasor is computed according to formula

$$U_2 = U_1 - I_1 Z$$

The device has three stages of operation. First stage is activated when phase angle between line ends becomes greater than 180 degrees. Second and third stages are activated after certain cycles of asynchronous operation. Cycle counter is reset if time between cycles exceeds certain value set by TRESET parameter. This brings the device to initial state.

The model has five output variables: one for each stage and two outputs which show whether the part of the system to which the model is connected goes faster or slower than the other part.

7.2. Notes on implementation

The logic of the device is implemented in macroautomaton macroblock ALAR. Corresponding macroautomaton shall be linked to controlled power transmission line. In addition user automatons shall be defined to control outputs of the device and trigger line tripping. Common framework may be observed in the example of implementation.

7.3. Model parameters description

Description of model parameters adjustable by user and their default values are given in the table below.

Table 13: Model parameters description

Name	Default value	Unit	Description
DELTA	15	degrees	Frame size for catching phase angle near 180
EXTBLOCK	0		External blocking
N2ST	2		Setpoint (number of cycles) for the second stage
N3ST	5		Setpoint (number of cycles) for the third stage
TRESET	2	s	Device reset time
Z	-	p.u.	Line impedance
PHI	-	degrees	Line impedance angle

7.4. Model testing

7.4.1. Sample power grid

The model was tested in a simple scheme shown at the figure.

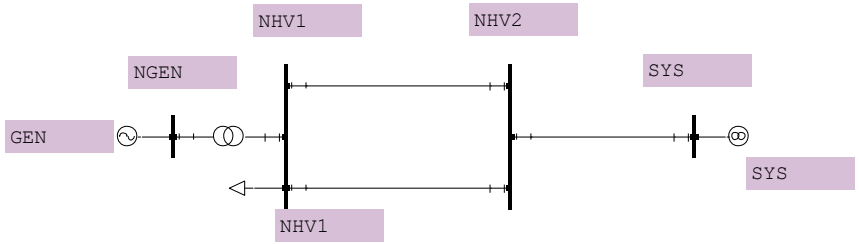

The device is supposed to be installed at NHV1 and control NHV1-NHV2-2 line.

Table 14: Input node data

Node name	Base voltage	Generated power		Load power	
		Active	Reactive	Active	Reactive
	kV	p.u.	p.u.	p.u.	p.u.
NGEN	24	6.00	0.67	0	0
NHV1	380	0	0	0	0
NHV2	380	0	0	0	0
SYS	380	4.91	-1.13	0	0

Table 15: Input branch data

Sending and receiving node names	Base power	Resistance	Reactance	Semi shunt conductance	Semi shunt susceptance	Ratio
	MVA	p.u.	p.u.	p.u.	p.u.	p.u.
NGEN-NHV1	100	0.00018	0.007690			1.05
NHV1-NHV2-1	100	0.00208	0.022850			
NHV1-NHV2-2	100	0.00208	0.022850			
NHV2-NHV3	100	0.00208	0.022850			

Results of steady state computation are shown in the tables below.

Table 16: Node voltages

Node name	Base voltage	Voltage magnitude	Voltage angle
	kV	p.u.	degree
NGEN	24	1.00	11.5
NHV1	380	1.05	9.1
NHV2	380	1.04	6.13
SYS	380	1	0.0

Table 17: Power flow

Sending and receiving node names	Power flow	
	Active	Reactive
	MW	MVAR
NGEN-NHV1	600.0	67.4
NHV1-NHV2-1	249.7	8.5
NHV1-NHV2-2	249.7	8.5
NHV2-NHV3	497.0	111.4

7.4.2. Test results

Below test results are shown. Each stage was tested separately with other stages disabled by setting corresponding automaton “Threshold 1” value to 10.

Test procedure consists of modeling three phase fault at NHV1 node that lasts from 10.0 to 10.7 s. This causes generator GEN1 loss of synchronism. For the time of short-circuit condition the device is blocked by setting corresponding setpoint to 1.

Then the respective device stage causes line tripping during first, second or fifth cycle of asynchronous operation.

Test for stage 1

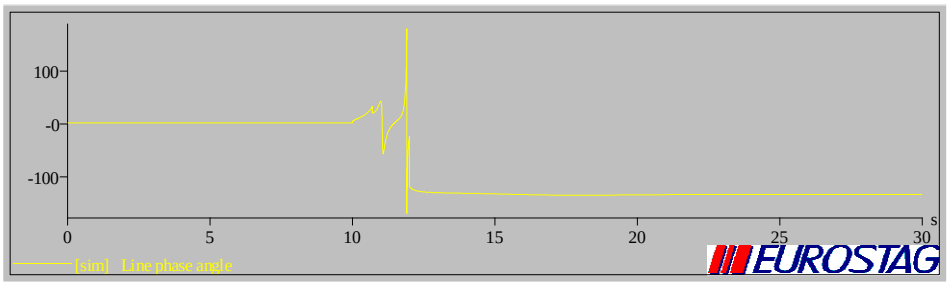

Figure 7-1: Test for stage 1

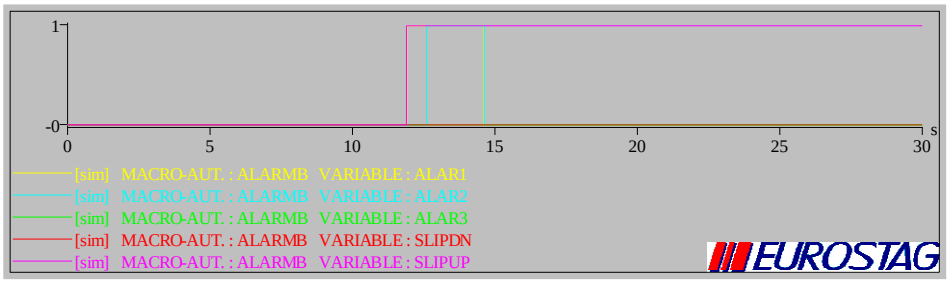

Figure 7-2: Test for stage 2

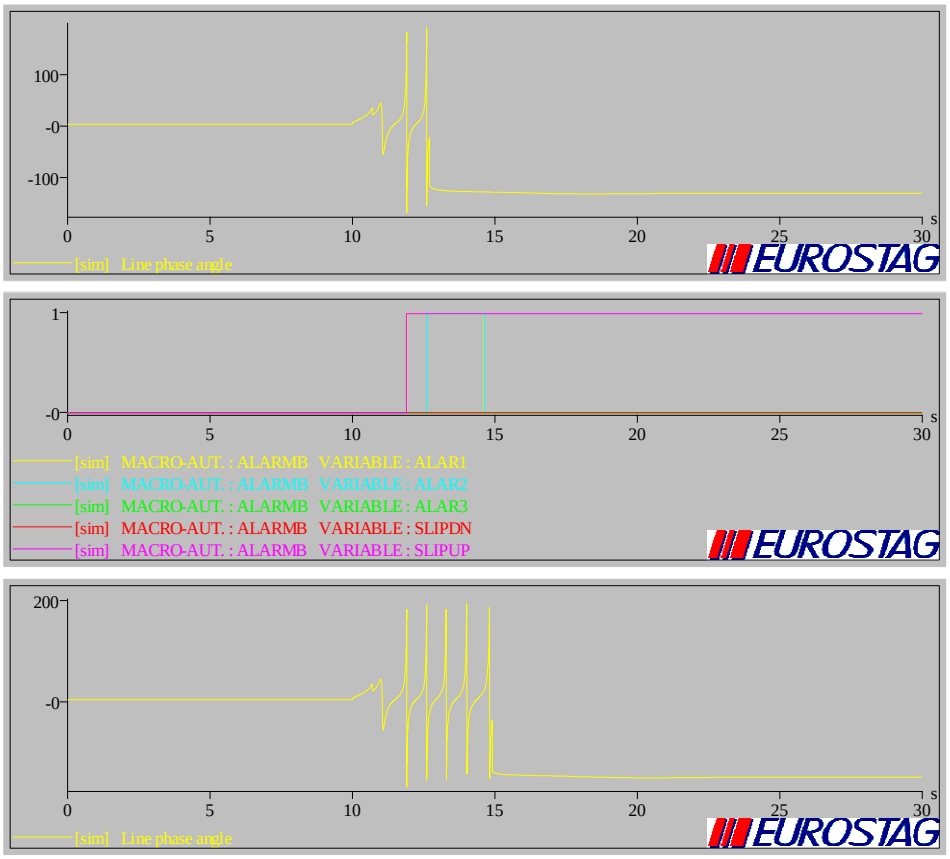

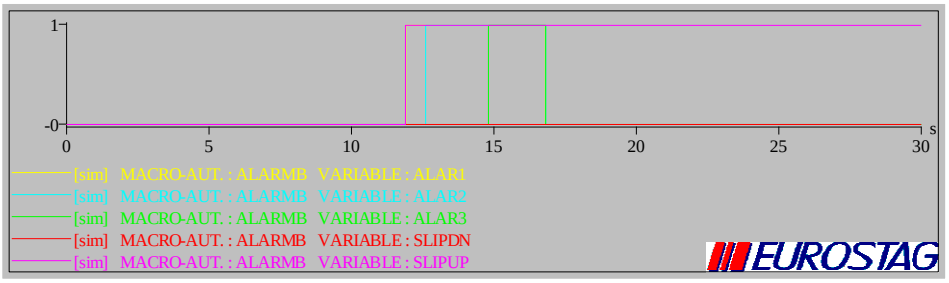

Figure 7-3: Test for stage 3

7.4.3. Conclusion on test results

Test results show that all parts of the model works as desired. Stage 1 output signal is set during first cycle of asynchronous operation; stage 2 and stage 3 signals are set after 2 and 5 cycles respectively. The model is reset to initial stage 2 second after last detected cycle.

As seen from diagrams, system is automatically split into two parts after corresponding signal becomes active. This shows correct operation of the complete system.

8. Thermal overload protection

Properties	Description
ANSI/IEEE C37.2 standard device number	49
IEC 61850 logical node name	PTTR
Input signal	Current (phase or positive sequence)
Output signal	Binary 0 or 1

Overloading transmission lines, cables, transformers, generators, motors, etc. beyond the nameplate rating can cause a rise of temperature of these devices above permissible level. As a result the insulation will deteriorate, resulting in accelerated loss-of-life of the equipment. The thermal overload protection is used to avoid it [1, 2].

ANSI 49 (IEC PTTR) thermal overload function is available in modern numerical protection relays. This function, depending on the protected object and specific implementation in the relay, uses some combination of ambient temperature, oil temperature, and measured current, to detect the presence of an over-temperature condition.

The scale of the PEGASE project restricts the size and complexity of the model, therefore it is suggested to apply the following simplified differential equation for thermal overload protection, omitting ambient temperature input signal, and some other typical but not substantial features [1, 2, 3, 4]:

$$\tau \cdot \frac{dH}{dt} + H = \left(\frac{I}{I_{max}} \right)^2 \quad (10)$$

where:

Symbol	Unit	Description
H	[pu]	Heat rise. For example, if H = 120 %, the protected object overheats by 20 % in relation to its rated operation conditions.
τ	[min]	Thermal time constant of winding or oil.
Imax	[A]	Maximum permissible current of the protected object.
I	[A]	Actual current.

Equation (10) is in accordance with IEC 60255-8 [3] and is used to track a first-order thermal image (replica) based on the measured current. The thermal replica model calculates a maximum temperature rise based on the measured current, the thermal time constant, and the maximum permissible current of the protected object.

The biggest advantage of using a thermal replica for temperature protection is the ease of implementation. The function involves only settings in the relay, with no need to physically install and connect temperature sensors. However, this method does not account for ambient temperature, and provides only a simple representation of oil or winding temperatures due to load, but is not truly the temperature of interest (oil, top-oil, winding, or hot-spot temperature). Functionally, therefore, this is essentially an over-current function, with an asymptotic time delay. Thermal replica based protection elements typically include several threshold settings, to alarm and trip on increasing temperature conditions.

The thermal replica model is widely used, it is incorporated in many protection devices by different manufacturers and it can be applied to different power system elements.

Protection tripping time can be easily calculated, assuming the protected object is loaded with constant current I [2, 3, 4]:

$$t_{trip} = \tau \cdot \ln \left[\frac{\left(\frac{I}{I_{max}} \right)^2 - H_{init}}{\left(\frac{I}{I_{max}} \right)^2 - 1} \right] \quad [min] \quad (11)$$

The calculated value will show how much time has left until the actual heat content H will exceed the set overload level H_{trip} (H_{trip} = 100 %).

In a similar way as with the protection tripping time, the alarm time can be estimated:

$$t_{alarm} = \tau \cdot \ln \left[\frac{\left(\frac{I}{I_{max}} \right)^2 - H_{init}}{\left(\frac{I}{I_{max}} \right)^2 - H_{alarm}} \right] \quad [min] \quad (12)$$

The calculated value will show how much time has left until the actual heat content H will exceed the set alarm level H_{alarm} (H_{alarm} = 80 %, for instance), assuming that the load current I will remain constant.

The previously mentioned operating principles are presented in the Figure 8-1 as a block diagram created in EUROSTAG environment.

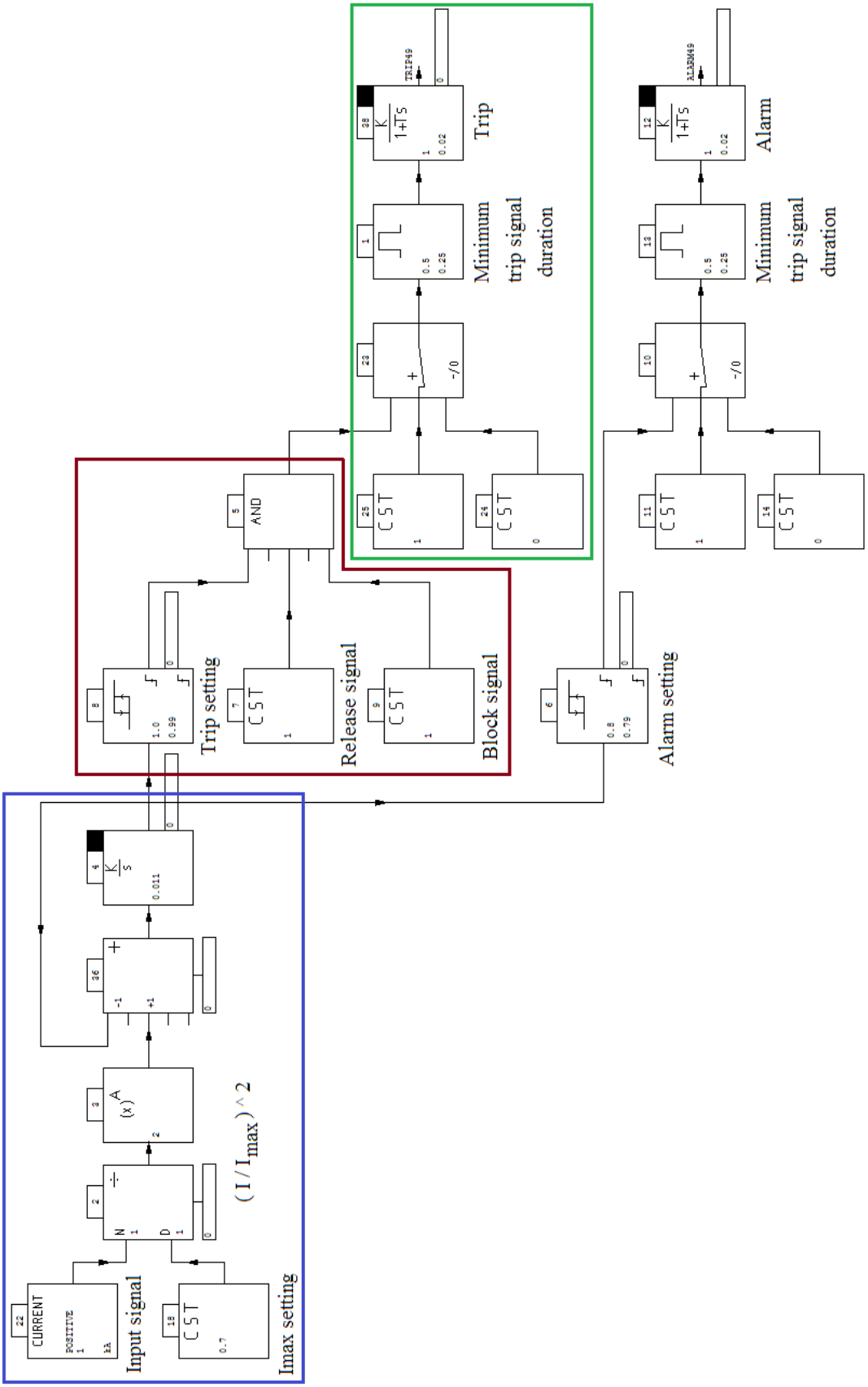

Figure 8-1: EUROSTAG block diagram of thermal overload protection

The thermal overload protection model is continuously fed with positive sequence current (i.e. this protection function is active throughout the simulation process).

The calculation of the heat content "H" is based on the fact that the temperature in the windings or oil is proportional to the square of the current, and that the temperature increases and decreases exponentially with a certain time constant [1, 2, 3, 4]. The part of the model that represents the equation (10) is given in Figure 8-2:

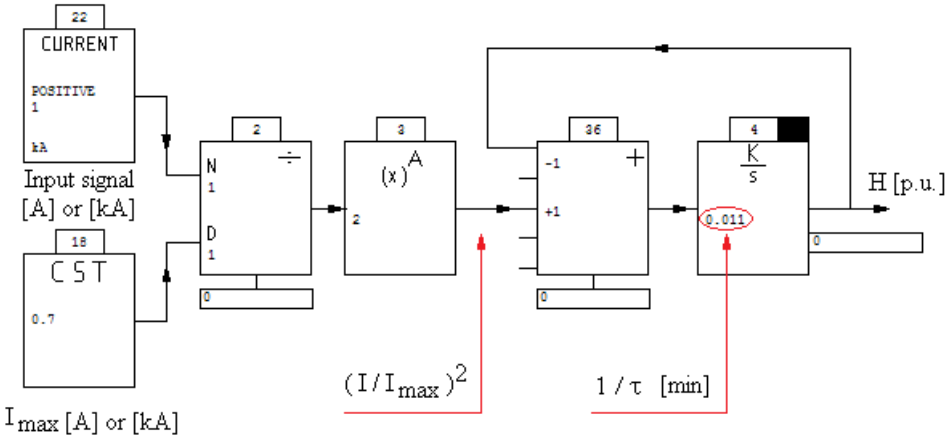

Figure 8-2: Part of the model that represents the equation (10)

Inclusion of two additional inputs (see Figure 8-3) significantly extends the application capabilities of model as very often protection functions are blocked or released according to some external criterion.

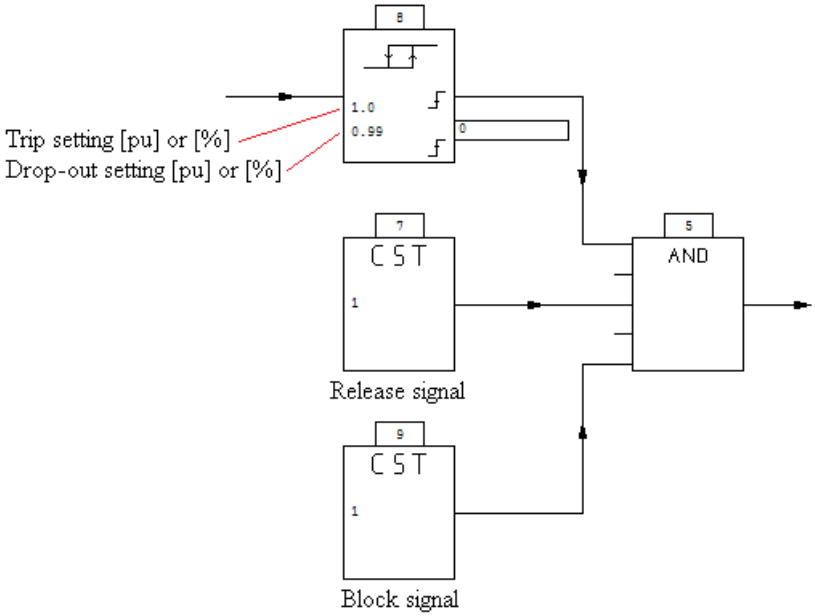

Figure 8-3: Additional blocking and releasing binary inputs

If the releasing or blocking input is not used then the binary "1" should be connected to the logical AND operator.

Blocking input could be supplemented with logical NOT operator so that binary "0" (instead of a "1") would result in "no blocking" condition.

Pickup of the thermal overload protection function is stabilized by setting the dropout value (see Figure 8-3) - the pickup condition is maintained until the current falls below the drop-out value, thus securing that the function does not drop-out too fast.

Drop-out ratio is mostly around 0.95 for new digital protection devices. For older electromechanical devices it is lower, for instance, 0.8.

The model is further extended to avoid an inconsistent length of tripping impulses that in some cases can be very short. See Figure 8-4 where the preset length of output signal is enforced. 0.25 s is a typical minimum trip command duration setting and it can be hard coded into a model.

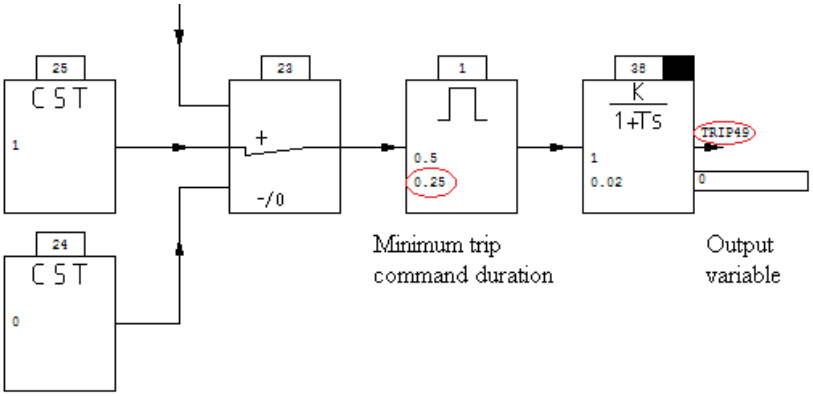

Figure 8-4: Modelling of preset length of output signal

As soon as calculated heat rise exceeds the trip setting (i.e. the maximum permissible temperature that corresponds to the maximum permissible current), the trip output signal appears and lasts at least 0.25 s. Trip setting usually is set in percent - in this example it is 100 %. The alarm stage is modeled in the same way as trip stage (albeit with the lower operation setting).

To consider that in EUROSTAG the best algorithmic performances are achieved when the output variable is the output of a differential block, or in case of an algebraic equation, when the variable is varying smoothly, a “Simple-Lag” element with short time constant is used as a last (or output) element of the model (see Figure 8-4).

It should be noted that all the necessary features of the model are included in the block diagram, though it would had been possible to transfer some of its features to the so called “User-automatons”.

For informative purposes the same model in MATLAB/SIMULINK environment is presented as well (Figure 8-5). It has some differences with EUROSTAG model due to the differences of available elementary blocks and modeling approach in both programs. In this and in the following chapters blocks of the Matlab models in yellow color represent input and output signals but blocks in blue color – the settings.

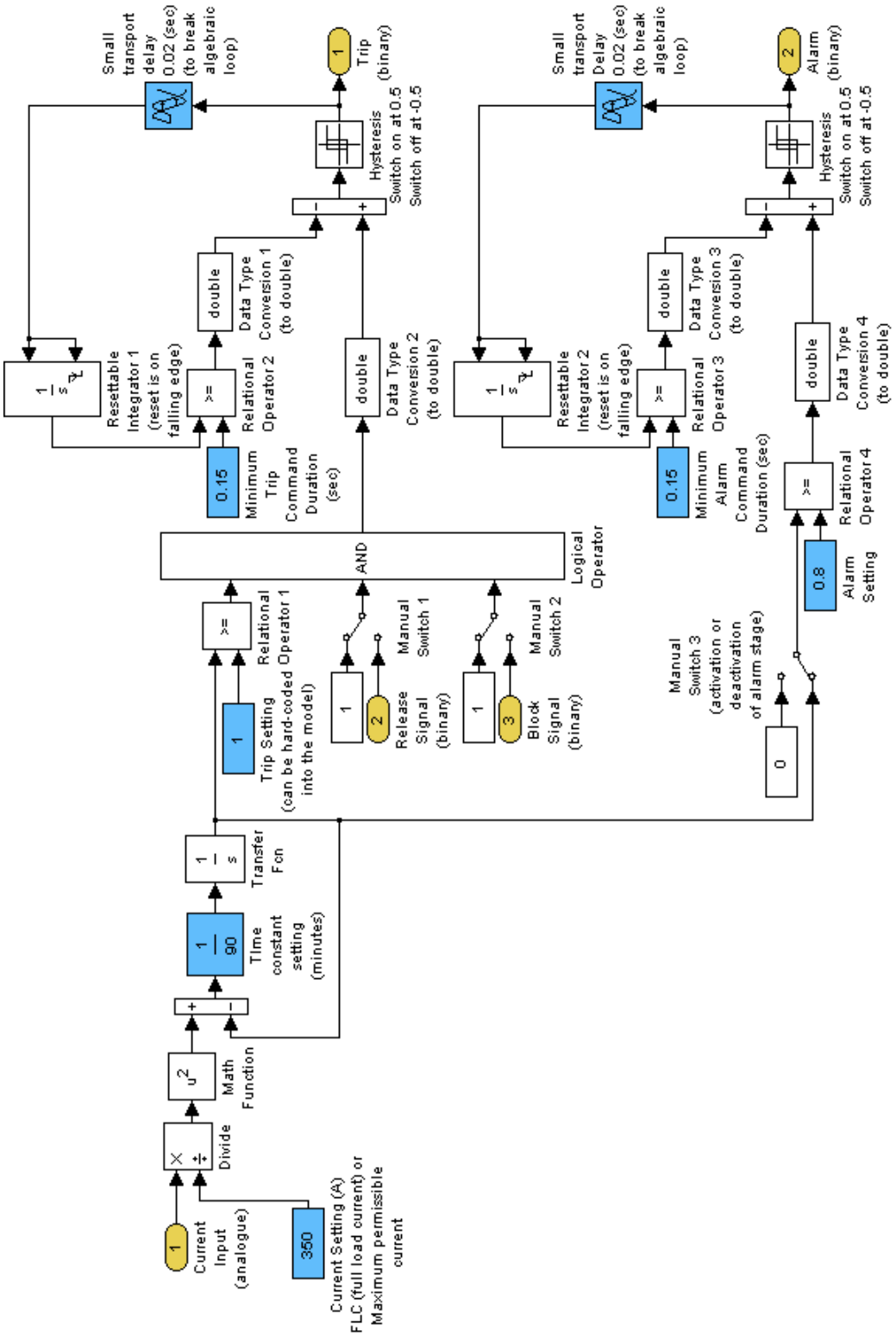

Figure 8-5: MATLAB / SIMLINK block diagram of thermal overload protection

Some typical features of thermal overload protection that were left out of the model in order to fit it better into the framework of PEGASE project are discussed below [4, 5, 6, 7].

Ambient temperature consideration. Some manufacturers modify the equation (10) to account the effect of variations in ambient temperature. That requires additional input signal for the thermal replica model. Also the rated temperature rise needs to be known.

Different thermal time constants. Other possible adjustment for equation (10) involves the use of two different thermal time constants. It can be essential for transformers to account for different cooling methods. The change of the transformer thermal time constants can be activated by the cooling equipment via a binary input. It is also important for self-ventilated electrical machines. In a self-ventilated machine the thermal time constant at standstill can differ considerably from the time constant of a continually running machine, since then the ventilation provides for cooling whereas at standstill only natural convection takes place. Machine standstill is detected and the thermal time constants are swapped when the current undershoots some preset threshold value.

Current limitation. In order that overload protection on occurrence of high short-circuit currents does not cause short trip times (possibly affecting time grading of different protection functions), in some relays it is possible to implement current limiting for the overload protection. Currents exceeding the specified value are limited to this value. For this reason, they do not further reduce trip time in the thermal memory.

Start-up of electrical machines. On startup of electrical machines the over-temperature calculated by the thermal replica may exceed the alarm over-temperature or even the trip over-temperature. In order to avoid an alarm or trip, the starting current sometimes is acquired and the resulting increase of temperature rise is suppressed. This means that the calculated temperature rise is kept constant as long as the starting current is detected.

Emergency start-up of electrical machines. When machines must be started for emergency reasons, operating temperatures above the maximum permissible operating temperatures sometimes are allowed (emergency start). Then exclusively the tripping signal can be blocked via a binary input. Since the thermal profile may have exceeded the tripping temperature after startup and dropout of the binary input has taken place, the protection function features a programmable run-on time interval which is started when the binary input drops out and continues suppressing a trip signal. Tripping by the overload protection is defeated until this time interval elapses. This binary input affects only the tripping signal. It has no effect on the fault condition logging nor does it reset the thermal profile.

Influence of the negative sequence current. To determine the heat rise of rotating machines, the relay can take into account the negative-sequence component. Indeed, the rotating field corresponding to the negative-sequence component induces a double frequency rotor current, which causes considerable losses.

Behavior in the case of input signal failure. The situation with a loss of input signal (actual current, temperature etc.) is considered here. Usually depending on the relay setting the value of the thermal replica is either reset to zero, or maintained in the memory. In the latter case, when the normal situation is restored, the thermal replica uses the stored value for calculation and matches it to the operating conditions.

Hot-spot temperature. Calculation of the hot-spot temperature and determination of the ageing rate according to IEC 60354 can also be considered (these quantities are considered in IEEE C57.91-1995 standard as well, however, there are terminological differences between IEC and IEEE standards when defining certain parameters). Hot-spot temperature is the hottest temperature spot in the transformer winding. The location of the winding hottest spot is dependent on the physical design of the transformer. The protection device calculates the hot-spot temperature from the input temperature data and the settings of the relay. When a settable threshold of the hot-spot temperature element is exceeded, an annunciation or a trip is generated. Hot-spot calculation is done with different equations depending on the cooling method.

Aging factor. The aging factor element detects transformer aging in per-unit normal insulation aging. The element can be set for alarm or trip whenever the computed aging factor is greater than the user-defined pickup setting for the specified time delay. The life-time of cellulose insulation refers to a temperature of 98 °C or 208.4 °F in the direct environment of the insulation. Experience shows that an increase of 6 K means half the life-time.

Loss-of-life. As the key goal of implementing thermal overload protection functions is to limit the loss-of-life of the transformer winding insulation the loss-of-life protection element sometimes is used as well. With constant rated load, the relative ageing rate L is equal to 1. For values greater than 1, accelerated ageing applies, e.g. if L=2 only half of the life-time is expected compared to the life-time under nominal load conditions.

9. Non-directional instantaneous/definite time over-current protection

Properties	Description
ANSI/IEEE C37.2 standard device number	50
IEC 61850 logical node name	PIOC (instantaneous), PTOC (definite time)
Input signals	Current (phase or positive sequence)
Output signals	Binary 0 or 1

When a fault occurs in a power system, the fault current is almost always greater than the pre-fault load current in any power system element. A very simple and effective relaying principle is the one using current magnitude as an indicator of a fault. Over-current relays can be applied to protect practically any power system element, i.e. transmission lines, transformers, generators, or motors. The operating principle of a relay can be defined as follows [3, 4, 8-13]:

$$\begin{aligned} I \geq I_{set.} &\Rightarrow \text{Trip} \\ I < I_{set.} &\Rightarrow \text{Do not trip} \end{aligned} \qquad (13)$$

The quantity $I_{set.}$ is known as the pickup setting of the relay. The equation (13) describes an ideal relay operating characteristic as shown in Figure 9-1. The relay does not operate (operating time is infinite) as long as current magnitude is less than $I_{set.}$ If current magnitude exceeds $I_{set.}$, relay operates taking a definite time T to close its contacts.

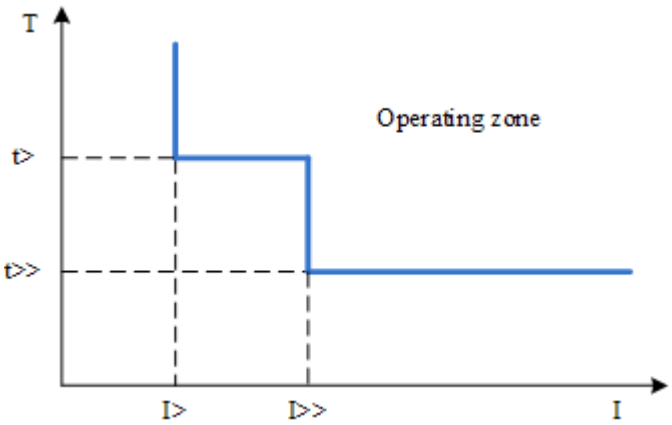

Figure 9-1: Tripping characteristic of two-stage over-current protection function

The previously mentioned operating principles are presented in the Figure 3.2 as a block diagram created in EUROSTAG environment.

In this model positive sequence current (see "Current" element No.22 in Figure 9-3) is continuously compared with the pick-up value (see "Schmidt-Trigger" element No.8 in Figure 9-3), that can be set in amperes or in per unit values, whichever is more suitable from the point of view of software developers. Phase current as an input quantity can be used as well.

As soon as positive sequence current exceeds the pick-up value (0.7 kA in this example), the binary "1" value appears at the output of the "Schmidt-Trigger" element (relay picks up). On the other hand – relay drops out as soon as current decreases below the drop-out value (0.6 kA in this example). The binary "1" is converted to "0.5" by the help of "Summer" element No.36 to form a convenient threshold signal for a "Relay" element No.11.

If the pick-up condition is maintained for a time period equal or greater than the time delay setting (0.50 s in this example) that is set by the help of "Summer" element No.21, the binary "1" value appears at the output of the "Relay" element No.23 (relay trips).

The resettable integrator is a main part of a logic that estimates for how long some criteria have been fulfilled. To obtain this functionality in EUROSTAG and Scilab the following equivalent scheme is used (see Figure 9-2 and Figure 9-3). The output signal is being reset by providing a large negative input to the integrator when necessary.

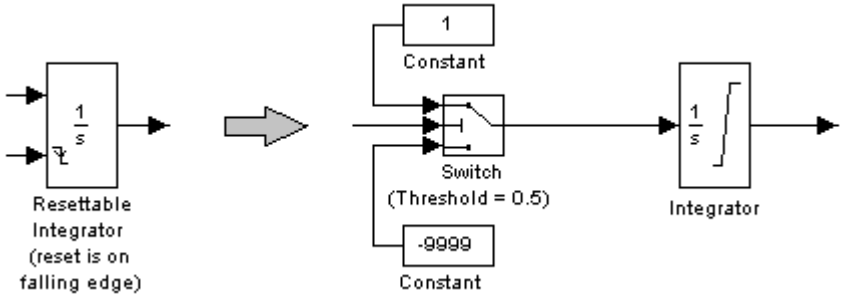

Figure 9-2: Modelling of resettable integrator

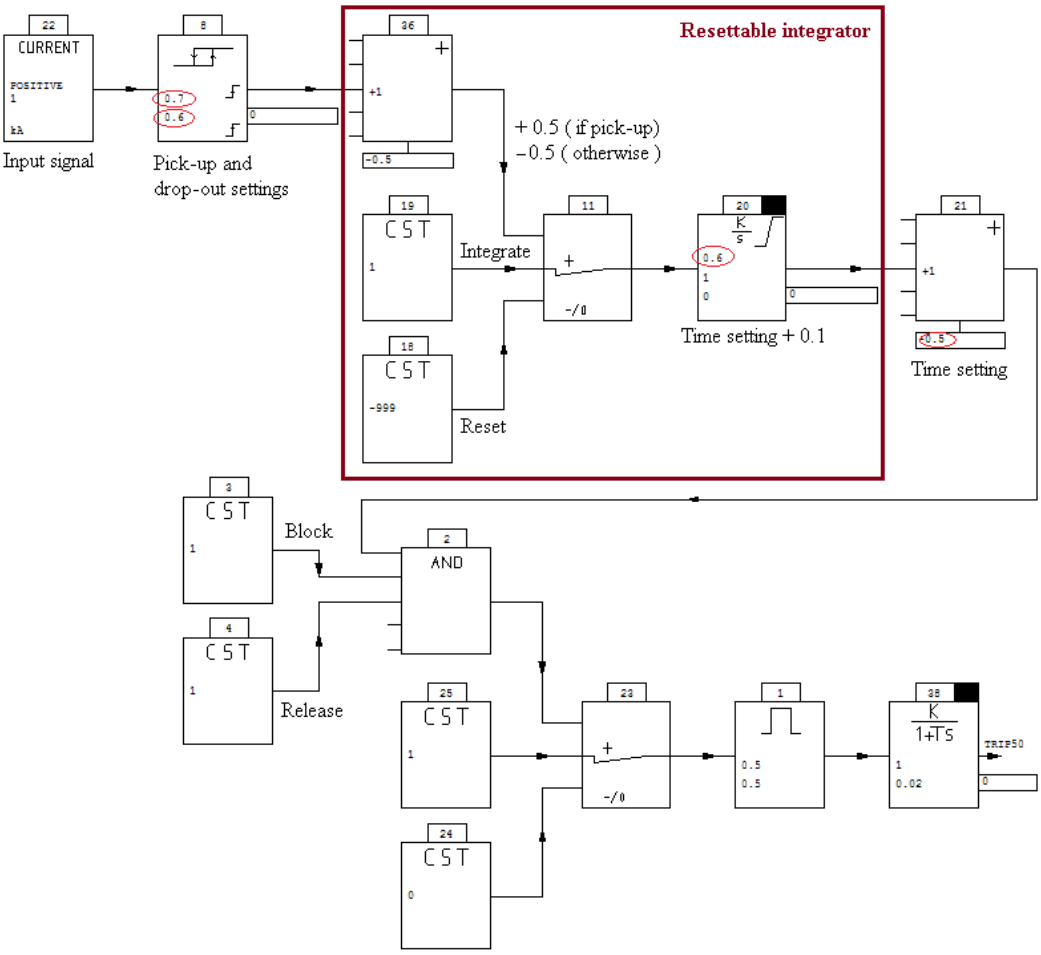

Figure 9-3: EUROSTAG block diagram of non-directional over-current protection

The same model is presented below in MATLAB/SIMULINK as well as SCILAB/XCOS environment as these programs are also used in PEGASE project.

Figure 9-4 shows the full block diagram of the non-directional instantaneous/definite time over-current protection that includes drop-out feature, blocking and releasing inputs, and provides a preset length of output signal.

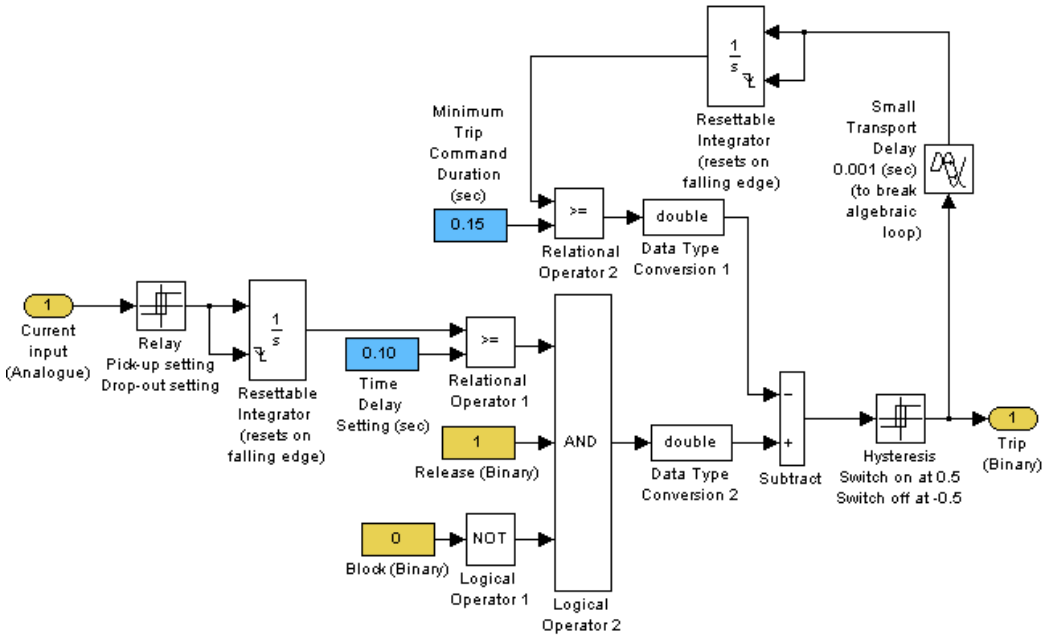

Figure 9-4: MATLAB/SIMULINK block diagram of non-directional over-current protection using resettable integrator

In Figure 9-5 the same model as in Figure 9-4 is presented with the exception of the resettable integrator element that is replaced with an equivalent scheme.

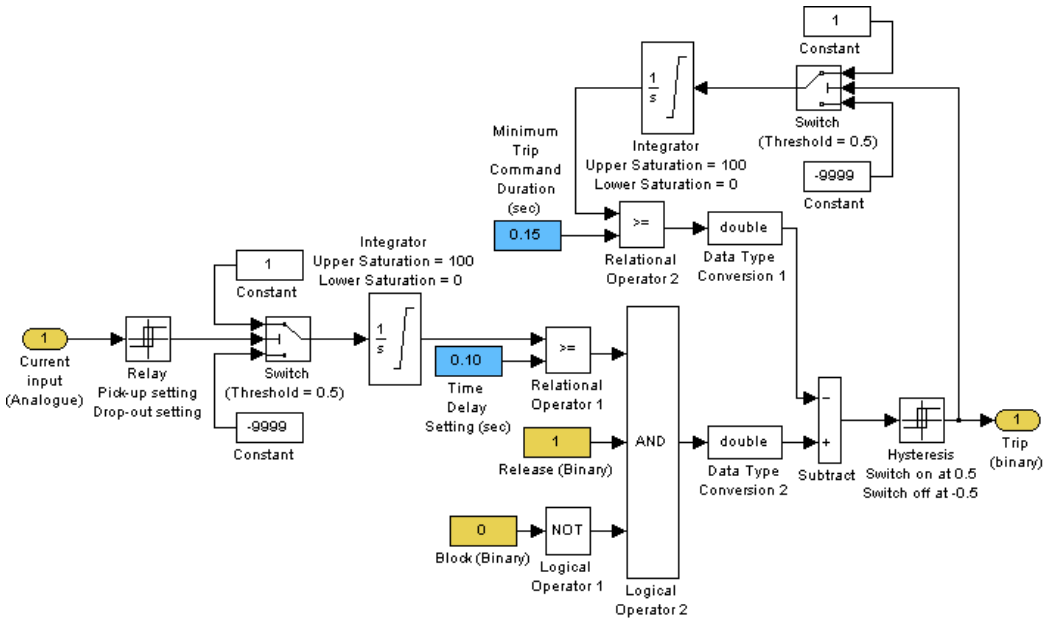

Figure 9-5: MATLAB/SIMULINK block diagram of non-directional over-current protection using equivalent scheme instead of resettable integrator

In case the short circuit duration is close to the relay time delay setting, the tripping impulse length can be very short. If software developers decide that they can deal with the variable length of output signal (simulation time step is decision making criterion here) then the model can be greatly simplified (see Figure 9-6).

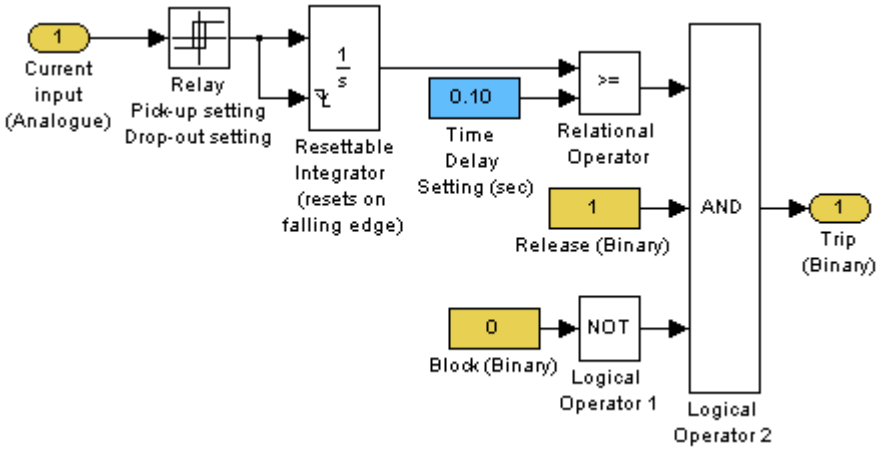

Figure 9-6: Simplified MATLAB/SIMULINK block diagram of non-directional over-current protection

In Figure 9-7 the full model of non-directional over-current protection is shown in Scilab format as well.

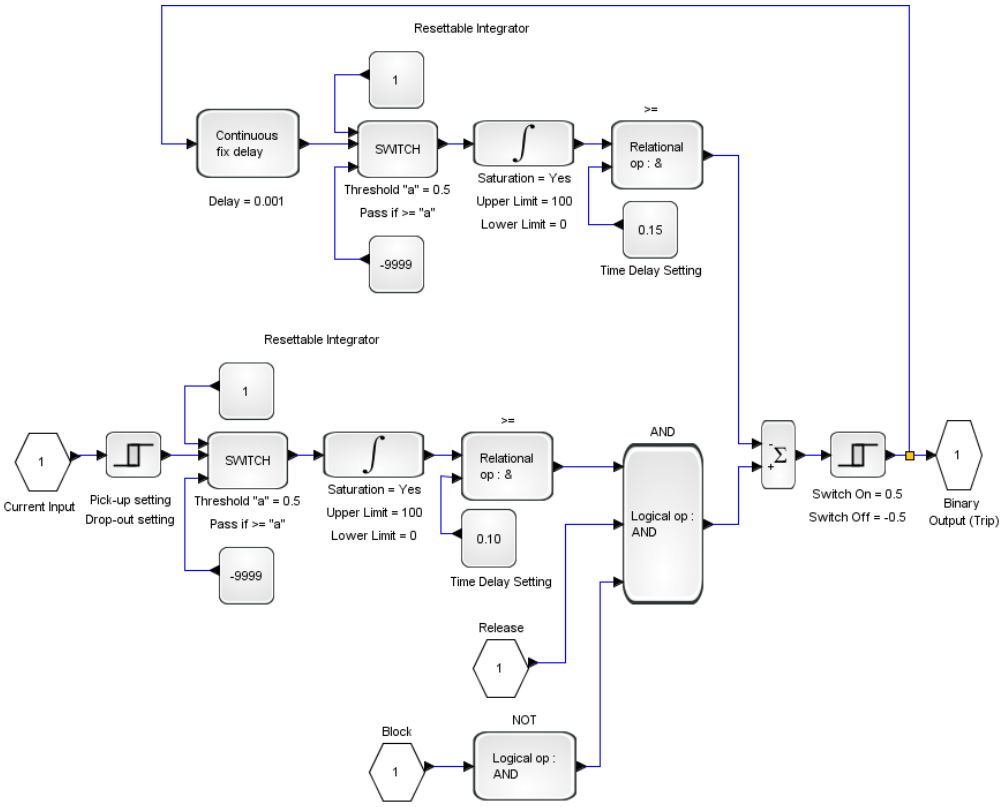

Figure 9-7: SCILAB/XCOS block diagram of non-directional over-current protection

Some additional features that can be modelled by the given model, using the blocking and releasing inputs [3, 4, 8-13]:

Dynamic cold load pickup function

Sometimes it may be necessary to dynamically increase the pickup values if, during starting, certain elements of the system show an increased power consumption after a long period of zero voltage (e.g. air-conditioning systems, heating installations, motors). Thus, a general raise of pickup thresholds can be avoided taking such starting conditions into consideration. A number of manufacturers have implemented such feature in their relays.

The dynamic cold load pickup feature can be simulated by blocking one over-current protection model and releasing the other when necessary.

Switch on to fault (SOTF) logic

The instantaneous high-current switch-onto-fault protection function is usually provided to disconnect immediately and without delay feeders that are switched onto a high-current fault. It is primarily used as fast protection in the event of energizing the feeder while the earth switch is closed, but can also be used every time the feeder is energized - in other words also following automatic re-closure.

If necessary, the SOTF function can be easily modeled by shortly releasing the advanced over-current protection model during feeder energization.

Voltage start

Voltage start logic can be implemented by releasing the protection if voltage decreases below a preset value.

Blocking during power swings or re-closure cycle

Protection can be blocked in case of power swings or during automatic re-closure cycle to avoid unwanted trip during these conditions.

Circuit Breaker Failure Protection

The circuit breaker failure function ensures fast back-up tripping of surrounding breakers. A current check with extremely short reset time is used as check criteria to achieve a high security against unnecessary operation. A current check can be performed using the non-directional over-current protection model.

Some typical features of non-directional over-current protection that were left out of the model in order to fit it better into the framework of PEGASE project [3, 4, 8-13]:

Inrush restraint

When the numerical relay is installed, for instance, to protect a power transformer, large magnetizing inrush currents can flow when the transformer is energized. These inrush currents may be several times the nominal transformer current, and, depending on the transformer size and design, may last from several milliseconds to several seconds.

Although pickup of the relay elements is based mostly only on the fundamental harmonic component of the measured currents, false device pickup due to inrush is still a potential problem since, depending on the transformer size and design, the inrush current also comprises a large fundamental harmonic component. For that reason relays often feature an integrated inrush restraint function. It prevents the pickup of the over-current elements if inrush conditions are present.

Inrush current contains a relatively large second harmonic component (twice the nominal frequency) which is nearly absent during a fault current. The inrush restraint therefore is based on the evaluation of the 2nd harmonic present in the inrush current. Digital filters are used to conduct a Fourier analysis of all three phase currents to detect the magnitude of 2nd harmonic.

Cross blocking

Since the harmonic restraint operates individually per phase, the protection is fully operative even when the transformer is switched onto a single-phase fault, whereby inrush currents may possibly be present in one of the healthy phases. It is, however, possible to set the protection in a way that when the permissible harmonic content in the current of only one single phase is exceeded, not only the phase with the inrush current but also the remaining phases (and over-current elements in them) are blocked.

Voltage restraint / Voltage control

For backup over-current protection, for instance, of generators, ordinary over-current relays are sometimes difficult to apply, due to the decaying characteristic of the fault current. The value of the fault current will be progressively reduced due to armature reaction, to a value less than full load current. Therefore, normal over-current relays set above the load current or maximum permissible overload, cannot be applied to provide time delayed backup protection as they will not operate for these fault conditions. For successful application of generator backup protection, the operating characteristics of the relay are required to be a function of voltage and current. There are two types of relay that are customarily used for these applications, namely voltage restrained and voltage controlled over-current relays.

With voltage restrained over-current relays, when the voltage falls below a set value, the operating time of the over-current characteristic is continuously reduced with declining voltage.

In voltage controlled over-current relays, the operating time characteristic is changed from the load characteristic to the fault characteristic when the voltage falls below a set level.

10. Non-directional inverse time over-current protection

Properties	Description
ANSI/IEEE C37.2 standard device number	51
IEC 61850 logical node name	PTOC
Input signals	Current (phase or positive sequence)
Output signals	Binary 0 or 1

From the modeling point of view the model of inverse time over-current protection is essentially the same as for instantaneous/definite time over-current protection. The only difference concerns the timer element [3, 4, 8-13].

The time delay depends on the ratio between the current measured and the operating threshold. The higher the current means the shorter the time delay (see Figure 10-1).

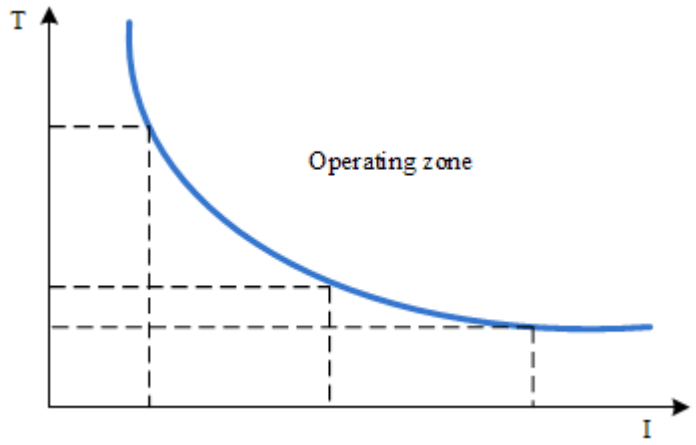

Figure 10-1: Inverse time protection

Inverse time protection operation is defined, for instance, by IEC 60255-3. This standard defines several types of inverse time protection that are distinguished by the gradient of their curves: standard inverse, very inverse or extremely inverse time protection [4, 10-12].

Trip time curves according to IEC:

Trip time curve	Equation
Normal Inverse (Type A)	$t = \frac{0.14}{\left(\frac{I}{Ip}\right)^{0.02} - 1} \cdot Tp \quad [s]$
Very Inverse (Type B)	$t = \frac{13.5}{\left(\frac{I}{Ip}\right)^{1} - 1} \cdot Tp \quad [s]$

Extremely Inverse (Type C)	$t = \frac{80}{\left(\frac{I}{Ip}\right)^2 - 1} \cdot Tp \quad [s]$
Long Inverse (Type B)	$t = \frac{120}{\left(\frac{I}{Ip}\right)^1 - 1} \cdot Tp \quad [s]$
For all characteristics	t – trip time in seconds Tp – setting value of the time multiplier I – fault current Ip – setting value of the pick-up current
Pickup threshold	Approximately 1.10·Ip
The tripping times for I/Ip ≥ 20 are identical with those for I/Ip = 20.	

When the current element picks up, the time delay of the trip signal is calculated using an integrated measurement process. The calculated time delay is dependent on the actual fault current flowing and the selected tripping characteristics. Once the time delay elapses, a trip signal is issued.

Let us take as an example IEC Normal Inverse (Type A) characteristic. The respective model in MATLAB/SIMULINK environment is presented in Figure 10-2. The attention should be drawn to the fact that the pick-up threshold in most relays is 1.1 times the current setting Ip in order to avoid division by zero that can take place when I = Ip (see the equations for inverse time characteristics) as well as very large calculated tripping times when I is just slightly larger than Ip.

In the current model tripping time calculation is switched on (see switch element in the block diagram) as soon as relay picks-up (I ≥ 1.1 Ip). To avoid negative calculated time values when the relay has not yet picked-up or division by zero, time delay calculation element is switched off if I < Ip.

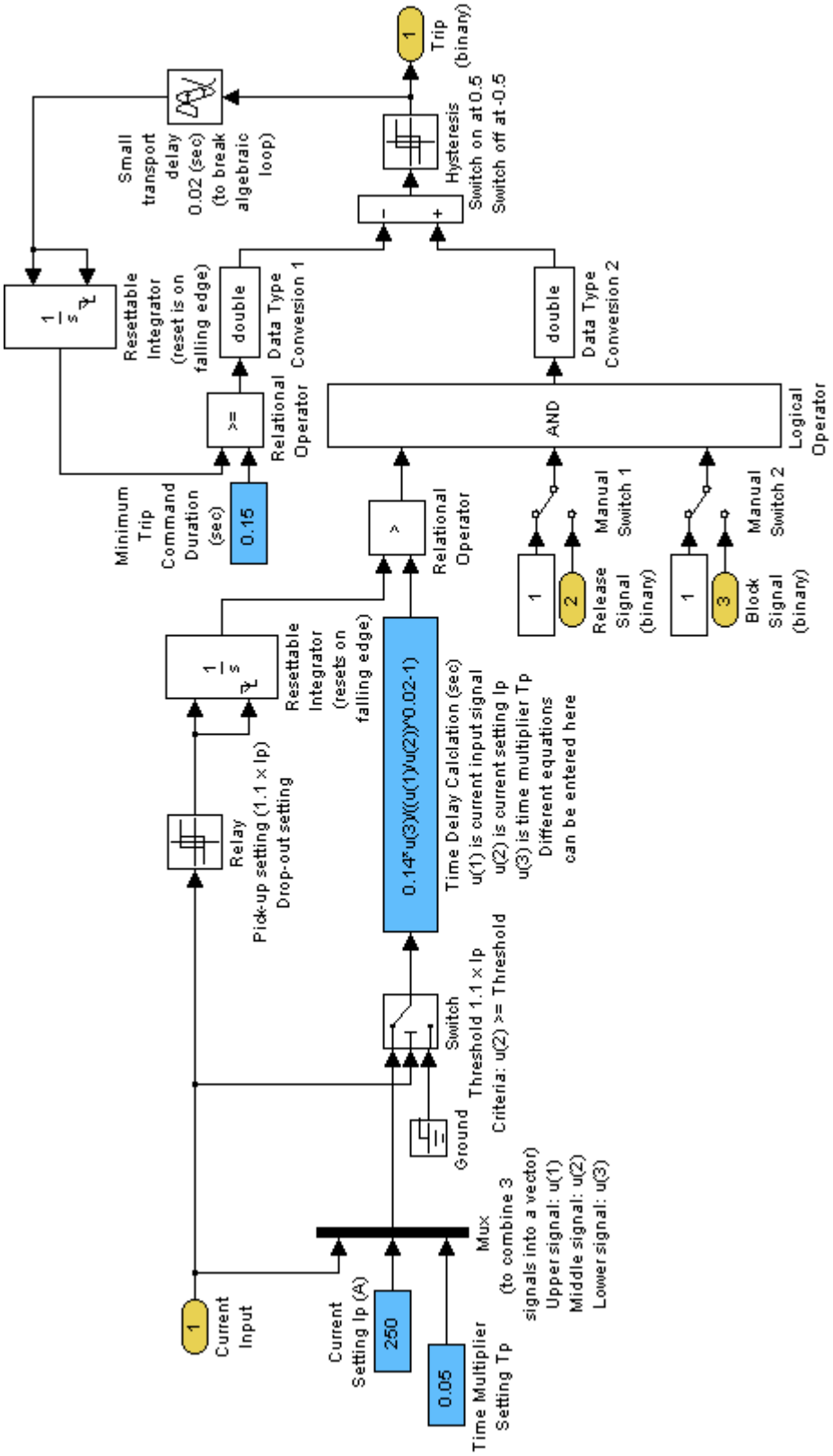

Figure 10-2: MATLAB/SIMULINK block diagram of O/C protection with inverse time delay characteristic

Although the equations for inverse time characteristics are relatively simple, the resulting model is not, if it is developed using standard mathematical blocks and transfer functions.

In Figure 10-3 (EUROSTAG) and Figure 10-4 (SIMULINK) a sample model is presented that includes one equation for inverse time characteristic (without logical protection against division by zero and negative or extremely large calculated tripping times).

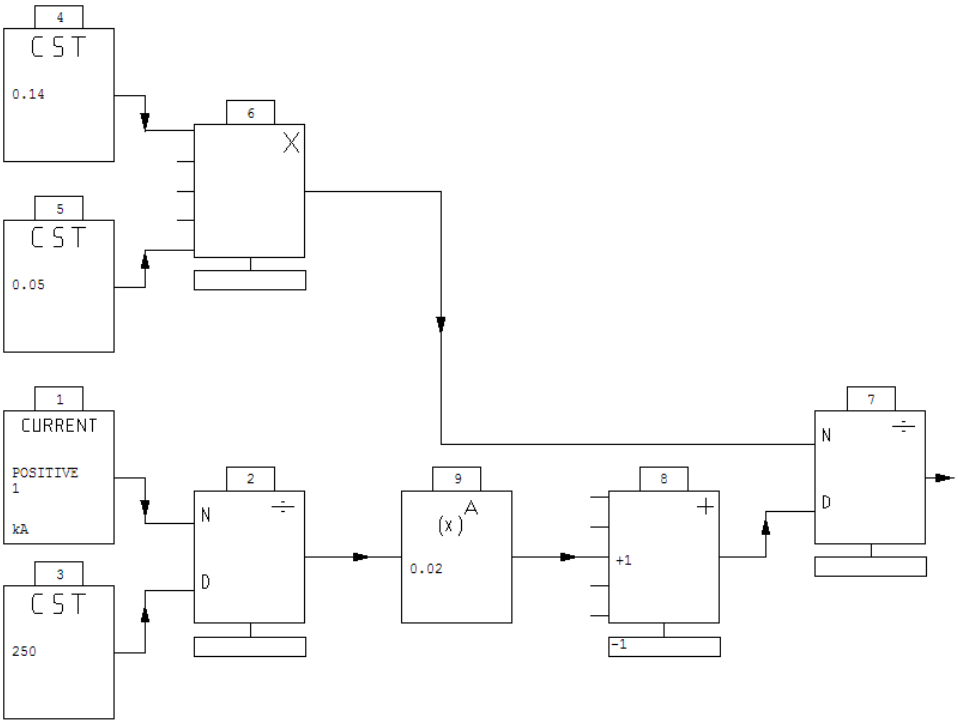

Figure 10-3: Equation for inverse time characteristic using EUROSTAG

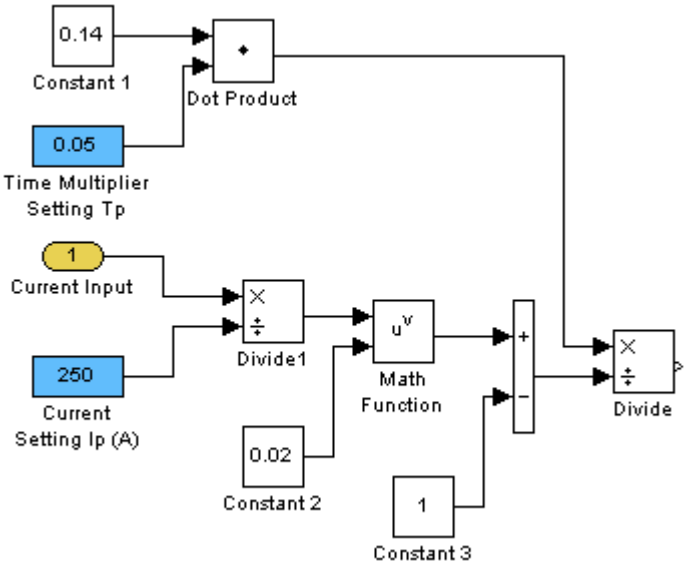

Figure 10-4: Equation for inverse time characteristic using SIMULINK

Even if the equation for inverse time characteristic can be written directly into some elementary function block, it is necessary to provide the possibility to switch between different characteristics. In Figure 10-5 a part of a model is presented in which it is possible to choose the necessary characteristic by providing appropriate control signal to the switching elements.

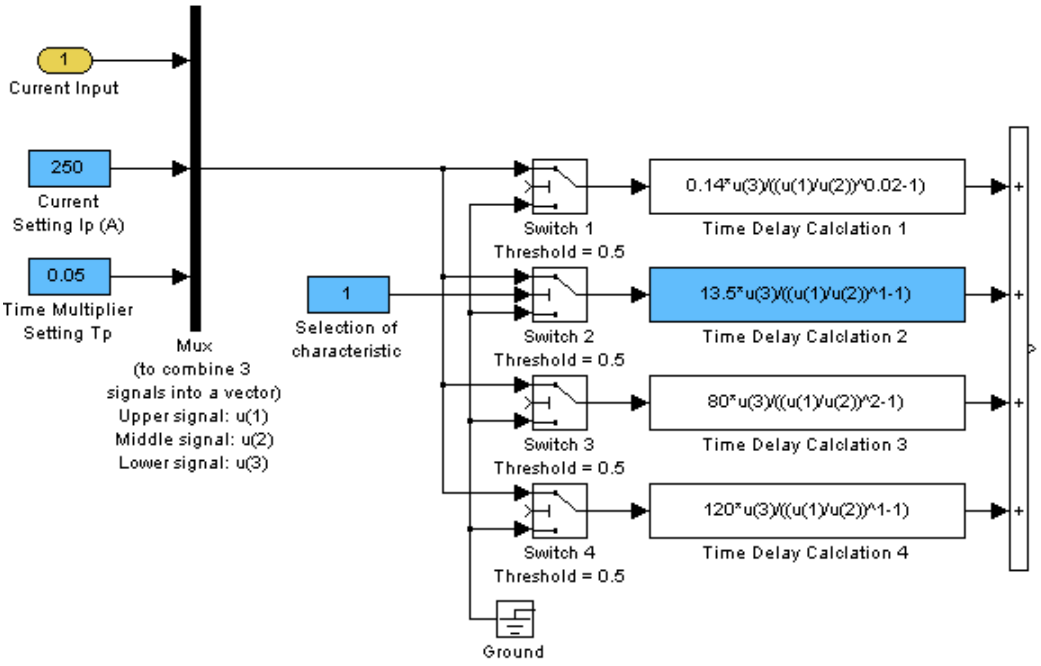

Figure 10-5: Part of a model for selection of necessary characteristic

The more characteristics are to be included the larger the model will be. Taking into account the scale of pan-European simulator, it seems that it would be better to develop programmatically a dedicated element that would include all the necessary characteristics and settings as shown in Figure 10-6:

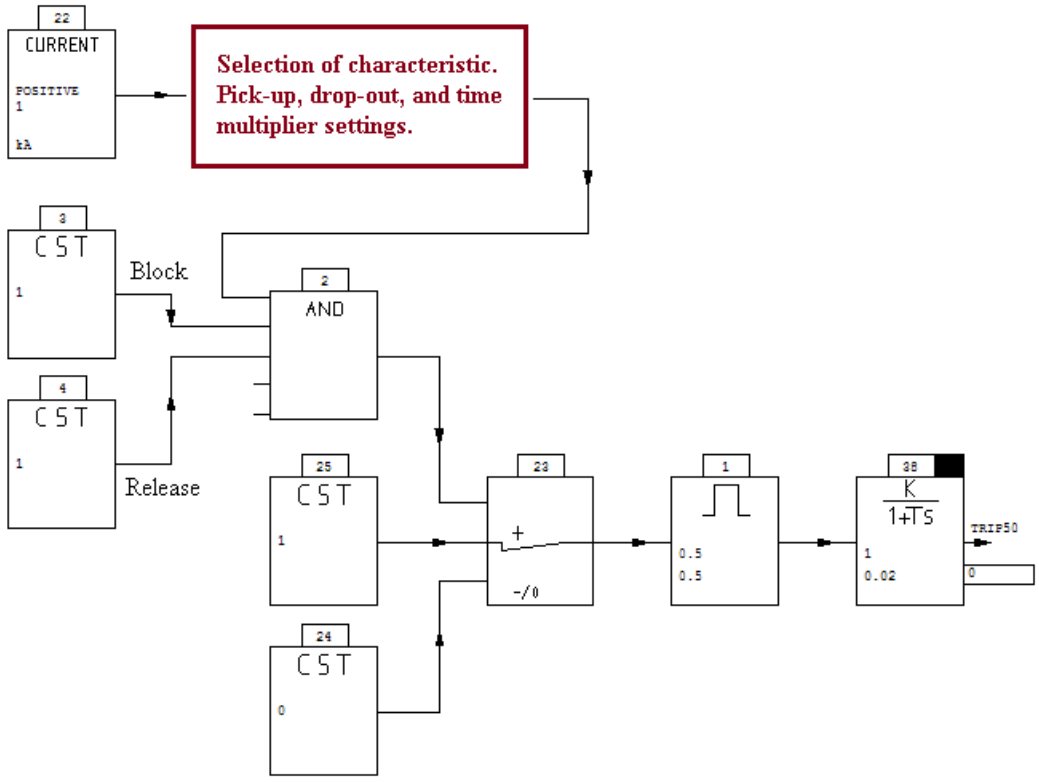

Figure 10-6: Pseudo EUROSTAG block diagram of O/C protection with inverse time delay characteristic

Some typical features of non-directional over-current protection that were left out of the model in order to fit it better into the framework of PEGASE project are discussed below [3, 4, 8-13].

User defined curves

It should be noted that some manufacturers offer the possibility to utilize user defined characteristics. These characteristics are then defined point by point. Thus, for instance, in SIEMENS 7SJ6 relays up to 20 pairs of values (current, time) may be entered. The device then approximates the characteristic, using linear interpolation. The dropout curve may be user-defined as well.

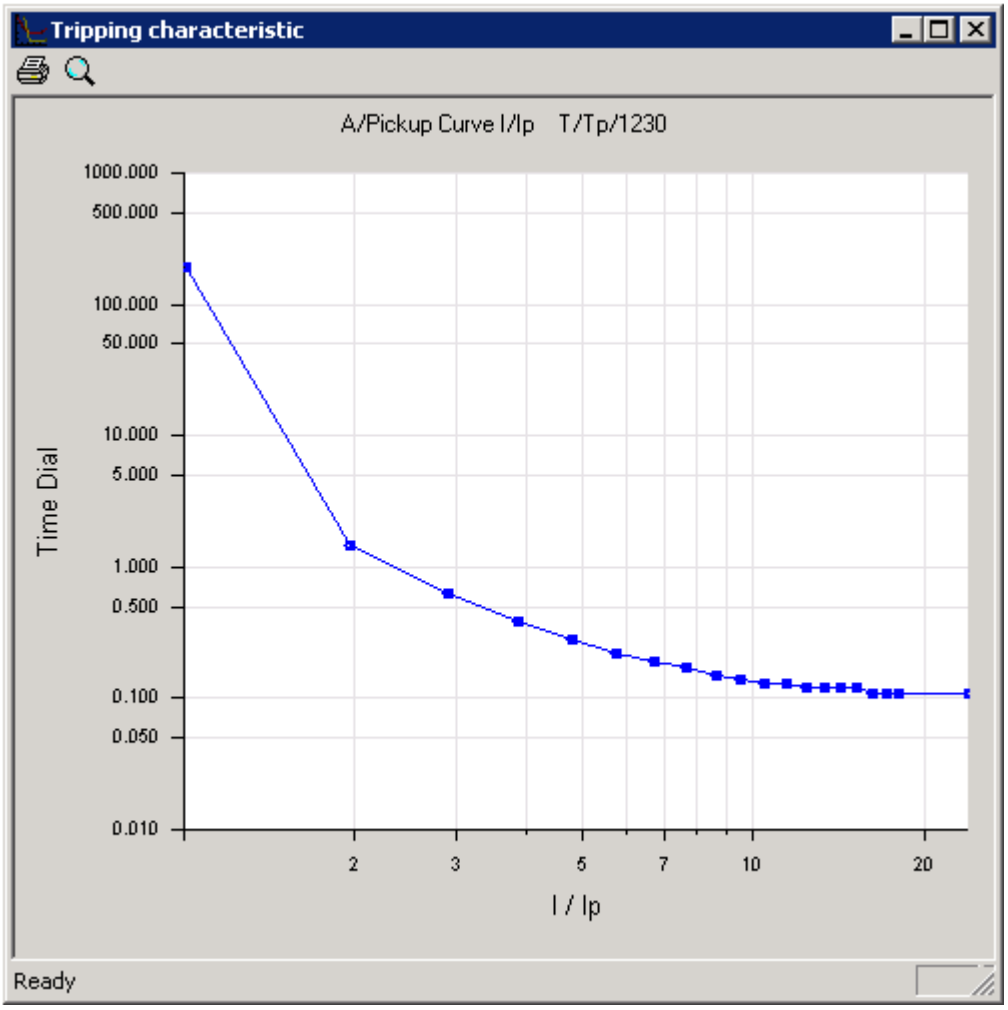

Figure 10-7: An example of user defined curve in SIEMENS 7SJ6 relay

Drop-out behaviour

Very often it is possible to select whether the dropout of an element is to occur instantaneously after the threshold has been undershot or whether dropout is to be performed according to some characteristic. “Instantaneously” means that pickup drops out when the pickup value of approx. 95 % is undershot. For a new pickup the time counter starts at zero.

Other curve shapes

IEEE, GE Type IAC, I2t and other standard curve shapes might be also considered (in addition to IEC).

11. Directional over-current protection

Properties	Description
ANSI/IEEE C37.2 standard device number	67
IEC 61850 logical node name	PTOC
Input signals	Current (phase or positive sequence)
Output signals	Binary 1 or 0

Directional over-current relays are constructed using a normal over-current unit plus a unit that can determine the direction of the power flow in the associated distribution system element. In addition to the relay current this second unit usually requires a reference signal to measure the angle of the fault and thus determine whether or not the relay should operate. Generally, the reference or polarization signal is a voltage but this can also be a current input [3].

The ability to differentiate between a fault in one direction or another is obtained by comparing the phase angle of the operating current phasor, which varies directly with the direction of the fault, and some other system parameter that is not dependent on the fault location. This constant parameter is referred to as the polarizing quantity.

For directional relays applied to operate during a fault, it is important to remember two facts [3, 4, 10-18]:

1. The system voltage will collapse at the point of the short circuit. Therefore the polarizing voltage must not include the faulted phase.

2. The fault power factor is low, i.e. the current lags the voltage by nearly 90°. The choice of connections to obtain correct directional discrimination for unbalanced faults usually is restricted to those shown in Figure 11-1. It is possible to determine the best connection of the three for any given set of system and fault conditions by analyzing the phasors within the relay for the most probable conditions of load angles, faults and the effect of arc resistance. If any of these conditions change, the preferred connection will also change. Since it is not reasonable to account for all of the possible variations, it is necessary to select the best compromise for the widest range of possibilities. Of the three shown, the 90° connection is usually preferred.

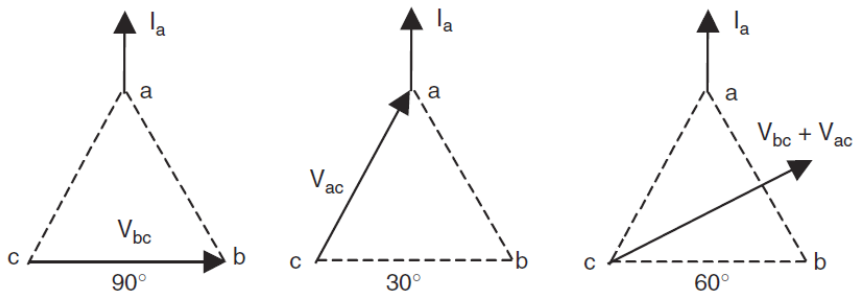

Figure 11-1: Conventional connections for directional phase relays

It is said that the protection detects the "direction of the current"; in reality it detects the sign of the active power. Thus, the phase displacement φ between the voltage and the short-circuit current must be known.

Directional phase over-current protection is activated if the following two conditions apply to a time equal to the time delay chosen:

- The current is higher than the setting threshold;

- The current phase in relation to the polarizing voltage is in a range referred to as the tripping zone.

Unfortunately in pan-European simulator only the positive sequence phasors are available; therefore it is not possible to reproduce any of the existing direction determination approaches.

Let us develop a simple directional element using only positive sequence quantities. The task is simplified by the fact that only three phase faults should be taken into account.

To begin with let us calculate the phase displacement φ between the positive sequence quantities as shown in equation (14) [3, 17, 18]:

$$\varphi = \angle I_1 - \angle U_1 \tag{14}$$

In this case the forward zone of the protection (see Figure 11-2) can be shown as a half plane where the active power detected by the protection is positive:

$$-\frac{\pi}{2} \le \varphi \le \frac{\pi}{2} \quad \Rightarrow \quad \cos(\varphi) \ge 0 \tag{15}$$

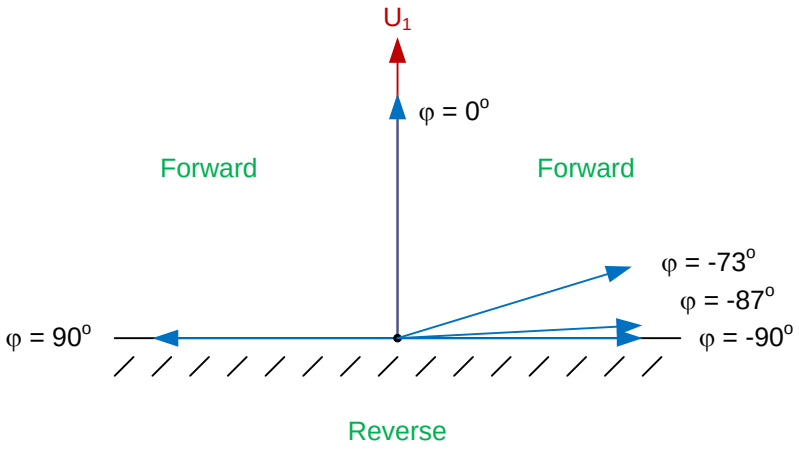

Figure 11-2: A plane that represents forward and reverse direction of current (active power). One voltage and five current phasors are displayed.

The reverse zone of the protection on its turn is a half plane where the active power detected by the protection is negative:

$$\frac{\pi}{2} \le \varphi \le \frac{3 \cdot \pi}{2} \quad \Rightarrow \quad \cos(\varphi) \le 0 \tag{16}$$

In purely resistive circuits voltage and forward current waveforms are in phase and the phase displacement is φ = 0°. In purely inductive and capacitive circuits it is respectively φ = -90° and φ = 90°. It means that the forward flowing current phasor will always be located in the forward plane of Figure 11-2.

The problem with the approach given in equation (14) is that the fault power factor usually is low, i.e. the current lags the voltage by nearly 90°. Thus for typical X to R ratios between 3 and 20 the phase displacement angle is 73° to 87° [3]:

$$3 < \frac{X}{R} < 20 \Rightarrow tg\varphi = \frac{X}{R} \Rightarrow 71.6° < \varphi < 87.1° \quad (17)$$

With angle values close to 90°, direction determination can becomes unreliable.

To resolve the issue that fault current is typically highly lagging, the directional unit can be optimized to detect lagging current conditions rather than 1.0 power factor conditions.

One approach, shown in Figure 11-3, is to phase shift the voltage phasor so that the shifted voltage phasor is in phase with current when current lags the 1.0 power factor condition by some setting (SHIFT).

$$\varphi = \angle I_1 - \angle U_1 + SHIFT \quad (18)$$

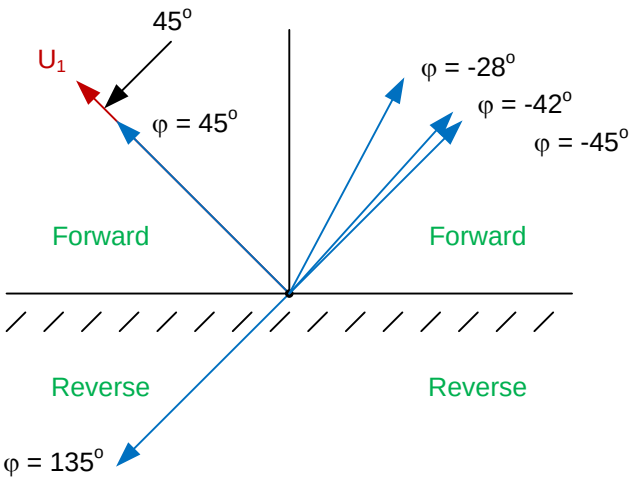

Figure 11-3: A plane that represents forward and reverse direction with voltage phasor shifted by 45°

Now, during a fault, the angle φ values are safely in the forward plane for reliable direction determination.

It should be noted that the optimization by equation (18) can lead to wrong direction determination as the phasor can go into the reverse plane even in case of a forward fault. Using, for instance, the plane showed in Figure 11-3, it can happen in case of a highly capacitive forward fault.

To avoid wrong direction determination, the angle φ should be limited within the ranges showed in Figure 11-4 and equations (19). Some margin (for instance, 2° in both directions) can be set to separate safely forward and reverse directions [3, 4, 16-18].

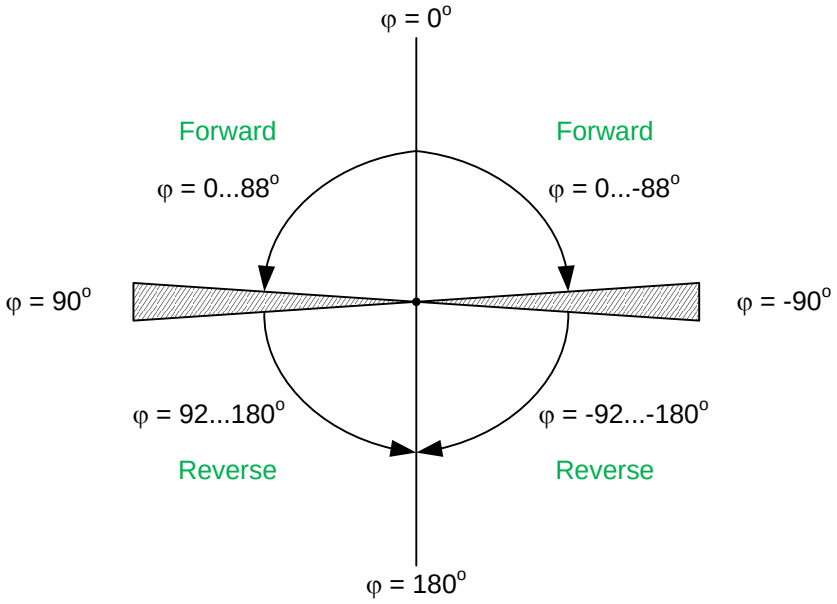

Figure 11-4: Limits of angle φ for reliable direction determination

$$\begin{aligned} &\text{Forward} \quad \text{if} \quad -88° \le \varphi \le 88° \\ &\text{Reverse} \quad \text{if} \quad -92° \le \varphi \le -180° \quad \text{or} \quad 92° \le \varphi \le 180° \end{aligned} \tag{19}$$

Since ω·t is continually growing quantity, the angle of current and voltage phasors is not constant (see Figure 11-5).

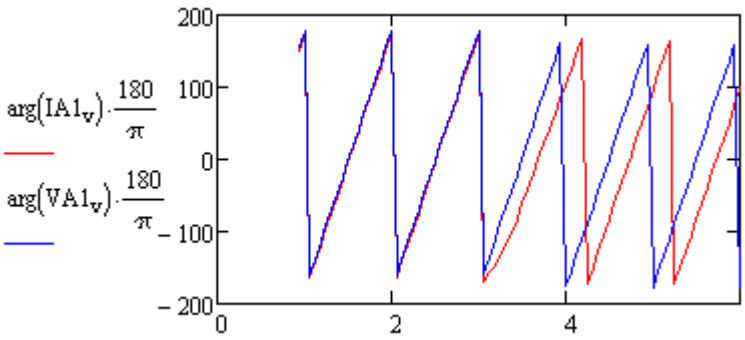

Figure 11-5: The continually growing angles of current and voltage

If the two waveforms seen in Figure 11-5 do not "reset" at the same time (due to angle difference between current and voltage), the angle difference calculation can lead to substantial inaccuracies (see Figure 11-7).

Graphical explanation of different reset times of voltage and current vectors is presented in Figure 11-6.

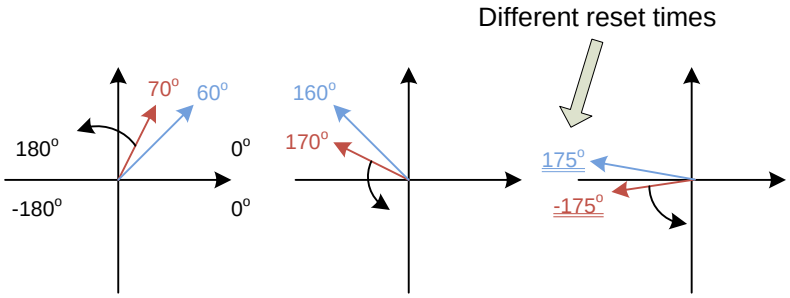

Figure 11-6: Graphical explanation of different reset times of voltage and current vectors

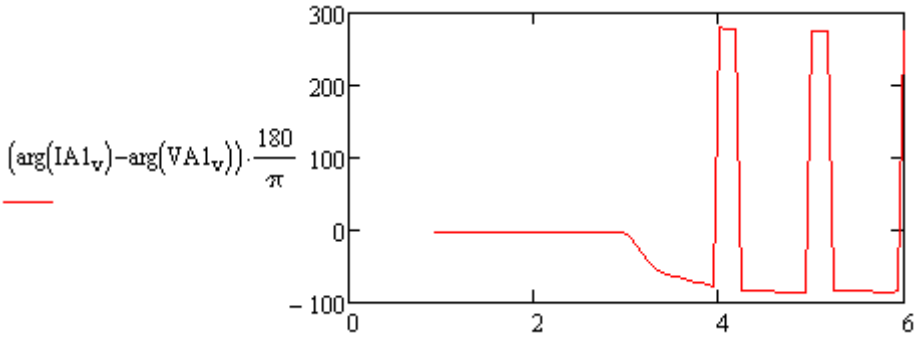

Figure 11-7: Possible problem with angle difference calculation due to different reset times of current and voltage

To avoid this, the angle difference can be calculated as shown in equation (20).

$$\begin{cases} \varphi = \angle I_1 - \angle U_1 & \text{if} \quad \left|\angle I_1 - \angle U_1\right| < \pi \\ \varphi = \angle I_1 - \angle U_1 - 2\cdot\pi & \text{if} \quad \left(\angle I_1 - \angle U_1\right) > \pi \\ \varphi = \angle I_1 - \angle U_1 + 2\cdot\pi & \text{if} \quad \left(\angle I_1 - \angle U_1\right) < -\pi \end{cases} \tag{20}$$

The block diagram of suggested directional determination unit is presented in Figure 11-8. It is modeled using equations (18), (19), and (20).

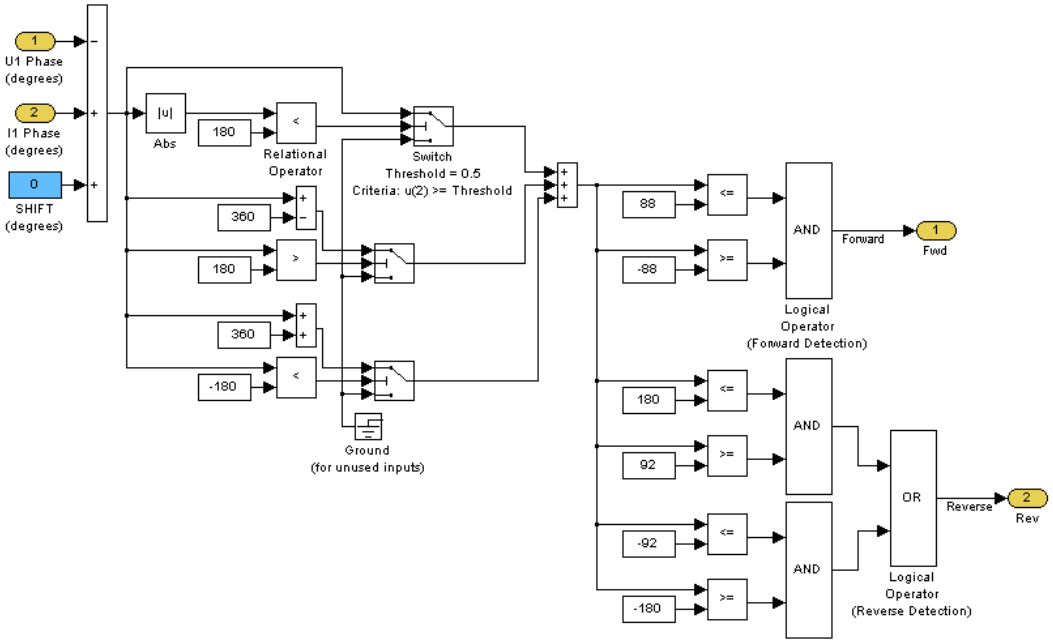

Figure 11-8: Block diagram of direction determination unit

As with inverse time over-current protection it seems it is better to develop a dedicated block for direction determination (as in Figure 11-9), possibly according to the previously presented algorithm.

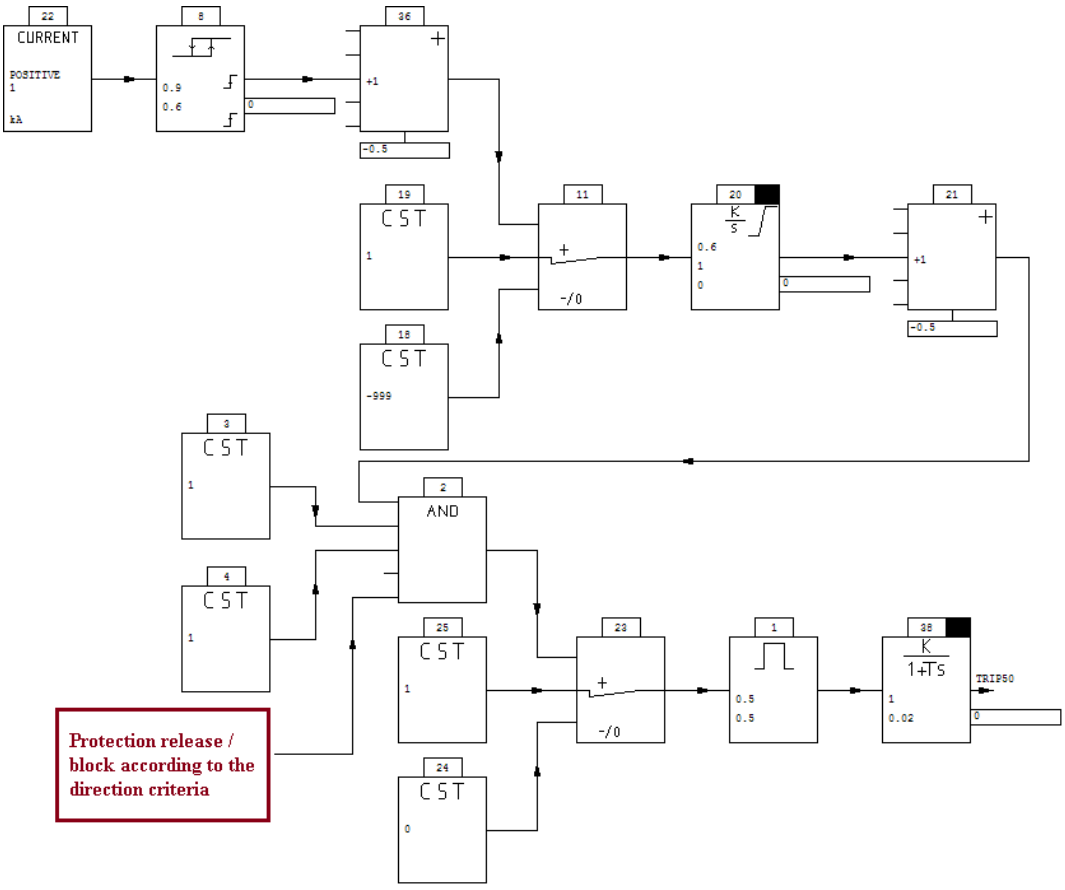

Figure 11-9: Pseudo model with dedicated direction determination element

This approach would be especially beneficial in case of directional inverse time over-current protection (see Figure 11-10)

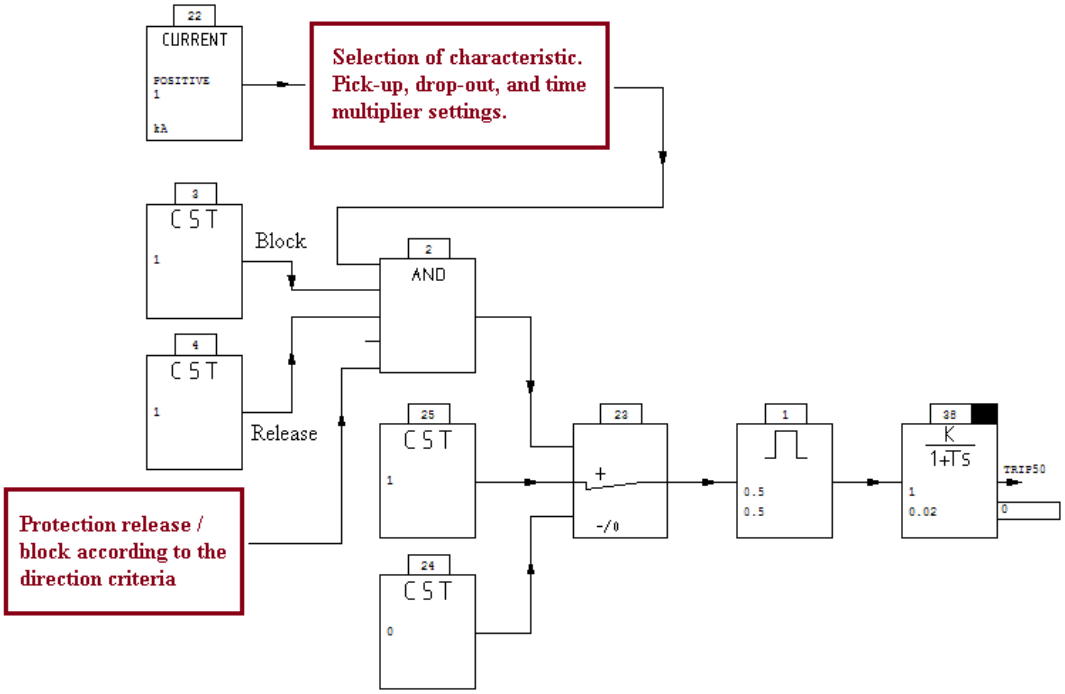

Figure 11-10: Pseudo model with dedicated elements for inverse time characteristic and direction determination

12. Zero (residual) and negative sequence over-current protection

Properties	Description
ANSI/IEEE C37.2 standard device number	46 (negative sequence over-current) 50N (instantaneous zero current) 51N (inverse time zero current) 67N (directional zero current)
IEC 61850 logical node name	PIOC (instantaneous) PTOC (definite time, inverse time)
Input signals	Current (zero or negative sequence)
Output signals	Binary 1 or 0

Zero sequence over-current protection is used to protect the network against earth faults. The protection is activated if the residual current 3I0 = I1 + I2 + I3 rises above the setting threshold. The residual current corresponds to the current flowing through earth [3, 4, 10-16].

Negative sequence over-current protection is used to protect a rotating machine (motor or generator) against current unbalances. This unbalance may come from:

- the power source (transformer or generator), which does not supply a symmetrical three-phase voltage;
- other consumers who do not constitute a symmetrical load causing the power supply network to have a voltage unbalance;
- from a two-phase power supply following a blown fuse or a phase being cut;
- from an inversion of phases due to a connection error.

Both protections operate in a similar way to the phase or positive sequence over-current protection. Therefore the same models can be applied, only with different input signals that can be easily obtained using EUROSTAG measurement blocks:

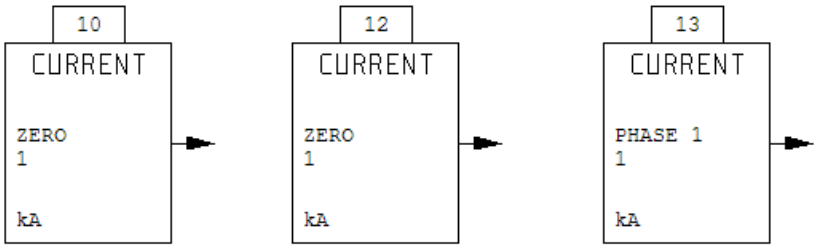

Figure 12-1: EUROSTAG measurement blocks for different current signals

13. Differential protection

Properties	Description
ANSI/IEEE C37.2 standard device number	87 87T (transformer) 87G (generator) 87B (busbar)
IEC 61850 logical node name	PDIF
Input signals	Current phase and angle (phase or positive sequence) from all sides of the protected object
Output signals	Binary 1 or 0

There are protection functions that are simple from the point of view of general operational principles but at the same time are very complicated from the point of view of development of simplified models. Let us take as an example the numerical busbar differential protection. Very stringent demands regarding security, availability and selectivity are imposed on the busbar protection as false operation of it can lead to very serious consequences [3, 5, 16, 19-24].

1) Security

The protection may not under any circumstances trip in the event of an external fault as the loss of a busbar in general causes shut-down of a large section of the system. Tripping is therefore always dependent on a number of criteria.

2) Availability

The failure to trip or the delayed tripping of a busbar fault creates the risk of system instability and may under critical circumstances cause a system collapse due to the voltage collapse on the busbar. Furthermore, severe damage could be caused at the fault location due to the very high short-circuit current level.

3) Selectivity

In multiple busbar substations, only the busbar section which is affected by the fault must be cleared, so that the power supply via the other busbars is ensured. For this purpose, a separate measuring unit for each bus section is required, along with a complex image of the isolator positions for the allocation of the feeder currents and distribution of the trip commands.

The stringent demands that are put on busbar differential protection result in very complicated internal logic.

In Figure 13-1 the structure of Siemens numerical busbar protection 7SS52 is presented as an example. This protection is fully numerical and consists of a central unit and de-centralized bay units [24].

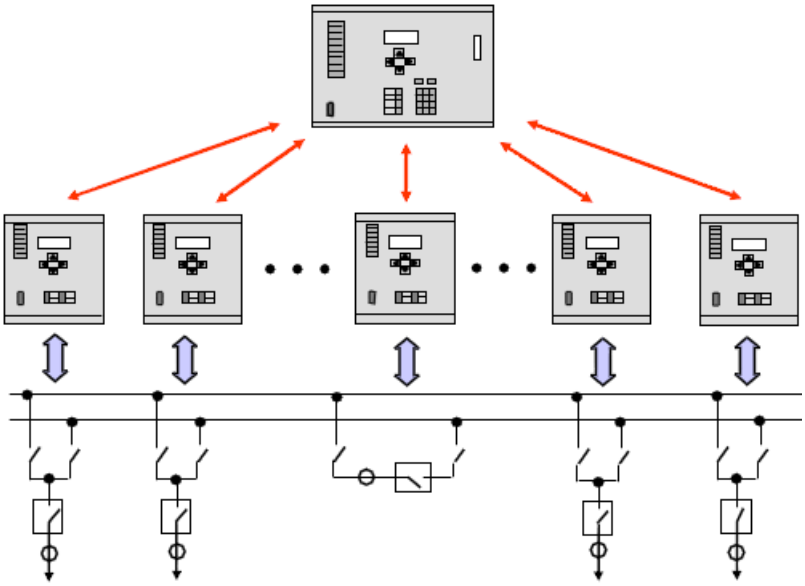

Figure 13-1: Structure of the numerical busbar protection 7SS52

Due to the simple current comparison, the principle of differential protection is very straight forward. If the current entering into the protected zone is not equal to the current leaving this zone, the current differences at the ends of the protected zone indicates the fault.

In real life application such as 7SS52 the fault recognition depends on the busbar configuration, current transformer placement, and position of all isolators and circuit breakers. This information along with measured currents is transferred from the bay units to the central unit for further processing.

Trip decision is based on 3 independent measurements. 2 measurements are based on busbar configuration (two independent processors execute the protection algorithm on alternate data samples), and the third measurement considers all busbar sections independent of the isolator replica (check zone). All three processors must reach a trip decision independently before the trip command is released.

Independent characteristics for check zone and bus-selective zone; modification of stabilization current so that it decays at the rate of $\tau = 64$ ms; special restraint to avoid over-stabilization by separate addition of the magnitudes of positive and negative currents and selection of the smaller sum; different algorithms working in parallel and many more factors influence the operation of 7SS52 [24].

As a result it is very hard to simplify the logic involved in 7SS52 (or any other similar device from ABB, GE, Areva etc.) so that the model would relatively accurately imitate the real protection device.

Fortunately there are two specific features of busbar differential protection that allow taking very simple approach regarding modeling. These features are:

1) Rarity of occurrence of busbar faults

Busbar faults are on occasion caused by mechanical or insulator defects, but are frequently caused by incorrect switching operations. Statistically one can count one busbar fault every 10 years (0.63 to 2 faults per feeder in 100 years according to CIGRE survey [21]).

2) 100% selectivity of busbar protection

Busbar protection is 100% selective and therefore only responds to faults within its protected zone. The boundary of the protected zone is uniquely defined by the location of the current transformers. Time grading with other protection systems is therefore not required, allowing for tripping without additional delay.

Therefore on those relatively rare occasions when there is a genuine fault inside the protection zone, one can be almost sure that this fault will be quickly and selectively isolated.

In case of pan-European simulator it means that it is not necessary to develop burdensome model at all. Any fault inside the busbar differential protection zone can be treated with immediate opening of respective circuit breakers (see Figure 13-2).

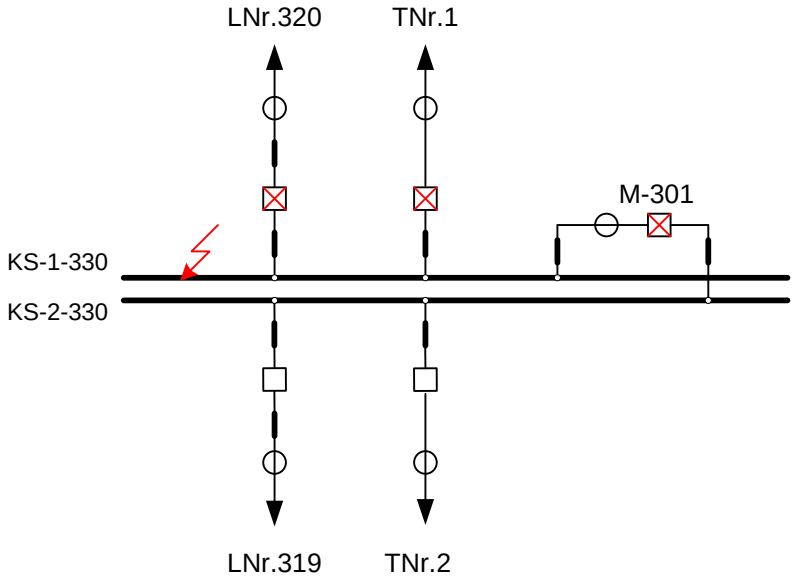

Figure 13-2: Selective isolation of busbar fault

Detailed primary schemes of stations and substations will not be applied in the pan-European simulator, except maybe for the most important nodes and for dispatcher off-line training simulations. However it must be noted that the arrangement and connection of incoming and outgoing feeders in stations and substations and the number of busbars have an important influence on the supply reliability of the power system. Knowledge of the exact primary schemes can be very useful for transmission system operators.

The same approach can be applied for other differential protections as well.

Let us suppose that pan-European simulator operator wants to simulate a fault at generator, transformer or line during off-line contingency studies. In this case the fault can be simulated by simply switching off the faulted power system element. This approach will be far more reliable than reliance on heavily simplified model.

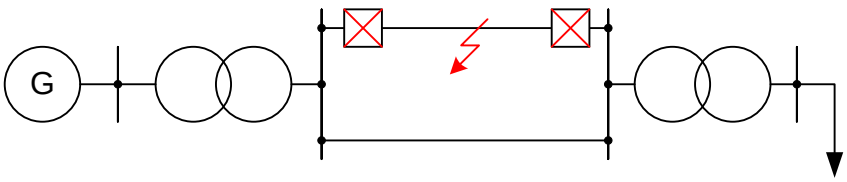

Figure 13-3: Imitation of operation of line differential protection

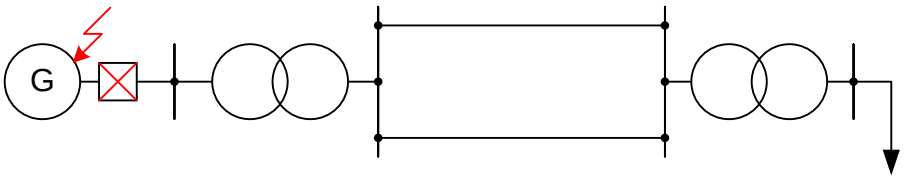

Figure 13-4: Imitation of operation of generator differential protection

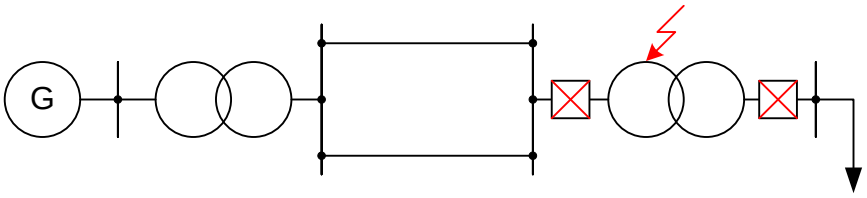

Figure 13-5: Imitation of operation of transformer differential protection

For off-line trainings a very simple and general differential protection element can turn out useful for demonstrative purposes. In this case the main point of model would be to show the differential principle and typical pick-up characteristic.

Let us develop a simple and general model for differential protection. To begin with the tripping characteristic should be chosen for the model.

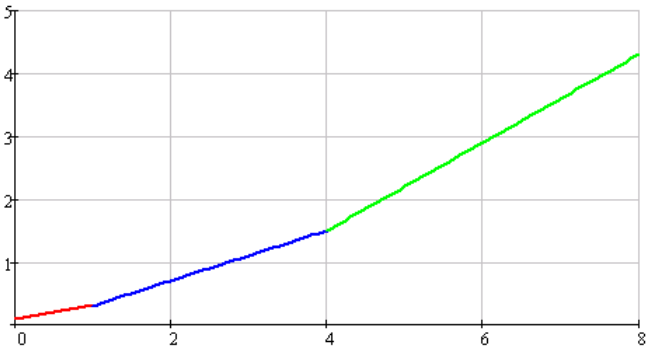

Figure 13-6: Typical three section tripping characteristic with differential current on y axis and restraint or bias current on x axis. Tripping area is above the characteristic

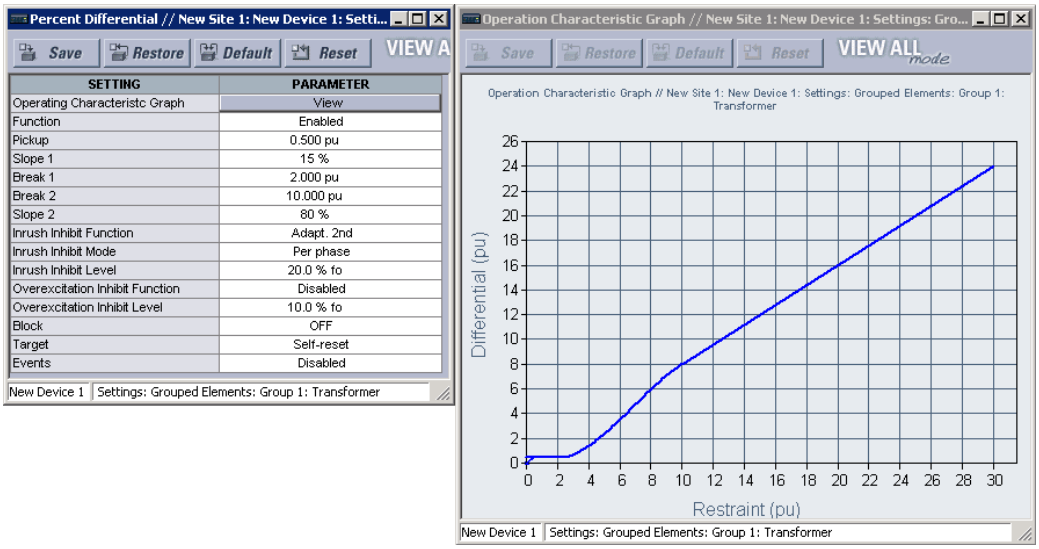

Figure 13-7: Atypical tripping characteristic and settings of differential protection for General Electric T60 relay using bended lines [5]

Tripping characteristic (see Figure 13-6) usually consists of two or three segments, characterized by pairs of points and slopes of segments. In rare occasions, that will not be taken into account, the characteristic is more complicated as shown in Figure 13-7 for General Electric T60 relay.

In general there are several different approaches in calculation of differential and restraining currents. Some of them are listed below. Currents in (21)…(24), of course, should be amplitude and vector matched [5, 6, 19-24].

For two-winding transformer protection:

$$\begin{aligned} I_{diff} &= \left|\underline{I}_1 + \underline{I}_2\right| \\ I_R &= \frac{1}{2}\cdot\left|\underline{I}_1 - \underline{I}_2\right| \end{aligned} \tag{21}$$

For two-winding transformers or other two terminal power system elements such as generators:

$$\begin{aligned} I_{diff} &= \left|\underline{I}_1 + \underline{I}_2\right| \\ I_R &= \left|\underline{I}_1\right| + \left|\underline{I}_2\right| \end{aligned} \tag{22}$$

Calculation of differential and restraining currents for three or four-winding protection:

$$\begin{aligned} I_{diff} &= \left|\underline{I}_1 + \underline{I}_2 + \underline{I}_3 + \underline{I}_4\right| \\ I_R &= \frac{1}{2}\cdot\left(\left|\underline{I}_1\right| + \left|\underline{I}_2\right| + \left|\underline{I}_3\right| + \left|\underline{I}_4\right|\right) \end{aligned} \tag{23}$$

For multi terminal protected objects such as busbars:

$$\begin{aligned} I_{diff} &= \left|\underline{I}_1 + \underline{I}_2 + \underline{I}_3 + \underline{I}_4 + \cdots + \underline{I}_n\right| \\ I_R &= \left|\underline{I}_1\right| + \left|\underline{I}_2\right| + \left|\underline{I}_3\right| + \cdots + \left|\underline{I}_n\right| \end{aligned} \tag{24}$$

A little bit more common is approach given in equations (22) and (24) for two terminal and multi terminal power system elements respectively.

Typical three segment characteristic can be defined in two ways. The first one is to use input data given in (25) and presented in Figure 13-8:

$$I_{d1},\quad I_{b1},\quad I_{b2},\quad I_{b3},\quad k_1,\quad k_2,\quad k_3 \tag{25}$$

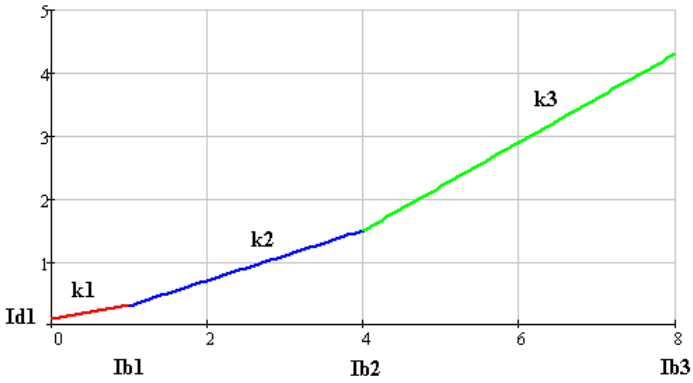

Figure 13-8: Possible input data for differential protection tripping characteristic

The tripping criterion for the considered input data is formulated as:

Segment 1:

a) if the restraint (bias) current is in the following region:

$$0 \le I_b \le I_{b1} \tag{26}$$

b) and differential current exceeds the one calculated by (27)

$$I_d > k_1 \cdot I_b + I_{d1} \tag{27}$$

c) then the trip signal can be issued.

Segment 2:

$$\begin{aligned} &I_{b1} \le I_b \le I_{b2} \\ &I_d > k_2 \cdot \left(I_b - I_{b1}\right) + k_1 \cdot I_{b1} + I_{d1} \end{aligned} \tag{28}$$

Segment 3:

$$\begin{aligned} &I_{b2} \le I_b \le I_{b3} \\ &I_d > k_3 \cdot \left(I_b - I_{b2}\right) + k_2 \cdot \left(I_{b2} - I_{b1}\right) + k_1 \cdot I_{b1} + I_{d1} \end{aligned} \tag{29}$$

The second way to define triple slope biased restraint characteristics is to determine it by the following four pair of points, see equations (30)…(33) and Figure 13-9. This approach is more flexible and allows easier to define the necessary characteristic.

$$\begin{matrix} I_{d1}, & I_{d2}, & I_{d3}, & I_{d4} \\ I_{b1}, & I_{b2}, & I_{b3}, & I_{b4} \end{matrix} \tag{30}$$

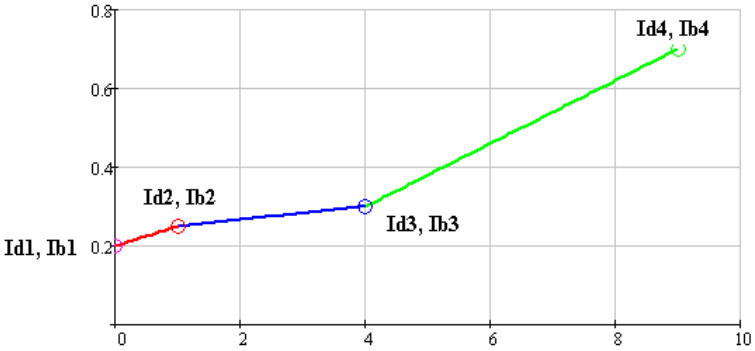

Figure 13-9: Tripping characteristic defined by four pairs of points

Segment 1:

$$\begin{aligned} & I_{b1} \le I_b \le I_{b2} \\ & I_d > \frac{I_b - I_{b1}}{I_{b2} - I_{b1}} \cdot \left(I_{d2} - I_{d1}\right) + I_{d1} \end{aligned} \tag{31}$$

Segment 2:

$$\begin{aligned} & I_{b2} \le I_b \le I_{b3} \\ & I_d > \frac{I_b - I_{b2}}{I_{b3} - I_{b2}} \cdot \left(I_{d3} - I_{d2}\right) + I_{d2} \end{aligned} \tag{32}$$

Segment 3:

$$\begin{aligned} & I_{b3} \le I_b \le I_{b4} \\ & I_d > \frac{I_b - I_{b3}}{I_{b4} - I_{b3}} \cdot \left(I_{d4} - I_{d3}\right) + I_{d3} \end{aligned} \tag{33}$$

Figure 13-10 illustrates a general model of differential protection for two terminal power system element. The right part of the model is the same as in previous chapters. In the left part equations (22), (30)…(33) are modeled. For conversion to per unit values a base current of 1000 A is used in this example.

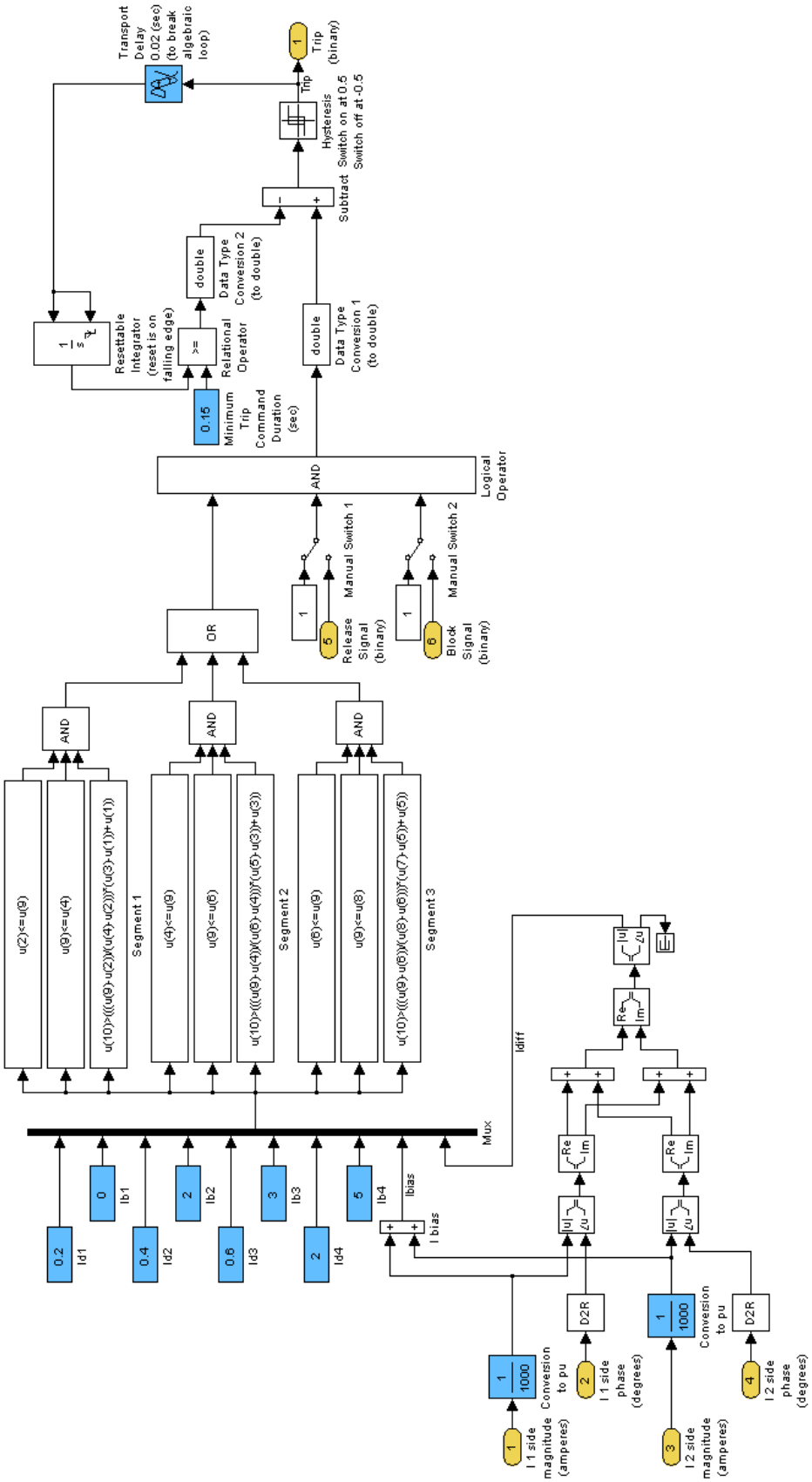

Figure 13-10: General model of differential protection for two terminal power system element

For the development of model of differential protection in EUROSTAG software an "Above Line" block could be used (see Figure 13-11), that describes a general line equation $A \cdot x + B \cdot y = C$ and returns binary 1 or 0 depending on the coefficient B and whether the given point lies above or below the defined line.

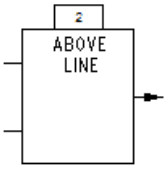

Figure 13-11: The "Above Line" block in EUROSTAG's model editor

The part of a model that outputs binary 1 if a point in tripping characteristic lies in the tripping area (see Figure 13-12) is presented in Figure 13-13.

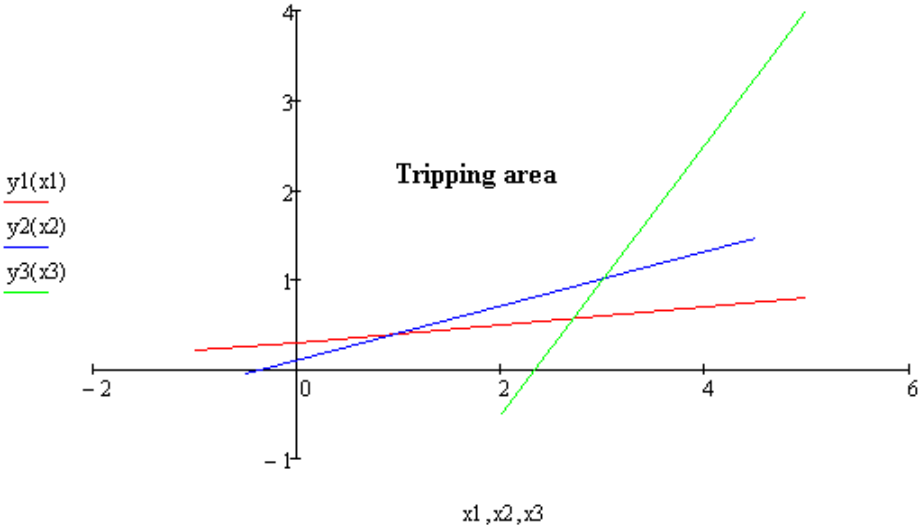

Figure 13-12: Tripping characteristic that is modelled in Figure 13-13 by the help of three "Above Line" blocks

Differential and bias currents in the following model are calculated according to the equation (22), taking into account that the calculation has to be done using complex values of currents from both sides of the protected object.

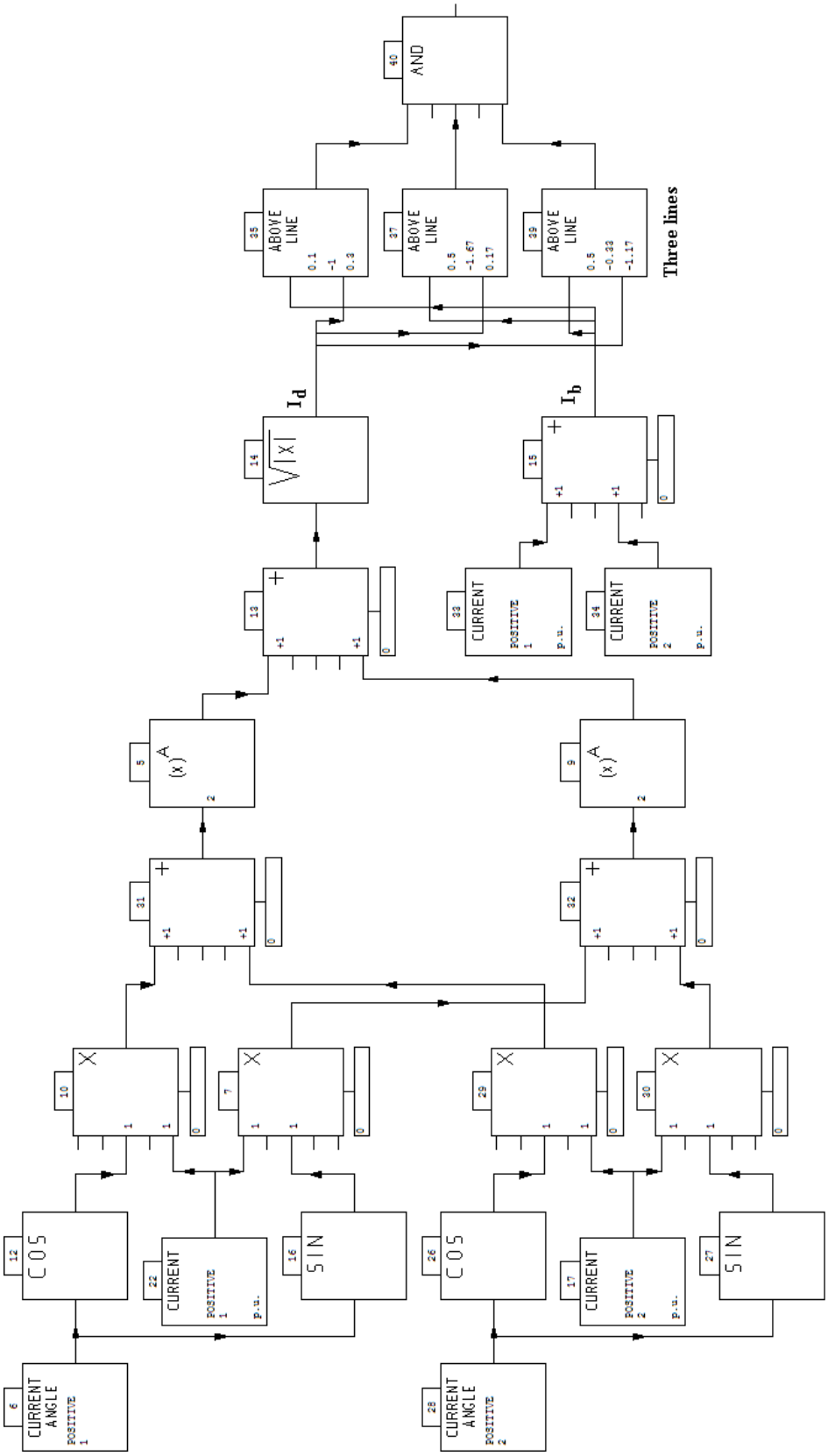

Figure 13-13: The part of a model that outputs binary 1 if a point in tripping characteristic lies in the tripping area

14. Distance protection

Properties	Description
ANSI/IEEE C37.2 standard device number	21
IEC 61850 logical node name	PDIS
Input signals	Current and voltage phase and angle
Output signals	Binary 1 or 0

Distance relay usually has 5 zones of phase fault and earth fault protection. Often it is possible to choose between quadrilateral (polygon) characteristics, or mho circles. Rectangular characteristics with 2 zones are common for generator distance protection. The faulted phase impedance must appear within a tripping zone in order to issue a tripping signal.

Some possible characteristics of distance elements are presented in the following table [25-29]:

Description	Characteristic	Equations
Quadrilateral	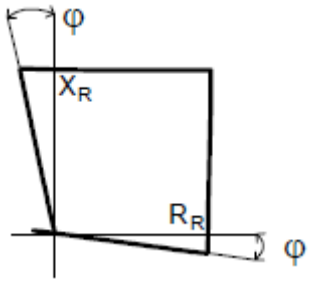	$X < X_R$ $R < R_R$ $X > -R \cdot tg(\varphi)$ $R > -X \cdot tg(\varphi)$
Universal polygon	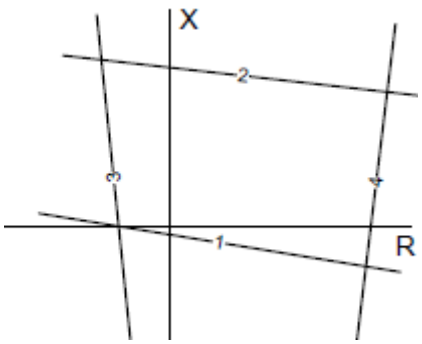	1. $X > a_1 \cdot R + b_1$ 2. $X < a_2 \cdot R + b_2$ 3. $R > a_3 \cdot R + b_3$ 4. $R < a_4 \cdot R + b_4$
Rectangular - tilted	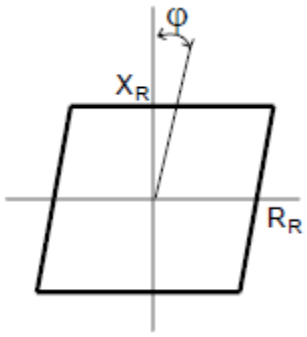	$\lvert X \rvert < X_R$ $R < R_R + X \cdot tg(\varphi)$ $R > -R_R + X \cdot tg(\varphi)$

Rectangular	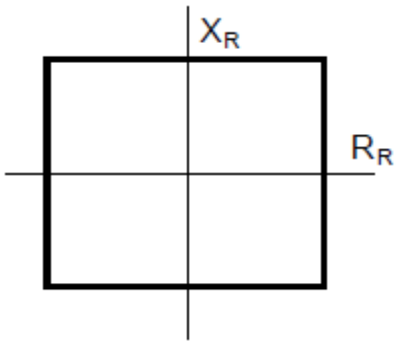	$\lvert X\rvert < X_R$ $\lvert R\rvert < R_R$
MHO - offset	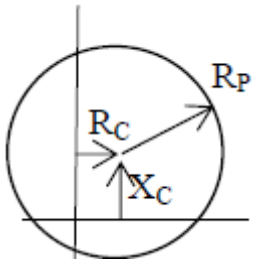	$\lvert(R+jX)-(R_C+jX_C)\rvert < \lvert R_P\rvert$
MHO	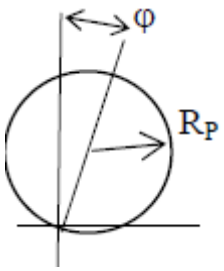	$\lvert(R+jX)-R_P\cdot e^{jANG}\rvert < \lvert R_P\rvert$
Circle	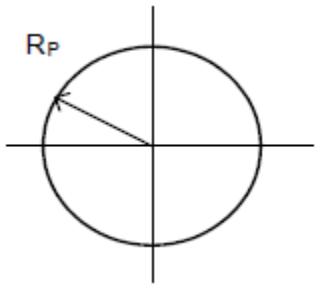	$\lvert R+jX\rvert < \lvert R_P\rvert$

Measured impedance Z for phase to phase (e.g. for loop consisting of phase "A" and "B") and phase to ground (e.g. for phase "A") elements are as follows [25-29]:

$$\underline{Z}_{ph-ph} = \frac{\underline{U}_A - \underline{U}_B}{\underline{I}_A - \underline{I}_B} \tag{34}$$

$$\underline{Z}_{ph-gnd} = \frac{\underline{U}_A}{\underline{I}_A + \underline{k}_E \cdot 3 \cdot \underline{I}_0} \tag{35}$$

Where $U_{A,B,C}$ and $I_{A,B,C}$ are phase voltages and currents phasors, I_0 is zero sequence current phasor and k_E is a compensation factor calculated from positive and zero sequence line parameters by equation (36):

$$\underline{k}_E = \frac{\underline{Z}_0 - \underline{Z}_1}{3 \cdot \underline{Z}_1} \tag{36}$$

If distance protection model is based upon calculated positive sequence impedance (where U1 is positive sequence voltage and I1 is positive sequence current) then the measured impedance is:

$$\underline{Z}_1 = \frac{\underline{U}_1}{\underline{I}_1} \tag{37}$$

Using, for instance, the equation (37) and equations defining the tripping characteristic, as well as some fragments from previous models we can easily create a model for distance protection (see Figure 14-1).

In the considered model two important features are missing [25-29]:

1) Power swing detection / blocking element,

   Distance protections are usually equipped with power swing blocking to prevent the switching of protected lines in case of the stable swings. Blocking is carried out by the measuring of elapsed time, between the passing of apparent impedance vector through outer and inner zone of blocking elements. If elapsed time is greater than defined value (usually 40 -50 ms) distance elements are blocked (inhibited). Blocking may affect either phase to phase elements or both phase to phase and phase to ground elements. Sometimes the smallest zone (the 1st stage) is not blocked.

2) Load encroachment detection / blocking element.

   To exclude the risk of unwanted fault detection by the distance protection during heavy load flow, the load region can be "cut out" from the characteristics. The cut out shape is defined by the minimum load resistance and the load area angle.

The first of these two features will be analyzed and modeled in the next chapter and, if necessary, can be added to distance protection model (to its blocking or releasing input). The other concerns mainly the last (reserve or back-up) zones of the distance protection which are not reasonable to take into account in the framework of PEGASE project.

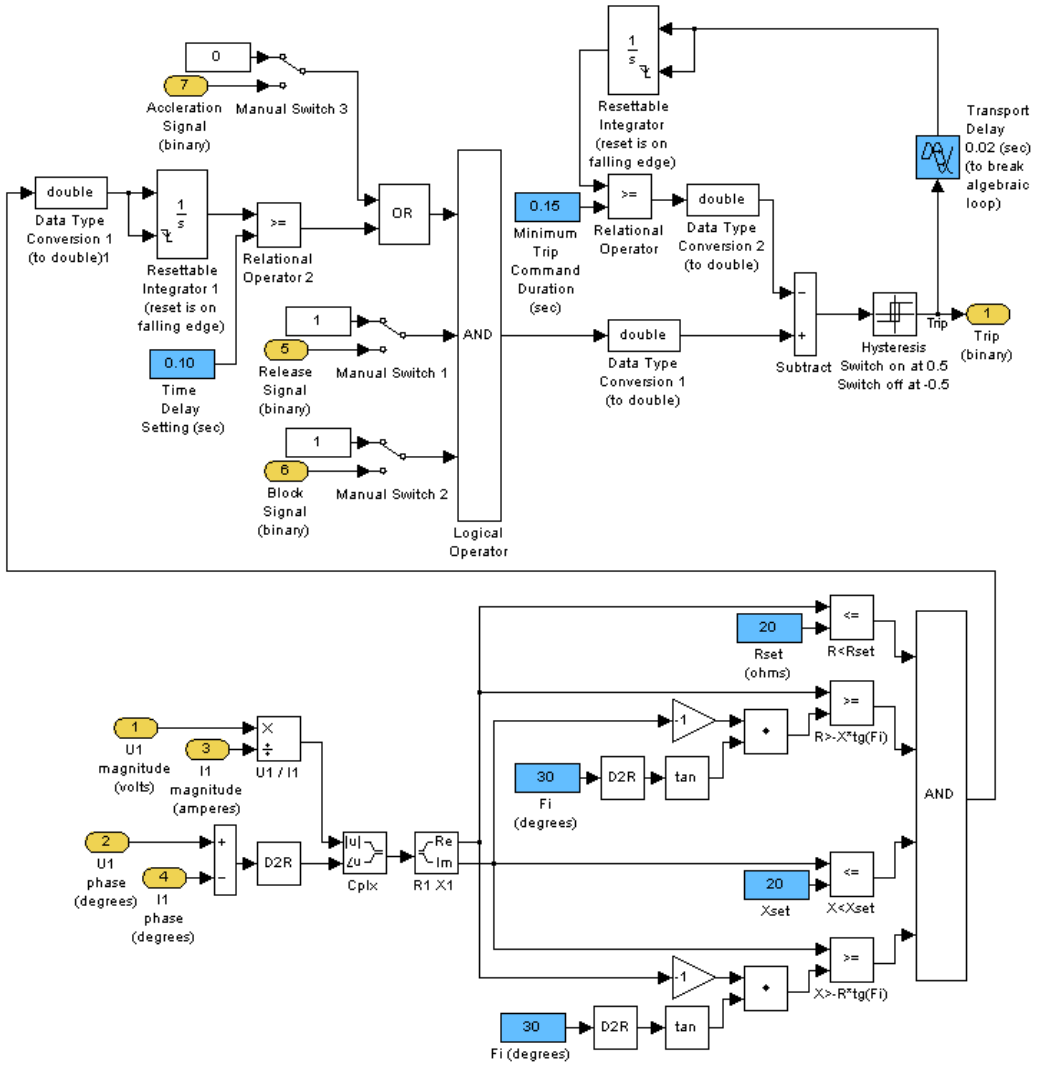

Figure 14-1: Block diagram of distance protection

When developing an EUROSTAG model of distance protection, a dedicated block "Inside Polygon" can be applied (see Figure 14-2). With this single block a complex polygon characteristic can be easily modeled.

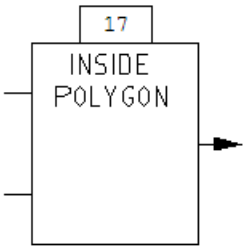

Figure 14-2: The "Inside Polygon" block in EUROSTAG's model editor

What remains to be done is to calculate impedance Z, split it into real and imaginary parts and connect R and X signals to the "Inside Polygon" block.

15. Power swing detection

Properties	Description
ANSI/IEEE C37.2 standard device number	78
IEC 61850 logical node name	RPSB
Input signals	Current and voltage phase and angle
Output signals	Binary 1 or 0

The loss of synchronism between power systems or a generator and the power system affects transmission line relays and systems in various ways. Some relay systems such as segregated-line differential relay systems will not respond to an OOS (out-of-step) condition and other relays such as over-current, directional over-current and distance relays may respond to the variations of voltage and currents and their phase angle relationship. In fact, some of the above relays may even operate for stable power swings for which the system should recover and remain stable [14, 25, 26, 30, 31].

Instantaneous phase over-current relays will operate during OOS conditions if the line current during the swing exceeds the minimum pickup setting of the relay. Likewise, directional instantaneous over-current relays may operate if the swing current exceeds the minimum pickup setting of the relay and the polarizing and operating signals have the proper phase relationship during the swing. Time-over-current relays probably will not operate, however, it most likely will depend on the swing current magnitude and the time delay settings of the relay.

Phase distance relays model measure the positive-sequence impedance for three-phase faults. The positive-sequence impedance measured at a line terminal during an OOS condition varies as a function of the phase angle separation δ between the two equivalent system source voltages. Distance relay elements will operate during a power swing, stable or unstable, if the swing locus enters the distance relay operating characteristic. Zone 1 distance relay elements, with no intentional time delay, will be the most prone to operate during a power swing. Also very prone to operate during swings are Zone 2 distance relay elements used in pilot relaying systems, for example blocking or permissive type relay systems. Backup zone step distance relay elements will not typically operate during a swing, depending on their time-delay setting and the time it takes for the swing impedance locus to traverse through the relay characteristic.

Figure 15-1 shows the operation of a Zone 1 distance relay when the swing locus goes through its operating characteristic [31].

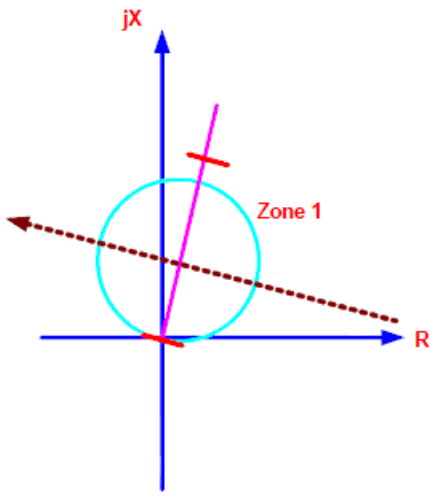

Figure 15-1: Zone 1 distance relay characteristic

It is important to recognize that the relationship between the distance relay polarizing memory and the measured voltages and currents plays the most critical role in whether a distance relay will operate during a power swing. Another important factor in modern microprocessor-type distance relays is whether the distance relay has a frequency tracking algorithm to track system frequency. Relays without frequency tracking will experience voltage polarization memory rotation with respect to the measured voltages and currents. Furthermore, the relative magnitude of the protected line and the equivalent system source impedances is another important factor in the performance of distance relays during power swings. If the line positive-sequence impedance is large when compared with the system impedances, the distance relay elements may not only operate during unstable swings but may also operate during swings from which the power system may recover and remain stable [31].

Out-of-step protection philosophy

The performance of protective relays that monitor power flows, voltages, and currents may respond to variations in system voltages and currents and cause tripping of additional equipment, thereby weakening the system and possibly leading to cascading outages and the shutdown of major portions of the power system. Protective relays prone to respond to stable or unstable power swings and cause unwanted tripping of transmission lines or other power system elements include: over-current, directional over-current, under-voltage, distance, and directional comparison systems.

The philosophy of out-of-step relaying is simple and straightforward: avoid tripping of any power system element during stable swings. Protect the power system during unstable or out-of-step conditions. When two areas of a power system, or two interconnected systems, lose synchronism, the areas must be separated from each other quickly and automatically in order to avoid equipment damage and shutdown of major portions of the power system. Uncontrolled tripping of circuit breakers during an OOS condition could cause equipment damage and pose a safety concern for utility personnel. Therefore, a controlled tripping of certain power system elements is necessary in order to prevent equipment damage, and widespread power outages, and minimize the effects of the disturbance.

Out-of-step detection methods and types of schemes

Out-of-step protection functions detect stable power swings and out-of-step conditions by using the fact that the voltage/current variation during a power swing is gradual while it is virtually a step change during a fault. Both faults and power swings may cause the measured apparent positive-sequence impedance to enter into the operating characteristic of a distance relay element.

A short circuit is an electromagnetic transient process with a short time constant. The apparent impedance moves from the pre-fault value to a fault value in a very short time, a few milliseconds. On the other hand, a power swing is an electromechanical transient process with a time constant much longer than that of a fault. The rate of change of the positive-sequence impedance is much slower during a power swing or OOS condition than during a fault and it depends on the slip frequency of the OOS. For example, if the frequency of the electromechanical oscillation is about 1 Hz and the impedance excursion required to penetrate the relay characteristic takes about half a period (a change in δ of 180°), the impedance change occurs in about 0.5 seconds. When δ approaches 180° during an OOS, the measured impedance falls into the operating characteristic of a distance relay for a particular transmission line. The impedance measurement by itself cannot be used to distinguish an OOS condition from a phase fault. The fundamental method for discriminating between faults and power swings is to track the rate of change of measured apparent impedance.

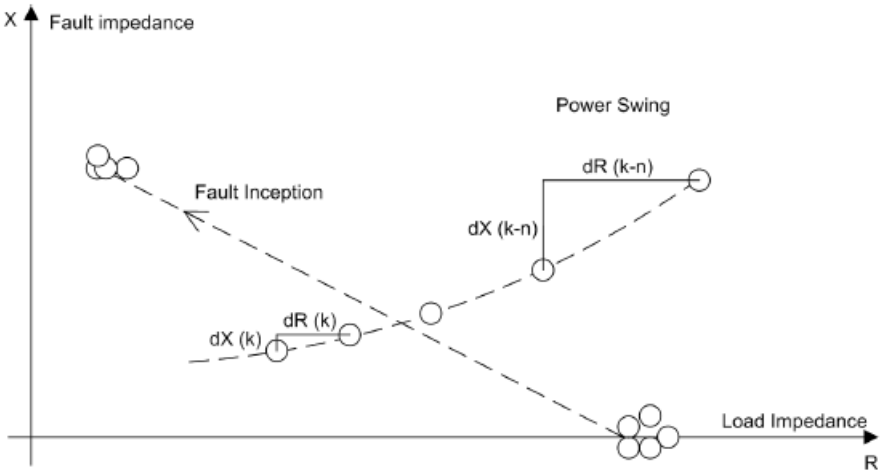

Figure 15-2: Impedance vector during power swing and fault [29]

The difference in the rate of change of the impedance has been traditionally used to detect an OOS condition and then block the operation of distance protection elements before the impedance enters the protective relay operating characteristics. Actual implementation of measuring the impedance rate of change is normally performed though the use of two impedance measurement elements together with a timing device. If the measured impedance stays between the two impedance measurement elements for a predetermined time, then an OOS is declared and an out-of-step blocking signal is issued to block the distance relay element operation. Impedance measurement elements with different shapes have been used over the time. These shapes include double blinders, concentric polygons, and concentric circles as shown in Figure 15-3 [31].

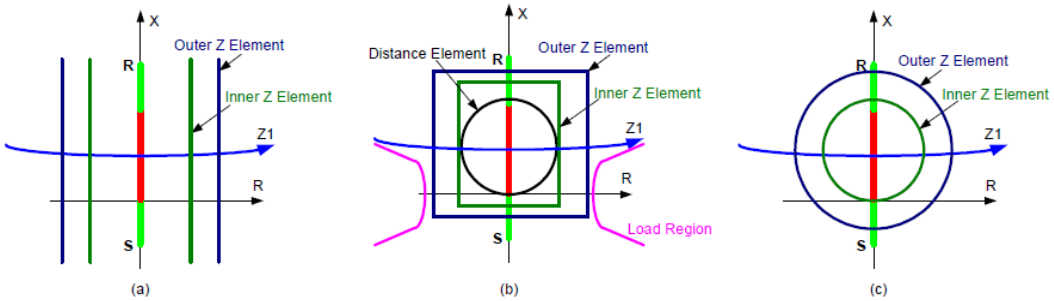

Figure 15-3: Different double blinder OOS characteristics

To guarantee that there is enough time to carry out blocking of the distance elements after an OOS is detected, the inner impedance measurement element of the OOS detection logic must be placed outside the largest distance protection region that is to be blocked. The outer impedance measurement element for the OOS detection has to be placed away from the load region to prevent inadvertent OSB logic operation caused by heavy loads. These relationships among the impedance measurement elements are shown in Figure 15-3 (b), using concentric polygons as OOS detection elements.

Below some definitions are given for clarity.

Power Swing: a variation in three phase power flow which occurs when the generator rotor angles are advancing or retarding relative to each other in response to changes in load magnitude and direction, line switching, loss of generation, faults, and other system disturbances.

Pole Slip: a condition whereby a generator or group of generators, terminal voltage angles (or phases) go past 180 degrees with respect to the rest of the connected power system.

Stable Power Swing: a power swing is considered stable if the generators do not slip poles and the system reaches a new state of equilibrium, i.e. an acceptable operating condition.

Unstable Power Swing: a power swing that will result in a generator or group of generators experiencing pole slipping for which some corrective action must be taken.

Out-of-Step Condition: Same as an unstable power swing.

Electrical System Center or Voltage Zero: it is the point or points in the system where the voltage becomes zero during an unstable power swing.

In this chapter we will develop a two-blinder model for power swing and out-of-step mode detection.

The two-blinder scheme shown in Figure 15-4 is based on the same principle of measuring the time needed for an impedance vector to travel certain delta impedance. The time measurement starts when the impedance vector crosses the outer blinder (RRO) and stops when the inner blinder (RRI) is crossed. If the measured time is above the setting for delta time, a power swing situation is detected. If the blinders are set in parallel to the line impedance, then they are optimized for the delta impedance measurement because the power swing impedance vectors will normally enter the protection zones at an angle of nearly 90 degrees to the line angle. Depending on certain network conditions, this may not be always correct but it can be assumed for simplification. One advantage of the blinder scheme for power swing detection applications is that it can be used independent of the distance zone characteristics. In addition, while the impedance vector is in this delta impedance area, the protective relay element can be blocked from tripping as this may be either heavy load or a stable power swing. If an unstable swing is detected, the mho element can be allowed to trip immediately (not recommended) or tripping can be delayed until the swing passes through thereby minimizing over-voltages across the opened breaker. To find the correct settings for the blinders is not always simple and requires a sophisticated grid analysis.

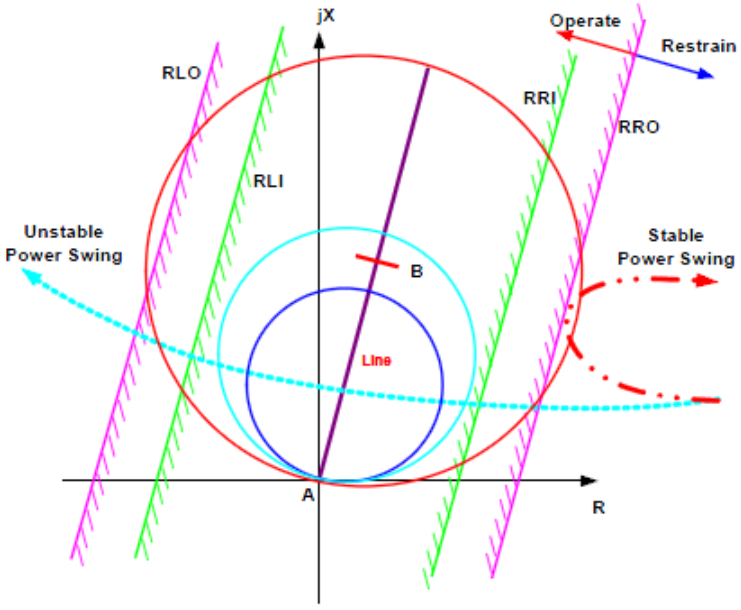

Figure 15-4: Two-blinder scheme [31]

Figure 15-5 illustrates the power swing detection model with two-blinder scheme.

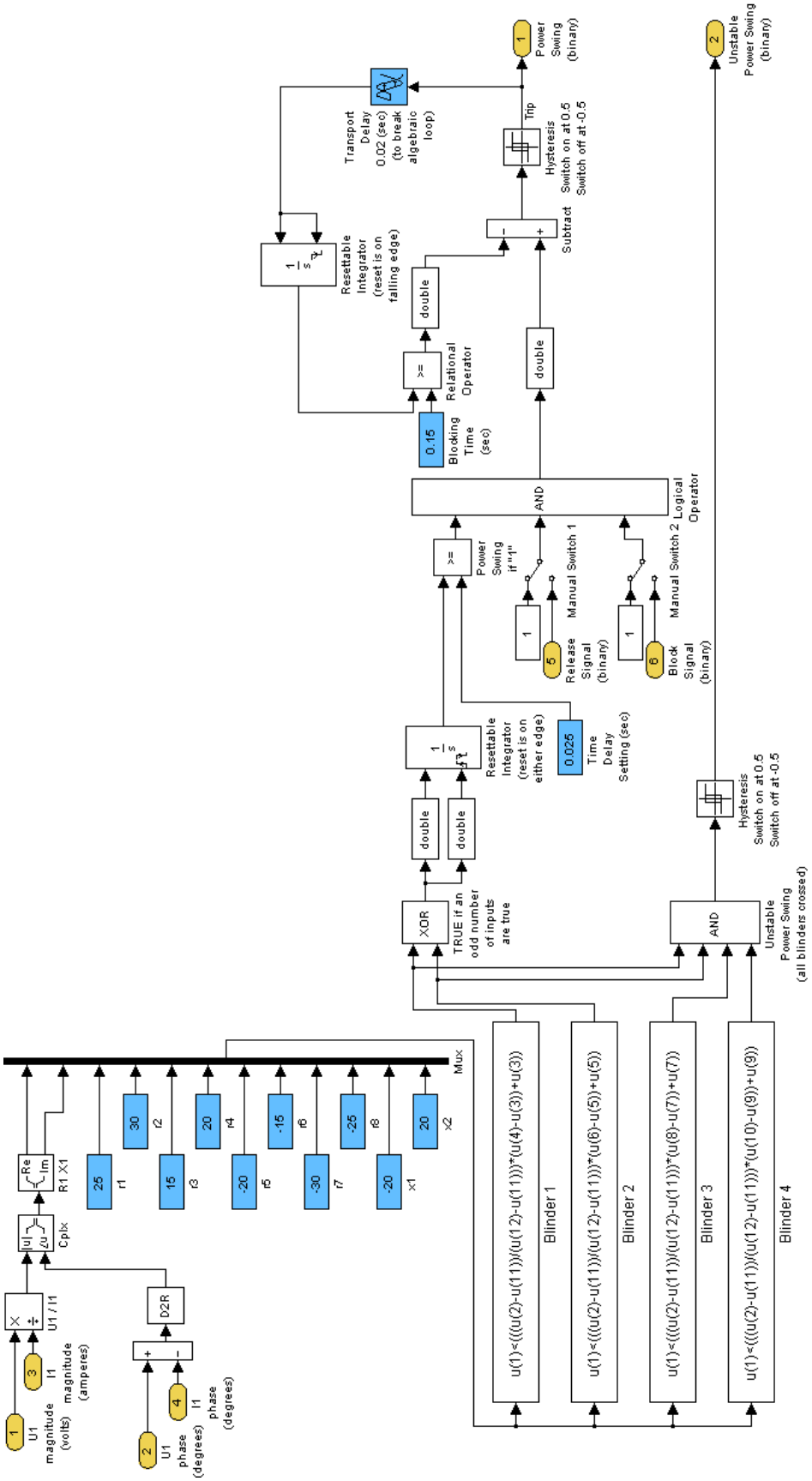

Figure 15-5: Block diagram of power swing detection model

Four lines in two-blinder scheme are defined in the model using eight pair of points and the following line equation (where r1, x1, r2, x2 are two pairs of points defining one line):

$$r(x) = \frac{x - x_1}{x_2 - x_1} \cdot (r_2 - r_1) + r_1 \tag{38}$$

The modeled two-blinder characteristic is presented in Figure 15-6.

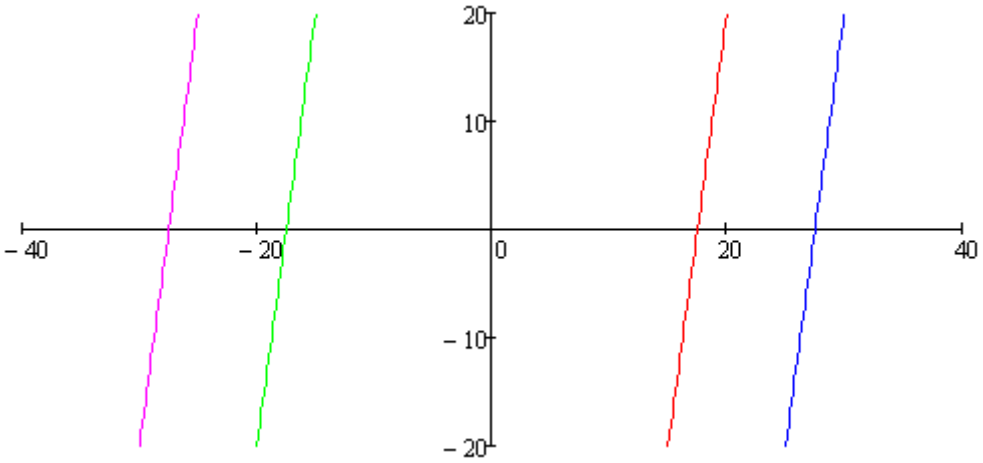

Figure 15-6: Example of two-blinder characteristic

In Areva P443 relay if the disturbance takes less than 25ms to cross two blinders, the relay will consider this to be a power system fault and not an out of step trip condition [25]. The timer of 25ms is a fixed timer in the logic and not user accessible. The same time delay is used in model (see Figure 15-5).

Instead of a minimum tripping time duration as in previous models, blocking time duration is set in this model.

The characteristic presented in Figure 15-6 can be easily modeled in EUROSTAG by the help of four “Above Line” elements:

In Figure 15-7 a part of a model that distinguishes a stable and unstable power swing is presented. Timers can be added to this model using the resettable integrator as shown, for instance, in Figure 9-3.

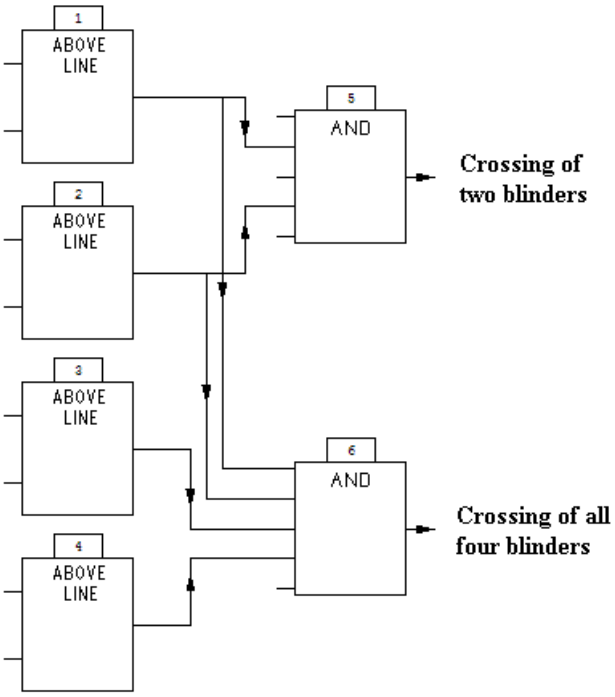

Figure 15-7: Part of a model that detects the crossing of blinders

16. Under-voltage and over-voltage protection

Properties	Description
ANSI/IEEE C37.2 standard device number	27 (under-voltage), 59 (over-voltage)
IEC 61850 logical node name	PTUV (under-voltage), PTOV (over-voltage)
Input signals	Voltage
Output signals	Binary 1 or 0

These protections are used to protect equipment against an abnormally low or high voltage. They can also be used [3]:

- To monitor the operation of voltage regulators;
- To load shed the non-priority consumer network when an overload occurs;
- To monitor the voltage before sources to carry out a power supply transfer.

The protection in its simplest form is activated when one or all three of the phase-to-phase (or phase-to-ground voltages) are lower/higher than the setting threshold. Positive sequence voltage can also be used. Generally, it includes a definite time delay.

Suggested block diagram of under voltage protection for PEGASE project is presented in Figure 16-2. In Figure 16-3 and Figure 16-4 the same model is split into two main parts.

When modeling under-voltage protection it should be noted that the reset setting of the protection has larger value than the trip setting, therefore standard hysteresis (Schmidt trigger) element cannot be applied. In order to model the pick-up/drop-out feature the logic depicted in Figure 16-1 can be used – if the operating point is below pick-up setting, then "+2" is set at the output of the block No.15 in Figure 16-2 and the relay picks up. If operating point is above the drop-out setting, then "-2" is set and the relay drops out. In case of "0" relay waits for further voltage changes.

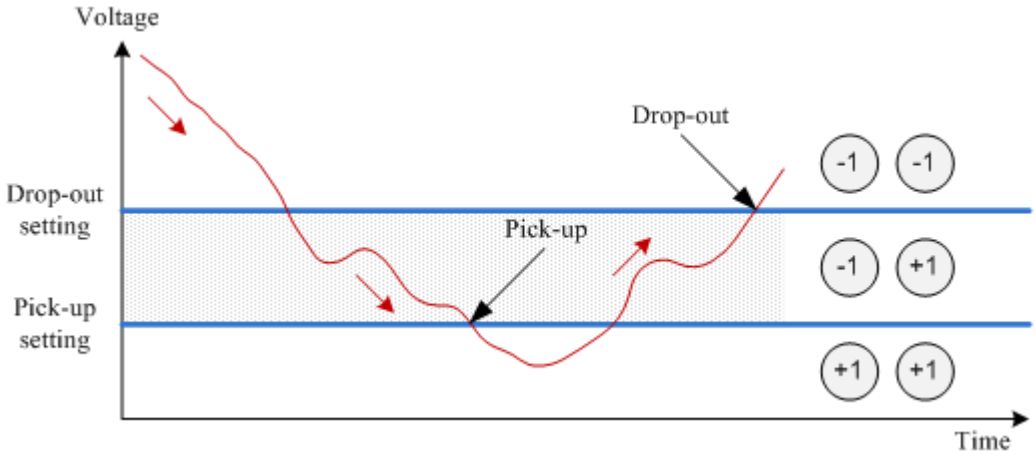

Figure 16-1: Pick-up and drop-out moments during transient process

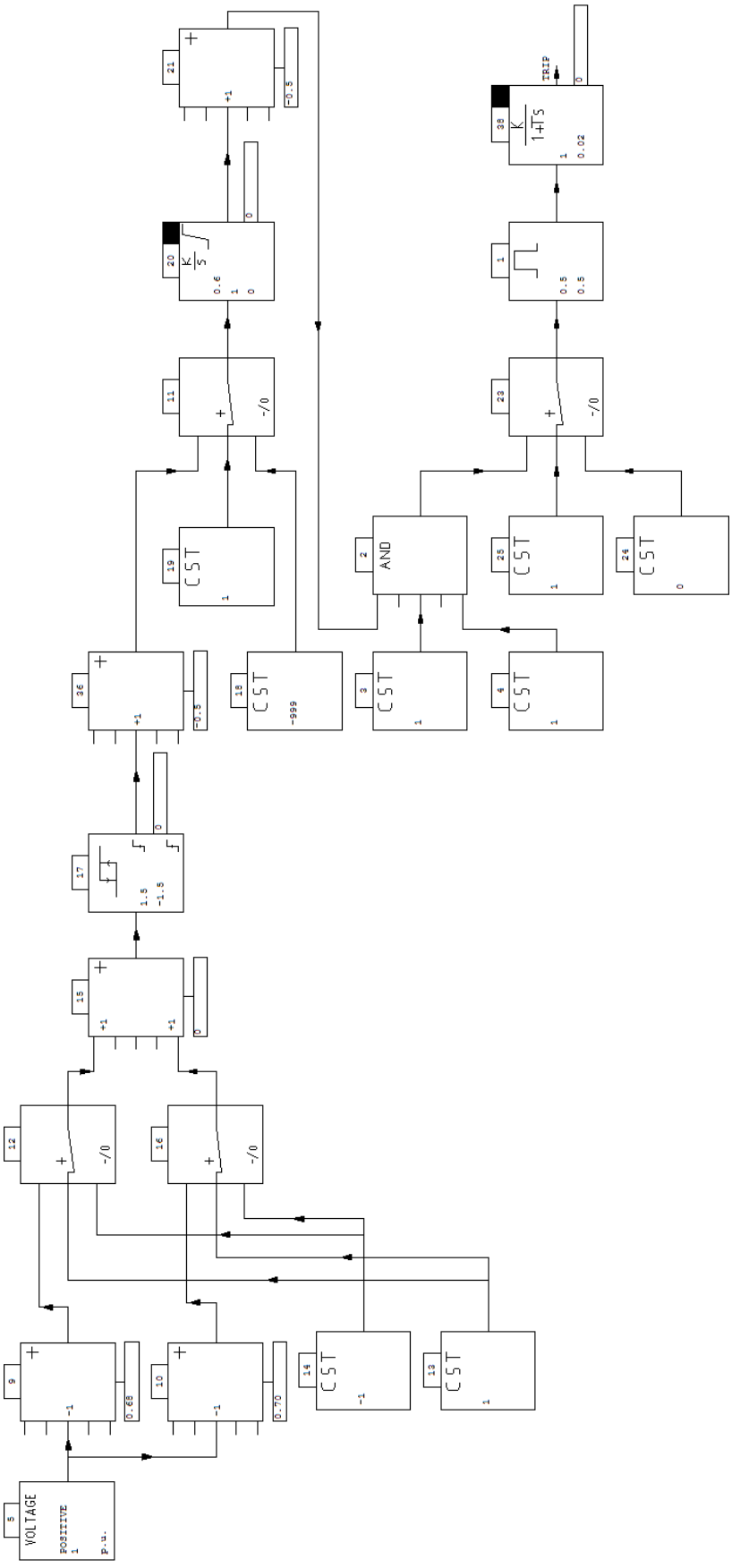

Figure 16-2: EUROSTAG model of under-voltage protection

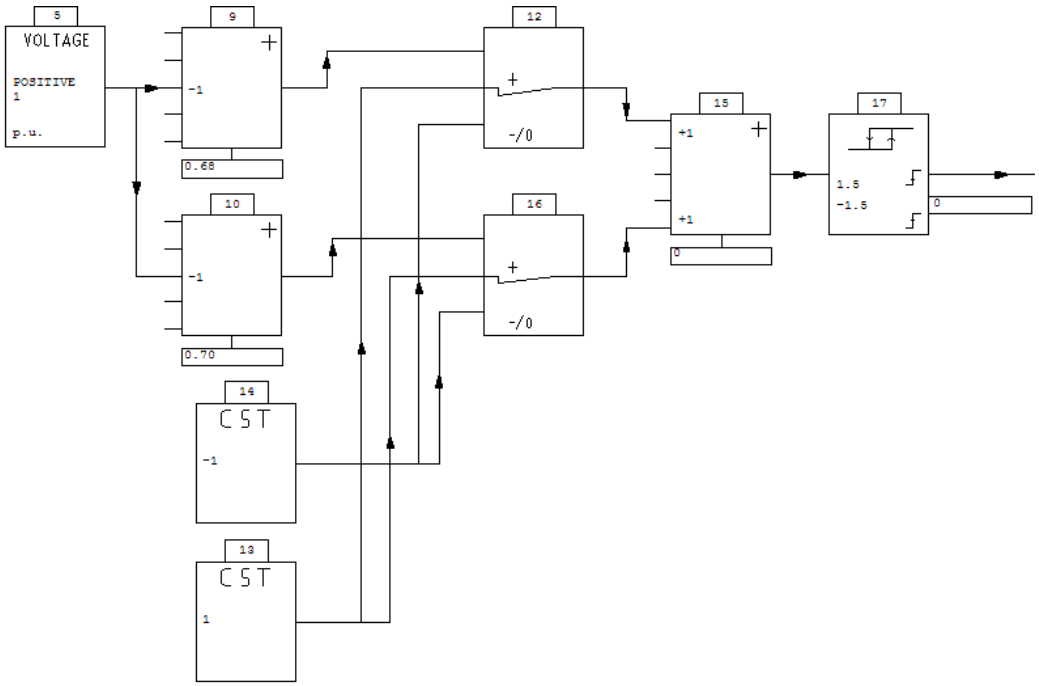

Figure 16-3: Tripping decision logic

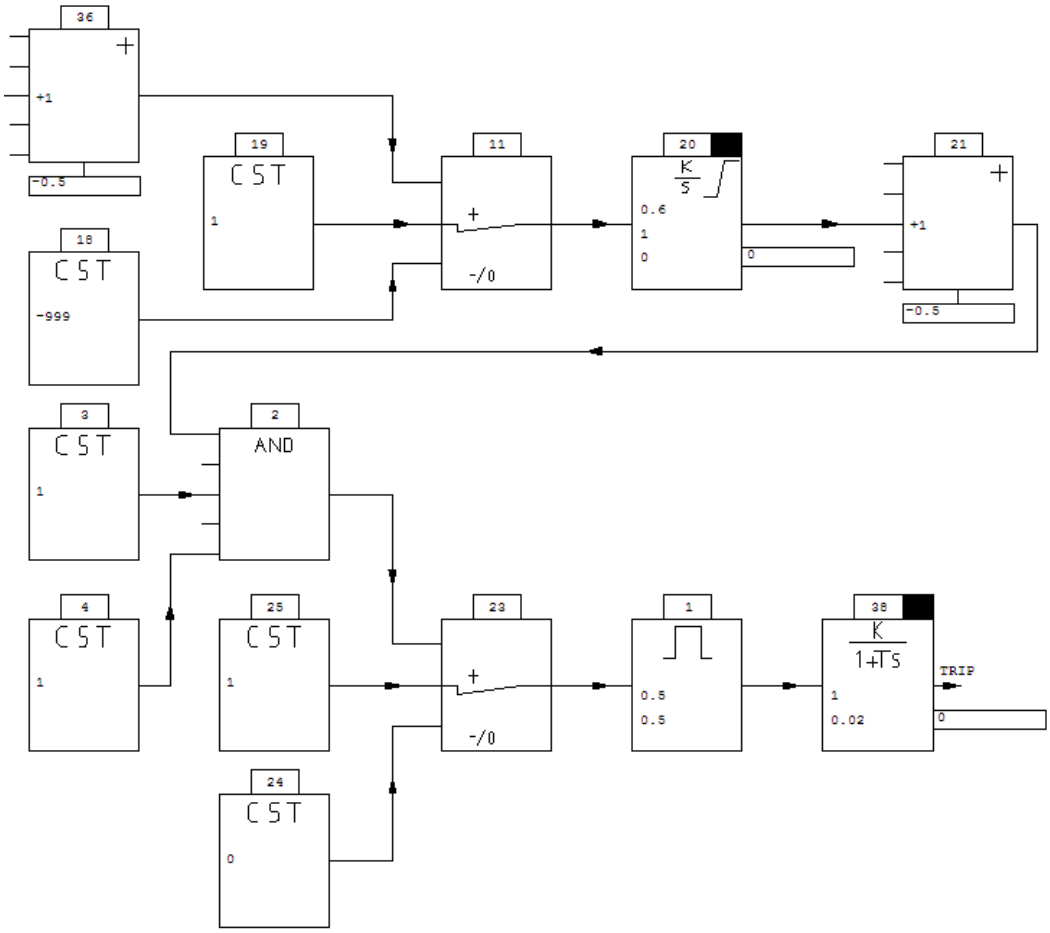

Figure 16-4: Modelling of time delay and preset length of output signal

Block diagram of under-voltage protection in MATLAB/SIMULINK environment is presented in Figure 16-5:

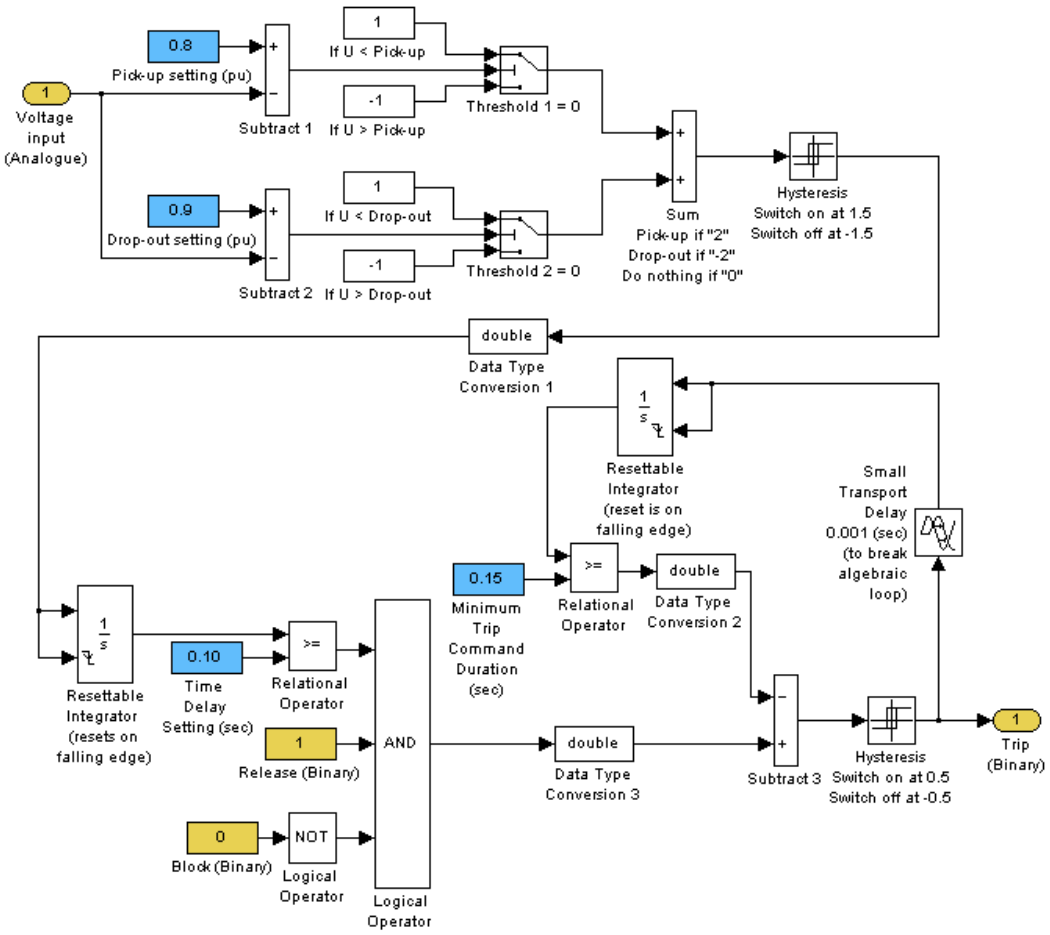

Figure 16-5: MATLAB/SIMULINK model of under-voltage protection

In case of over-voltage protection the model is simpler as the hysteresis (Schmidt trigger) element can be applied. EUROSTAG and MATLAB/SIMULINK models of over-voltage protections are presented in Figure 16-6 and Figure 16-7 respectively.

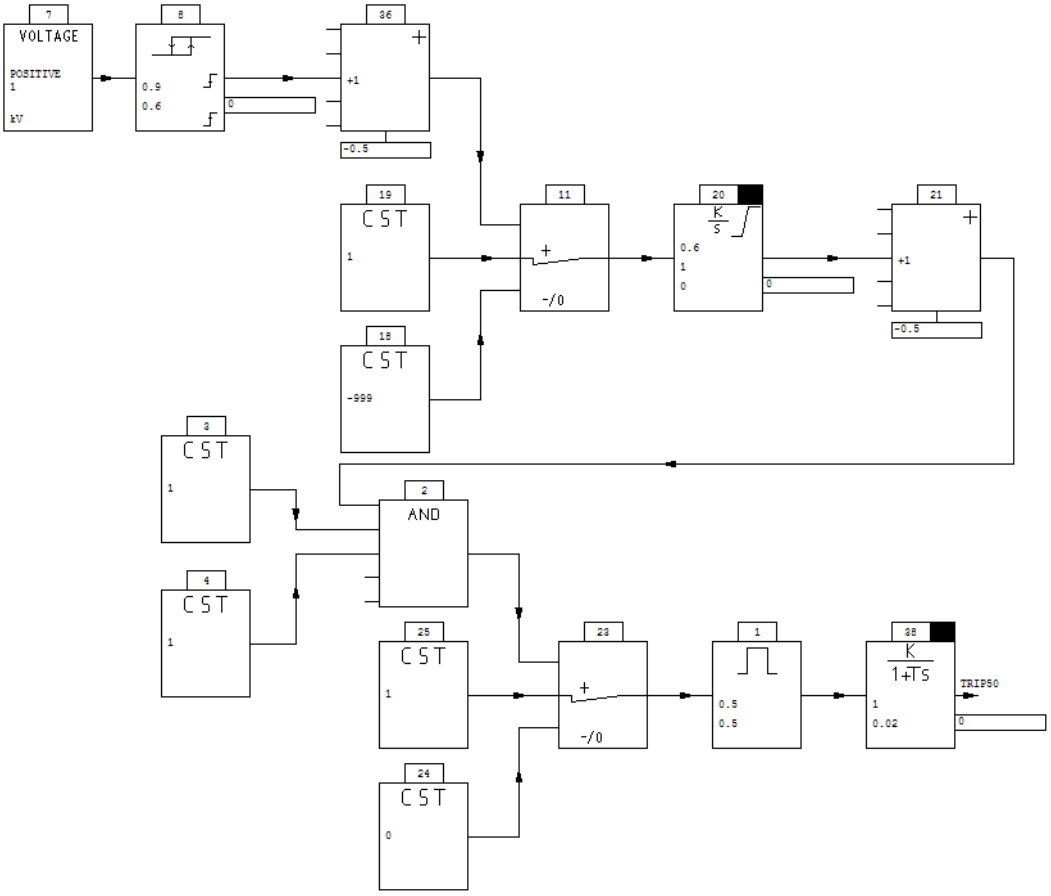

Figure 16-6: EUROSTAG model of over-voltage protection

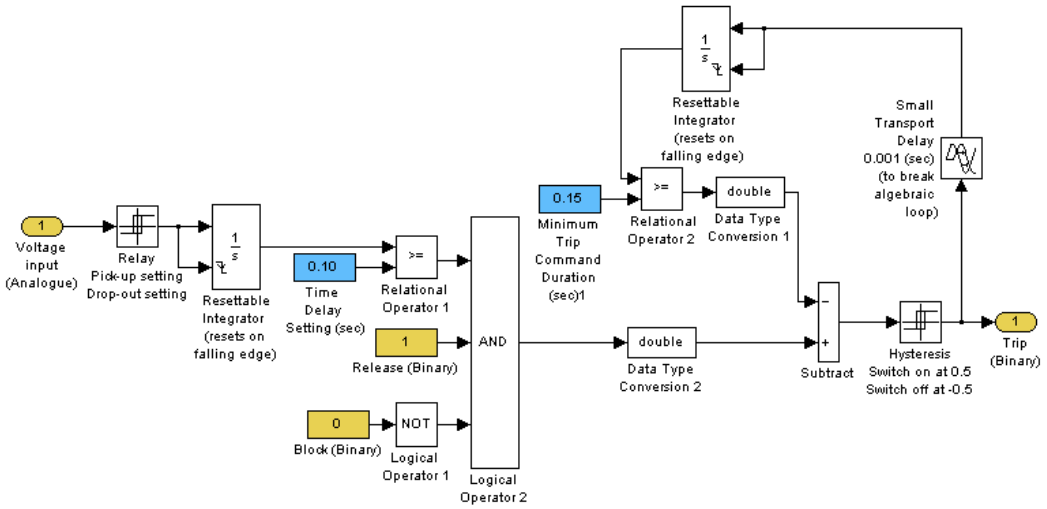

Figure 16-7: MATLAB/SIMULINK model of over-voltage protection

17. Under-frequency and over-frequency protection

Properties	Description
ANSI/IEEE C37.2 standard device number	81U (under-frequency), 81O (over-frequency)
IEC 61850 logical node name	PTUF (under-frequency), PTOF (over-frequency)
Input signals	Frequency
Output signals	Binary 1 or 0

Variations in the power supply frequency may be due to [3]:

- Overloads when the network is fed by a limited power source (internal generation plant operating while cut off from the utility network);
- Faulty operation of a generator frequency regulator;
- Cutting off of a generation plant from an interconnected network;
- Power supply being cut off in an installation fitted with large motors. The motors then feed the installation the time it takes for the flux to be extinguished with a decreasing frequency.

The protection in its simplest form compares the network frequency to a minimum or maximum threshold frequency. Generally, it includes a definite time delay.

Structurally models for over/under frequency and voltage protection are the same; therefore models for frequency protection are given in Figure 17-1 and Figure 17-2 without further explanation.

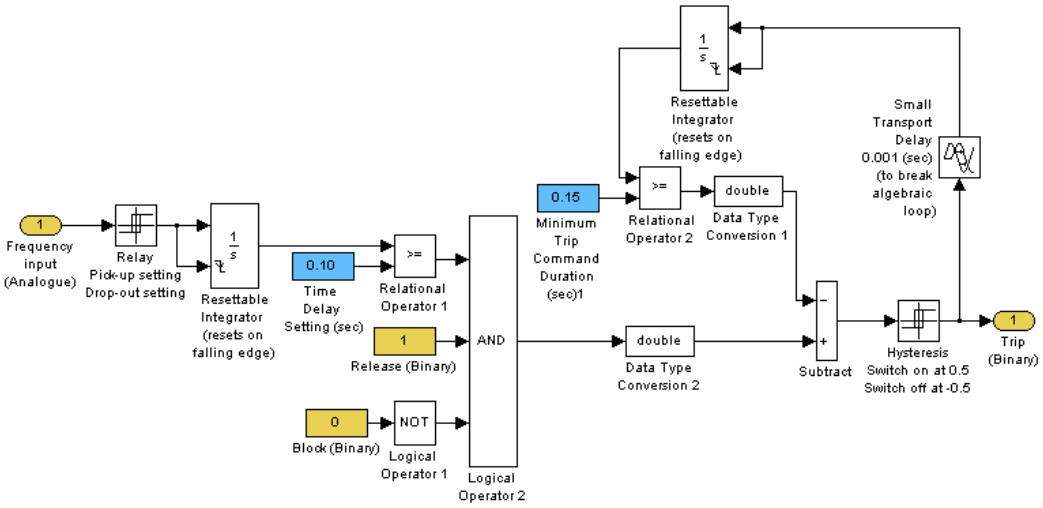

Figure 17-1: Model of over-frequency protection

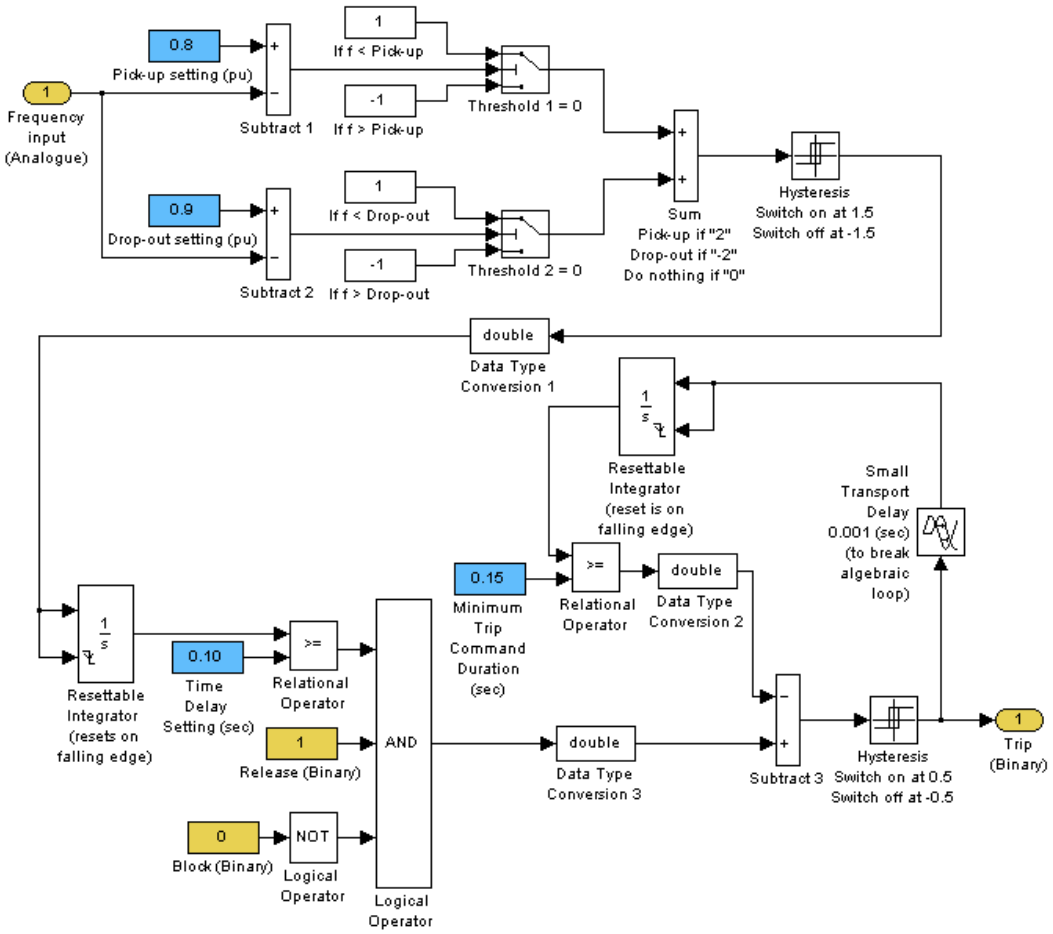

Figure 17-2: Model of under-frequency protection

18. Under-frequency load shedding

During emergency situation in the power system caused by generating power deficiency frequency decline takes place. Dynamics of under-frequency during the deficiency of generation in the power system can have very different character. It depends on the value of disturbance, response of emergency automation and governor system.

For gradual increase in load, or for sudden but mild overloads, electric power system generating units' governors will sense speed change and increase power input to the generator. Here so called primary and secondary frequency control is activated. Severe system disturbances can result in fast frequency drop, which makes impossible fast governor and boiler response. To restore frequency load shedding or spinning reserve involvement may be activated. If governor action cannot activate spinning reserve quickly enough to restore the system to its normal operating frequency, frequency actuated automatic load shedding (UFLS) serves as a last-resort tool to prevent the system from collapse.

Up-to-date automatic load shedding system practically in the most power systems foresees disconnection without time delay or with small delay part of the load on under-frequency. The number of load shedding steps and value of load to be shed vary for the different power systems. Some power systems use rate-of-change of frequency as additional factor to shed a load.

As under-frequency load shedding is tracking frequency and operates when the frequency decreases below some preset value, the model for one stage of UFLS is essentially the same as model for under-frequency protection. By combining several models of under-frequency protection it is possible to create a typical UFLS model. If necessary, rate-of-change of frequency can be used as input signal, using frequency measurement and derivative-lag elements (see Figure 18-1).

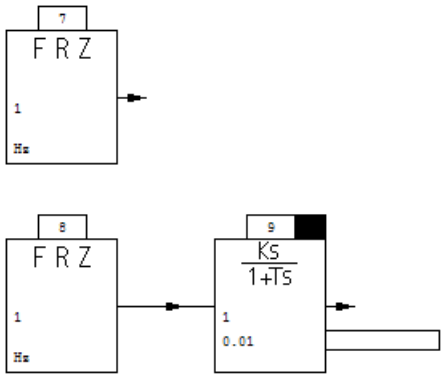

Figure 18-1: Frequency and rate-of-change of frequency signals

19. General protection model

It can be seen from the previous chapters, that all the models that operate according to some "-over" or "-under" criteria (current/voltage/frequency) are actually identical.

For the framework of PEGASE project it means that it is enough to have two models to cover a wide range of protections functions that operate according to "-over" and "-under" criteria. In addition to the already inspected protection functions, the general model can be applied also, for instance, as active (P), reactive (Q), apparent power (S) protection, or generator speed protection using the available measurement elements in EUROSTAG software (see Figure 19-1). The only difference concerns the input signal. For convenience the over/under voltage models are repeated in this chapter (see Figure 19-2, Figure 19-3), that can be used to monitor different power system parameters as well.

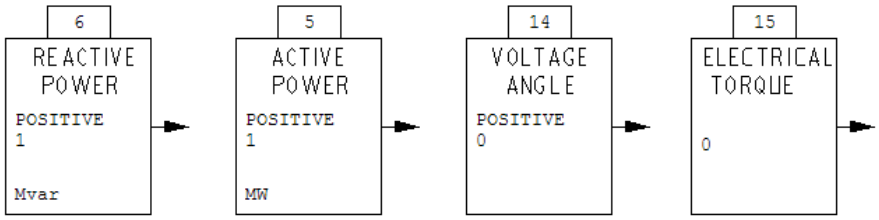

Figure 19-1: Measurement blocks in EUROSTAG software

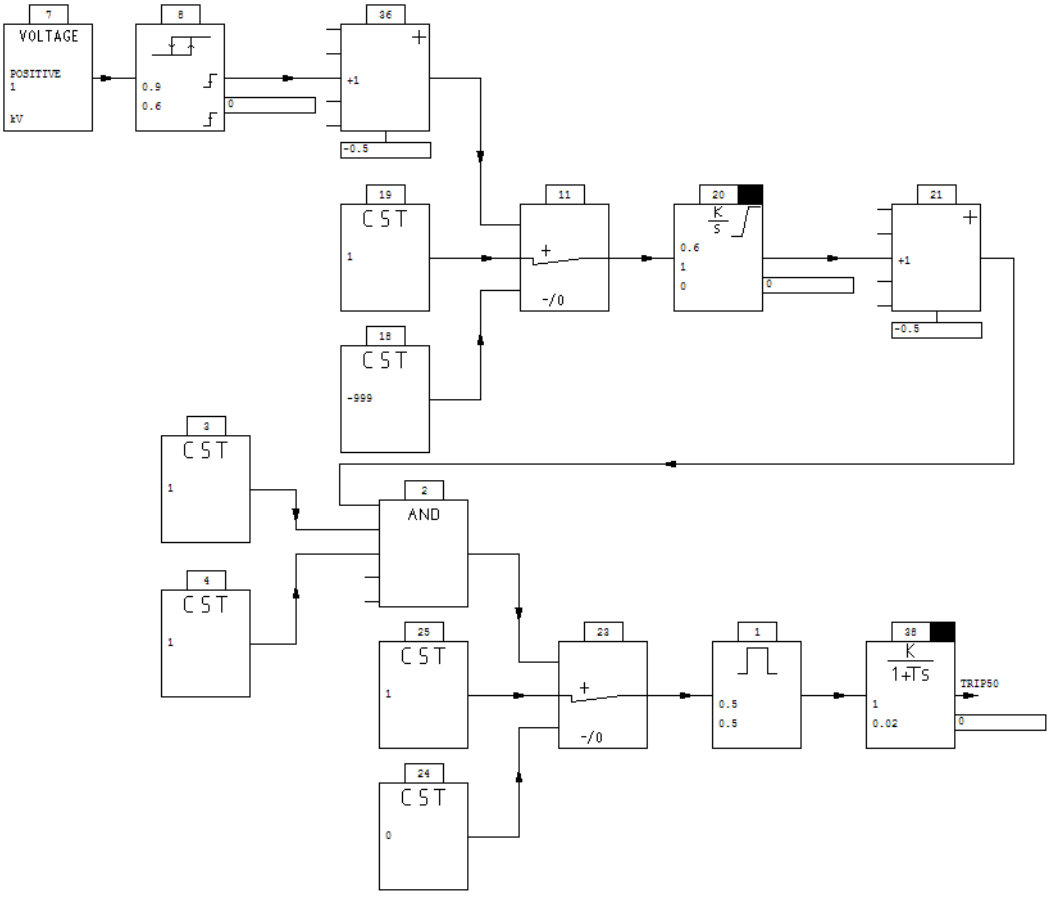

Figure 19-2: EUROSTAG model of over-(P, Q, S ...) protection

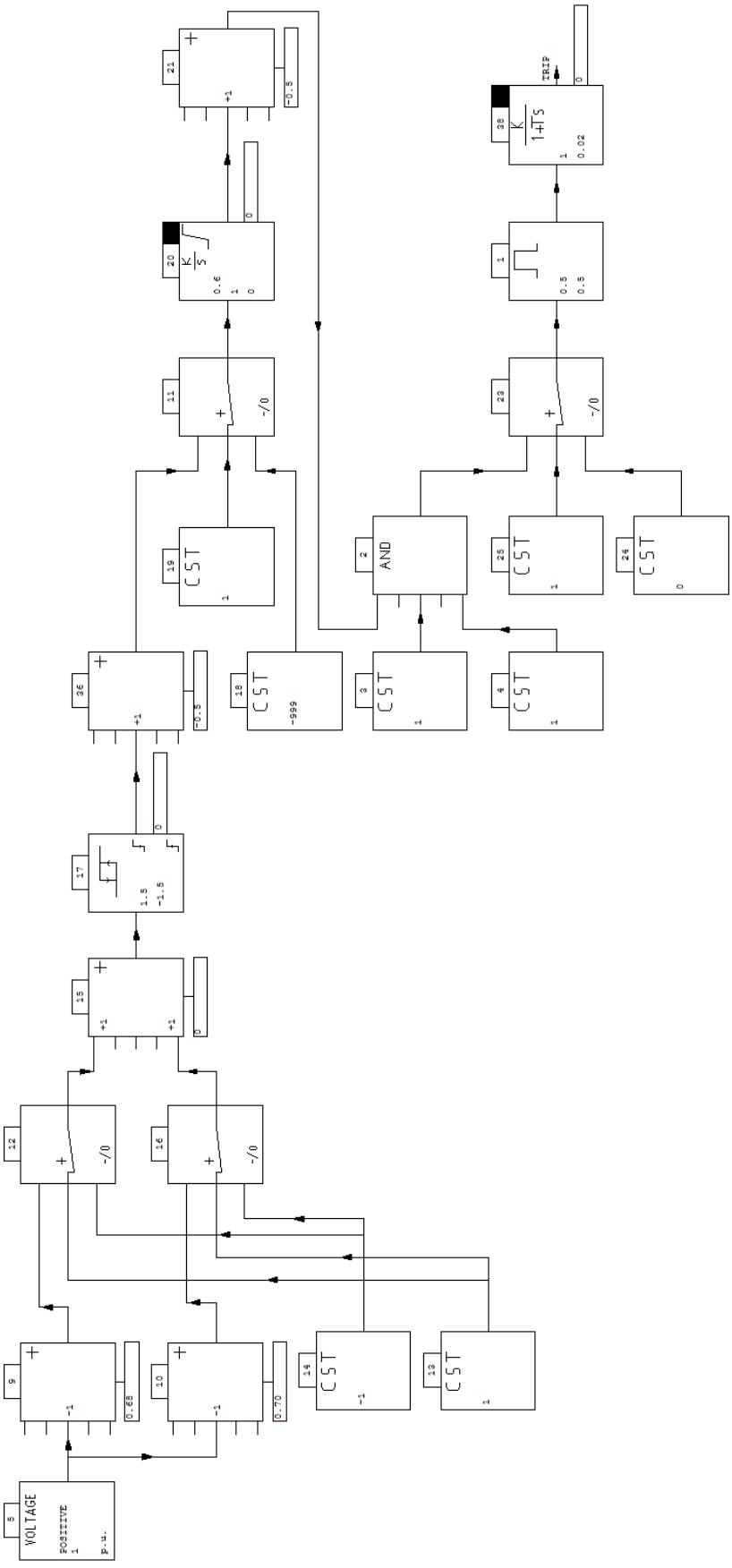

Figure 19-3: EUROSTAG model of under- (P, Q, S, ...) protection

These general models can be used also as a part of larger protection or automation systems taking advantage of the existence of blocking and releasing binary inputs.

20. Special Protection Schemes (SPS)

Due to great variety of special protection schemes and wide area protection and automation systems authors consider that it is impossible to create ready to use models. It is better to have a library of standard elements (see Figure 20-1) as well as standard protection and automation models so that end user can create any complex system he wants.

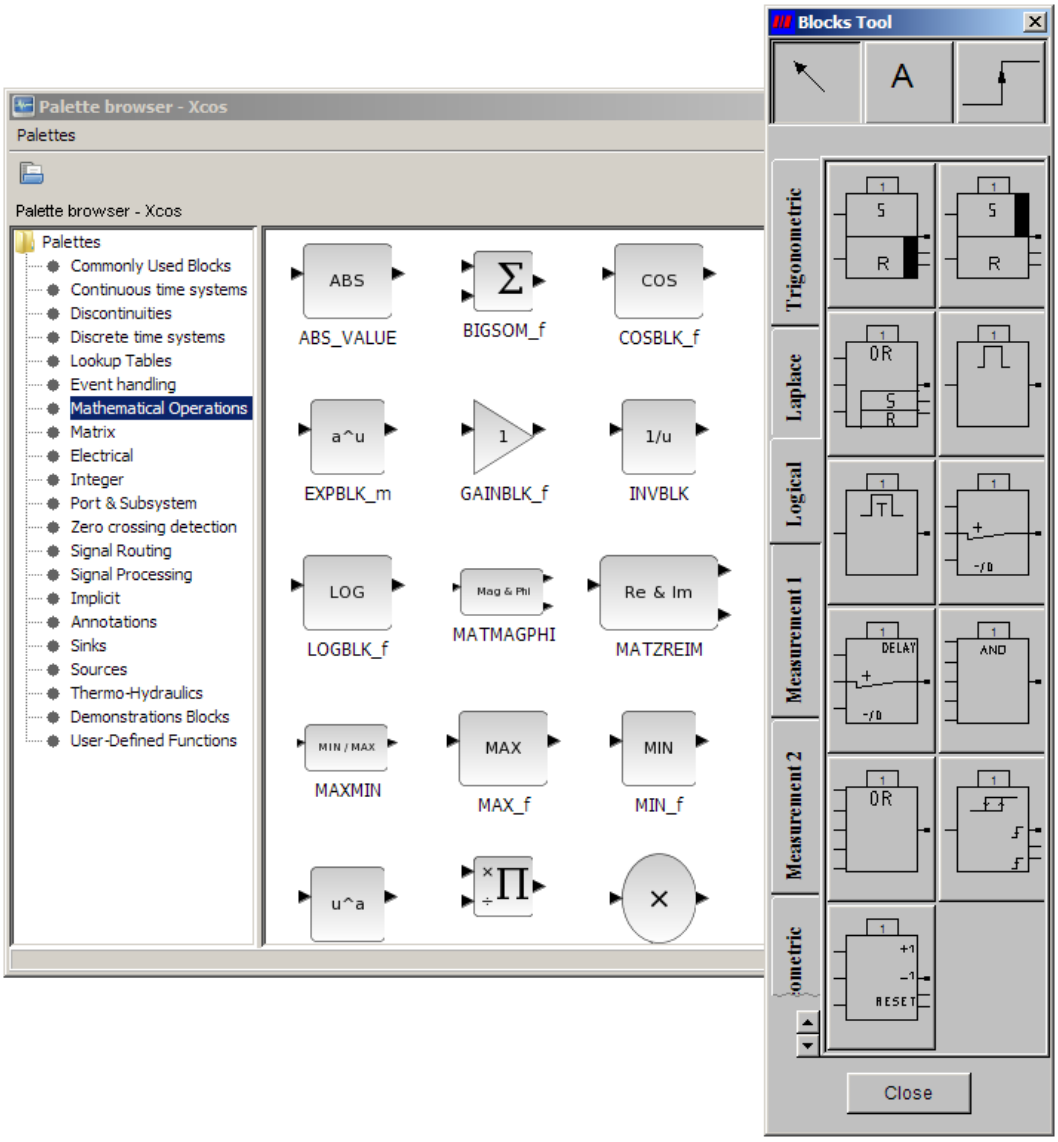

Figure 20-1: Library of standard elements in SCILAB/XCOS and EUROSTAG software

Let us take as an example the SPS of Kurskaya nuclear power plant in Russia. Kurskaya NPP is situated in the southern part of Center UPS near Ukrainian border. Its total capacity is equal to 4000 MW that is allocated in 4 generating units. Kurskaya NPP is connected to the power system by three 750 kV overhead lines and several 330 kV lines. A simplified plot of the surrounding power grid is shown in Figure 20-2.

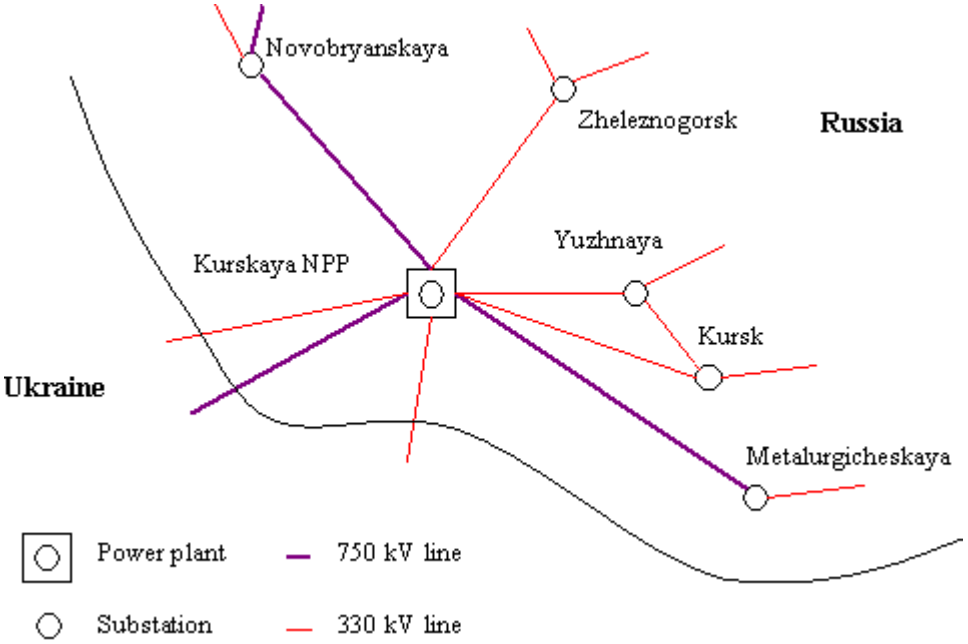

Figure 20-2: Region of Kurskaya NPP

Anti-emergency system of Kurskaya NPP includes two parts: out-of-step protection at each generator and automatic unloading system. The latter system is only enabled when Russian and Ukrainian power systems are not operated in parallel and therefore the grid is weakened. It automatically reduces NPP total generation by dropping a generator when one of predetermined events (short-circuit or grid element disconnection) occurs.

The logic that determines which generator and in what conditions it should be dropped is presented in Figure 20-3, this logic can be implemented in EUROSTAG using Macroblocks to define the conditions of generator dropping and Macroautomatons to enable the dropping via events.

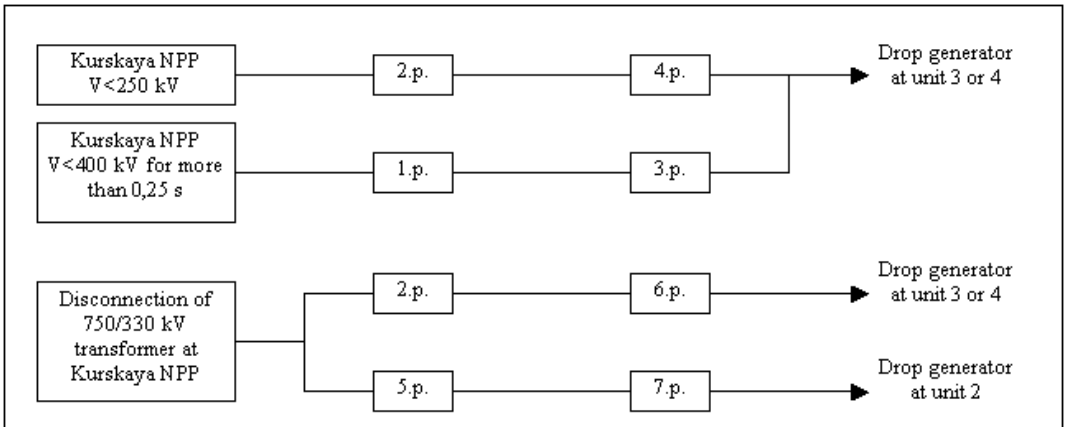

Starting factor		Control action
Total generation of units 1-2:	Total generation of the NPP	
1.p. – more than 800 MW	3.p. – more than 2500 MW	
2.p. – more than 1100 MW	4.p. – more than 2850 MW	
	750/330 kV trans former load:	
Generation of unit 2:	6.p. – more than 500 MW to 330 kV bus	
5.p. – more than 700 MW	7.p. – more than 300 MW to 750 kV bus	

Figure 20-3: Part of a station's unloading logic unit

21. References

[1] M. Behnke, et al : Development and Validation of WECC Variable Speed Wind Turbine Dynamic Models for Grid Integration Studies, *AWEA's 2007 WindPower Conference, Los* Angeles, California, June 4–7, 2007

[2] Fortmann, J.; Engelhardt, S.; Kretchmann, J.; Feltes, C.; Janssen, M.; Neumann, T. & Erlich, I. Generic Simulation Model for DFIG and Full Size Converter Based Wind Turbines 9th International Workshop on Large-Scale Integration of Wind Power into Power Systems as well as on Transmission Networks for Offshore Wind Power Plants, Oct. 2010 Quebec City, Quebec, Canada

[3] *Feltes, C.; Wrede, H.; Koch, F.W. & Erlich, I.* Enhanced Fault Ride-Through Method for Wind Farms Connected to the Grid Through VSC-Based HVDC Transmission IEEE Transactions on Power Systems, 2009 Vol. 24 No. 3 pp. 1537-1546

[4] *Shewarega, F.; Erlich, I. & Rueda, José L.* Impact of Large Offshore Wind Farms on Power System Transient Stability IEEE PES Power Systems Conference & Exposition, March 2009 Seattle, WA USA

[5] *Feltes, C.; Wrede, H. & Erlich, I.* Dynamic Behaviour of DFIG-Based Wind Turbines During Grid Faults IEEJ Transactions on Industry Applications, 2008 Vol. 128 No. 4 pp. 396 - 401

[6] Jiuping Pan, Reynaldo Nuqui, Le Tang and Per Holmberg: "VSC-HVDC Control and Application in Meshed AC Networks", IEEE-PES General meeting, Pittsburgh, Pennsylvania, July 20-24, 2008. Feltes, C.; Erlich, I. & Koch, F.

[7] Fault Ride-Through of DFIG-based Wind Farms connected to the Grid through VSC-based HVDC Link 16th Power Systems Computation Conference, July 2008 Glasgow, Scotland

[8] Lidong Zhang and Hans-Peter Nee, " Multivariable Feedback Design of VSC-HVDC Connected to Weak AC Systems", Member, IEEE, and, Senior Member, PowerTech 2009 28 June - 2 July 2009, Bucharest, Romania

[9] Rich Hunt, Michael L. Giordano, "Thermal Overload Protection of Power Transformers – Operating Theory and Practical Experience," 59th Annual Protective Relaying Conference, Georgia Tech, Atlanta, Georgia, April 27th – 29th, 2005.

[10] Christophe Preve, "Protection of Electrical Networks," ISTE Ltd., 2006. ISBN-10: 1-905209-06-1.

[11] IEC 60255-8 Electrical Relays - Thermal Electrical Relays, Second Edition, 1990.

[12] SIPROTEC Multi-Functional Protective Relay with Local Control 7SJ62/64 V4.7, Manual, Siemens.

[13] T60 Transformer Management Relay, UR Series Instruction Manual, Revision 5.2x, GE Multilin, 2007.

[14] MiCOM P139 Feeder Management and Bay Control, Software Version: 605/611/612, Technical Manual, Areva.

[15] Transformer Protection IED RET670, Technical Reference Manual, ABB, 2006.

[16] Blackburn J.L, Domin T.J., "Protective relaying, Principles and Applications," 3rd Edition, CRC Press, 2007, ISBN 1-57444-716-5.

[17] Hewitson L. G., Brown M., Balakrishnan R., "Practical Power System Protection," Elsevier, 2004, ISBN 0-7506-6397-9.

[18] MiCOM P125, P126, P127 Directional/Non-directional Relay, Version 6D, Technical Guide, Areva.

[19] MiCOM P141, P142, P143 Feeder Management Relays, Technical Guide, Areva.

[20] F650 Digital Bay Controller, User manual, Firmware version: 3.7X, GE Multilin, 2007.

[21] Elmore W. A., "Protective Relaying Theory and Applications," 2nd Edition, Marcel Dekker Inc., 2003, ISBN 0-82470-972-1.

[22] Reimert D., "Protective Relaying for Power Generation Systems," Taylor & Francis, 2006, ISBN 0-8247-0700-1.

[23] Horowitz S. H, Phadke A. G., "Power System Relaying," 3rd Edition, John Wiley & Sons, 2008, ISBN 978-0-470-05712-4.

[24] Network Protection and Automation Guide, Alstom, 2002, ISBN 2-9518589-0-6.

[25] Jeff Roberts and Armando Guzmán, "Directional Element Design and Evaluation," Schweitzer Engineering Laboratories, Inc., 2006.

[26] John Horak, "Directional Overcurrent Relaying (67) Concepts," Basler Electric, 2006.

[27] MiCOM P631, P632, P633, P634 Transformer Differential Protection, Software Version: 610, Technical Manual, Areva.

[28] SIPROTEC Differential Protection 7UT613/63x V4.60, Manual, Siemens.

[29] Ziegler G., "Numerical Differential Protection," Publicis Corporate Publishing, 2005, ISBN 3-89578-234-3.

[30] Busbar Differential Protection IED REB670, Technical Reference Manual, ABB, 2006.

[31] SIPROTEC Multifunctional Machine Protection 7UM62 V4.6, Manual, Siemens, 2005.

[32] SIPROTEC Distributed Busbar/ Breaker Failure Protection 7SS522 V4.6, 7SS523 V3.3, 7SS525 V3.3, Manual, Siemens, 2007.

[33] MiCOMho P443 and P445 Distance Relay, Software Version: 33, Technical Manual, Areva.

[34] Ziegler G., "Numerical Distance Protection," 2nd Edition, Publicis Corporate Publishing, 2006, ISBN 3-89578-266-1.

[35] SIPROTEC Line Differential Protection with Distance Protection 7SD52/53 V4.60, Manual, Siemens.

[36] Karel Máslo, Martin Kaňok, "Distance Protection Model for Network Simulators," 8th International Conference CONTROL OF POWER SYSTEMS '08, June 11-13, 2008 Štrbské Pleso, High Tatras, Slovak Republic.

[37] SIPROTEC Distance Protection 7SA6 V4.61, Manual, Siemens.

[38] P. Kundur, Power System Stability and Control, McGraw-Hill, Inc. 1993.

[39] Power Swing and Out-of-Step Considerations of Transmission Lines, IEEE PSRC WG D6, 2005.